



The
University
Of
Sheffield.

Flames in Tubes

by

Fouzi Mossa

Supervisor: Dr. Robert Woolley

A Thesis submitted for the degree of Doctor of Philosophy

Department of Mechanical Engineering

The University of Sheffield

October, 2014

Summary

The tube method has been widely used to determine the laminar burning velocity of gaseous and liquid fuels, and examine flame propagation in a confined space. This method has been suspended since 1960; therefore the main goal of this study is to re-improve this method.

This research focuses on studying the flame shape, flame speed, unburned gas velocity, surface area of the flame and the laminar burning velocities of premixed fuel and air mixtures in a range of equivalence ratios, with both ends open and with orifice plates fitted at both ends. Experiments were conducted at room temperature and atmospheric pressure for propane-air mixtures, and then modified for investigating the flames behaviour at elevated temperature for propane and acetone.

The experimental data were repeatable. The flame speed and the laminar burning velocities increased with temperatures and we are also shown to be influenced by gravity using the upward and downward propagations.

The gas velocity a head of the flame front was measured using Laser Doppler Velocimetry (LDV). As a result the values of laminar burning velocities obtained in this study are in good agreements with previous studies. However, the results obtained at high temperatures have a slightly different value compared with the literature data. These errors are due to the uncertainty temperature inside the tube and the surface area measurements and hence some improvements in this technique are recommended.

Dedication

To my **Parents**

To my beloved wife **Nagwa**

To my **Brothers** and **Sisters**

To my beautiful daughters **Rufeda** and **Mawda**

Acknowledgements

To my God, who made all things possible

I would like to express my sincere gratitude to my supervisor **Dr. Rob Woolley** for providing me an interesting research topic and for his support, help, advice and criticism throughout the course of this research work.

Also I would like to thank for **Mr. Malcolm Nettleship** for his help in building the test rig in the lab and spending long times with me during experiments.

I gratefully acknowledge the Ministry of Higher Education in Libya who supported me financially during my study. The University of Omar Al-Mukhtar is also acknowledged for nominating and giving me this opportunity to pursue my study.

My wife **Nagwa**, and my daughters **Rufeda & Mawda** for their support and patience during all time of my studies.

I express my thanks and appreciation to my father, mother, brothers, sisters and all my friends for their support and encouragements.

I would like also to give thanks to Kenneth K. Kuo the author of *Principle of Combustion*, and the publisher Hoboken, N.J: Wiley, 2005 2nd ed. for the permission to reproduce the figures 2.1 and 2.2 in this work.

Also thanks to Chung K. Law the author of *Combustion Physics*, and the publisher Cambridge University press, 2006 for the permission to reproduce the figure 2.3 in this work.

Finally, thanks for Royal Society of Chemistry for given permission for some figures presented in this work.

Table of Contents

Summary	i
Dedication.....	ii
Acknowledgements.....	iii
List of Figures	vii
List of Tables.....	xi
Nomenclature.....	xii
1. Introduction.....	1
1.1 Overview	1
1.2 Flame characteristics.....	2
1.3 Definitions.....	3
1.3.1 Laminar burning velocity of premixed flame.....	3
1.3.2 Flammability limits.....	3
1.3.3 Ignition.....	4
1.4 Flame structure.....	4
1.5 Flame temperature.....	5
1.6 Motivation for the present work.....	5
1.7 The specific objectives	6
1.8 Structure of the thesis.....	6
2. Literature review	8
2.1 Methods used to measure laminar burning velocity	8
2.2 Comparison of values of burning velocity.....	18
2.3 Factors affecting the laminar burning velocity	19
2.3.1 Equivalence ratio.....	19
2.3.2 Temperature.....	20
2.3.3 Pressure.....	21
2.4 Flammability limits.....	23
2.5 Flame stretch in laminar flames	24
2.6 Propane	25
2.7 Acetone.....	27
2.8 Flame surface area	29
2.9 Laser Doppler Velocimetry (LDV) application.....	31
3 Experimental Apparatus.....	33
3.1 Original apparatus.....	33

3.2	Tubing	34
3.3	Calculation of the required fuel volume	36
3.4	Igniter	37
3.5	Removal of remaining fuels and combustion products.....	39
3.6	Orifice plates	39
3.7	Recording the flame.....	40
3.8	Flame speed processing.....	40
3.9	Unburned gas velocity measurements.....	41
3.9.1	Laser Doppler Velocimetry (LDV) specification	41
3.9.2	The measuring volume	42
3.9.3	Signal processing.....	43
3.9.4	Seeding particles.....	43
3.9.5	Set up of the LDV	44
3.10	High temperature measurements	46
3.11	Measurement errors.....	48
4	Results of Flame propagation in a tube at open both ends.....	51
4.1	Results of horizontal tube with open both ends to atmosphere	51
4.1.1	Reasons for the performance of the flame	60
4.2	Results of upwards and downwards propagation in a vertical tube position open at both ends.....	66
4.2.1	Results of upwards propagation in a vertical position with open both ends to atmosphere	66
4.2.2	Results of downward wards propagation in a vertical position with open both ends to atmosphere	74
4.3	Results of a horizontal tube with open both ends to the atmosphere, using high speed camera with a rating of 3000 fps.....	76
5	Results of flame propagation with orifice plates at both ends.....	80
5.1	Results of horizontal tube with orifice plates at both ends.....	80
5.2	Results of upwards and downwards propagation in a vertical tube, with orifice plates at both ends.....	91
5.2.1	Upwards propagation in a vertical tube with 5 mm orifice plate at both ends... 91	
5.2.2	Upwards propagation in a vertical tube with 1 mm orifice plate at both ends... 94	
5.2.3	Downwards propagation in a vertical tube with 1 mm orifice plates..... 97	
5.3	Propane at elevated temperature	101
5.3.1	Results observation.....	101

5.4	Discussion	104
5.5	Comparisons	107
5.6	Liquid Fuel (Acetone).....	107
5.6.1	Results observation.....	108
5.6.2	Flame behaviour.....	110
6	Measurement of laminar burning velocity.....	111
6.1	Unburned gas velocity	112
6.2	Flame surface area	115
6.3	Laminar burning velocity	119
6.4	Laminar burning velocity of propane-air mixture at 333 K	122
6.5	Comparisons	126
6.6	Discussion	128
6.6.1	Results of unburned gas velocity.....	128
6.6.2	Effect of temperature	128
6.6.3	Effects of equivalence ratio and fuel structure.....	129
6.6.4	Reliability of tube method.....	129
7	Conclusions.....	131
7.1	Future work	133
	References	134
	Appendix A.....	146
	Appendix B.....	147
	Appendix C.....	153
	Appendix D.....	155
	Appendix E	156
	Appendix F	157
	Appendix G.....	158
	Appendix H.....	159
	Appendix I	160
	Appendix J.....	161
	Appendix K.....	162
	Appendix L	163
	Appendix N– Published	165

List of Figures

Figure 1.1 Laminar flame structure, showing preheat and reaction zones	4
Figure 2.1 Schematic of a premixed laminar flame shown above a Bunsen burner [13].....	9
Figure 2.2 A flat-flame burner setup [13].....	13
Figure 2.3 Schematic showing a counterflow configuration	14
Figure 2.4 A comparison of reported laminar burning velocities at room temperature and atmospheric pressure	18
Figure 2.5 Effect of equivalence ratio on the laminar burning velocity of propane-air mixture at 300 K and 1 bar [72].....	20
Figure 2.6 Relationship between unburned mixture temperatures and the laminar burning velocity for various fuels [13].....	20
Figure 2.7 Effect of the laminar burning velocities on the pressure of propane-air mixture at $\phi = 0.89$, at a temperature of 343 and 408 K [75]	22
Figure 2.8 Laminar burning velocities of Propane-air mixtures from literature data at ambient and elevated temperatures and atmospheric pressure.....	27
Figure 2.9 A comparison of laminar burning velocity values of acetone-air mixtures, from published data, at room temperature and atmospheric pressure	29
Figure 2.10 Image and sketch flame areas.....	29
Figure 2.11 Vertical and horizontal images of flame shapes.....	30
Figure 2.12 Flame curvature method.....	31
Figure 3.1 Schematic diagram of the experimental rig.....	34
Figure 3.2 Effect on flame velocity by increasing the tube diameter [116].....	35
Figure 3.3 Distance to maximum velocity as overall tube length increase, tube with 5 cm diameter and closed at both ends [7].....	36
Figure 3.4 Gas lighter ignition	38
Figure 3.5 Effect of ignition source on the flame speed in the tube for a $\phi = 0.9$	38
Figure 3.6 Four sets of orifice plates.....	39
Figure 3.7 Images at different step of the process.....	40
Figure 4.1 (c) Images of flames propagating down tubes, at different equivalence ratios, and a framing rate of 420 fps. Tube opens at both ends.....	54
Figure 4.2 Normalized CH^* chemiluminescence yield as a function of equivalence ratio [126]	56

Figure 4.3 Flame distance against time for tube open at both ends	57
Figure 4.4 Variations in flame speed (obtained from a linear fit), with equivalence ratio, for a tube at open both ends.....	60
Figure 4.5 Photographs of flame shape propagation down the tube at close both ends.....	62
Figure 4.6 Vertical position	66
Figure 4.7 Flame shapes propagating upwards in a vertical tube with a 20 mm ID	67
Figure 4.8 Images of non-uniform flames propagating upwards, at mixtures equivalence ratio 1.1	68
Figure 4.9 Images of non-uniform flames propagating upwards, at mixture equivalence ratio 1.3.....	68
Figure 4.10 Images of non-uniform flames propagating upwards, at mixture equivalence ratio 1.4.....	69
Figure 4.11 Flame distance versus time, for upward propagation for a tube open at both ends.....	72
Figure 4.12 Flame propagation upward with an equivalence ratio of 0.8 at open both ends, processed by Corel Paint Shop application	72
Figure 4.13 Equivalence ratio against flame speed of upward propagation at open both ends	73
Figure 4.14 A comparison flame speed of horizontal and upward propagation in a tube open at both ends	74
Figure 4.15 Consecutive images of flame propagating down tubes. A framing rate 3000 fps was used.....	78
Figure 4.16 Flame distance versus time for tube open at both ends, a frame rate of 3000 fps	79
Figure 5.1 Flame shape across equivalence ratios of 8, 5, 3 and 1 mm orifice plates	81
Figure 5.2 Images of flame propagation down tube with orifice plates of 8 mm at both ends. Mixture equivalence ratio = 1.3.....	82
Figure 5.3 Flame distance against time for a tube fitted with 8 mm orifice plates	83
Figure 5.4 Flame distance against time for a tube fitted with 5 mm orifice plates	84
Figure 5.5 Flame distance against time for a tube fitted with 3 mm orifice plates	85
Figure 5.6 Flame distance against time for a tube fitted with 1 mm orifice plates	86
Figure 5.7 Flame shape across equivalence ratios of 5/3 and 5/1 mm orifice plates.....	87
Figure 5.8 Flame speeds with the various orifice plates in flame tube	89
Figure 5.9 Flame speeds with the combination orifice plates in flame tube	90
Figure 5.10 Vertical experimental apparatus	91

Figure 5.11 Upwards propagation flame shape across equivalence ratios of 5 mm orifice plates.....	92
Figure 5.12 Flame distance against time of orifice plate 5 mm, at upward propagation.....	92
Figure 5.13 Flame speed with a range of equivalence ratios for upward propagation in a vertical tube with 5 mm orifice plate	93
Figure 5.14 A comparison of horizontal and vertical propagation in tube	94
Figure 5.15 Images of flames propagating upward with orifice plate of 1 mm at various equivalence ratios	95
Figure 5.16 Flame distance against time of orifice plates 1 mm, at upwards propagation.....	95
Figure 5.17 Flame speed with a range of equivalence ratios for upward propagation of 1 mm orifice plate	96
Figure 5.18 Images of flames propagating downward with orifice plate of 1 mm at various equivalence ratios	97
Figure 5.19 Images of flame propagating downward in the tube. Mixture equivalence ratio = 1.2, with orifice plate of 1 mm.....	98
Figure 5.20 Flame distance against time of orifice plate 1 mm, at downwards propagation..	98
Figure 5.21 Flame speed with a range of equivalence ratio for upward and downward flames in 20 mm I.D tube with 1 mm orifice plate	100
Figure 5.22 Flame shape of propane at 333 K across equivalence ratios of 5 mm orifice plate	101
Figure 5.23 Flame distance against time of 5 mm orifice plate of propane at 333 K	102
Figure 5.24 Flame speed with various equivalence ratios of 5 mm orifice plate at 333 K....	103
Figure 5.25 Results of 5/0 mm orifice plates [130]	105
Figure 5.26 A comparison of flame speed propagating in a horizontal tube at both ambient and 333 K with 5 mm orifice plates placed at both ends.....	107
Figure 5.27 Flame shape of acetone at 333 K across equivalence ratios of 5 mm orifice plates.....	108
Figure 5.28 Flame distance against time of 5 mm orifice plate of acetone at 333 K.....	109
Figure 5.29 Flame speed of acetone with various equivalence ratios of 5 mm orifice plates at 333 K.....	110
Figure 6.1 Results of unburned gas velocity of propane-air mixtures for equivalence ratio of 0.8.....	112
Figure 6.2 Unburned gas velocity of propane-air mixtures as a function of equivalence ratios with orifice plates of 5 and 5/3 mm, at ambient condition	113

Figure 6.3 Unburned gas velocity as a function of observed flame speed of 5 mm orifice plates at both ends.....	114
Figure 6.4 Unburned gas velocity as a function of observed flame speed of 5/3 mm orifice plates.....	114
Figure 6.5 Propane flame shape of top observation with 5 and 5/3 mm orifice plate.....	116
Figure 6.6 Flame shape (a) top image and (b) front view (an example of $\phi = 1.1$), produced by Solidworks software.....	116
Figure 6.7 Frustum of right circular cone.....	117
Figure 6.8 Example of computing flame surface area for equivalence ratio of 1.1, with 5 mm orifice plates.....	118
Figure 6.9 Flame surface area of $\phi = 1.1$, computed by Solidworks software.....	118
Figure 6.10 Laminar burning velocity of propane-air mixtures as a function of equivalence ratios with 5 mm orifice plates at both ends and at normal temperature and pressure	120
Figure 6.11 A comparison of measured laminar burning velocity of propane-air mixture at room temperature and atmospheric pressure.....	122
Figure 6.12 Propane flame shape of side and top observation with 5 mm orifice plates.....	123
Figure 6.13 Laminar burning velocities of propane-air mixtures with 5 mm orifice plates fitted at both ends	125
Figure 6.14 A comparison of laminar burning velocities of propane-air mixtures with 5 mm orifice plates at both ends	127

List of Tables

Table 2.1 Summary of previously experimental work for the laminar burning velocity of acetone-air mixture, for various methods.....	28
Table 3.1 Flammability limits of propane in the atmospheric air [67]	37
Table 3.2 System volume measurements.....	37
Table 4.1 Observed flame speeds for a tube open at both ends. Data are the averages from eight tests.....	59
Table 4.2 Flame speed variation of upward propagation.....	73
Table 5.1 Velocities and correlation data for least squares linear fits for tube with 8 mm orifice plates	87
Table 5.2 Velocities and correlation data for least squares linear fits for tube with 5 mm orifice plates	87
Table 5.3 Velocities and correlation data for least squares linear fits for tube with 3 mm orifice plates	88
Table 5.4 Velocities and correlation data for least squares linear fits for tube with 1 mm Orifice Plates.....	88
Table 5.5 Flame speed variation in test data 5 mm orifice plates of upward propagation	93
Table 5.6 Flame speed variation in test data 1 mm orifice plates of upward.....	96
Table 5.7 Flame speed variation in test data 1 mm orifice plates of downward	99
Table 5.8 Flame speed variation in test data 5 mm orifice plates at 333 K.....	102
Table 5.9 Flame speed variation of acetone in test data 5 mm orifice plates at 333 K.....	109
Table 6.1 Table of Calculated Unburned Gas Velocities for the 5mm and 5/3 orifice plates	115
Table 6.2 Surface area measurements of propane at room temperature and atmospheric pressure.....	119
Table 6.3 Laminar burning velocity calculations for both configurations.....	120
Table 6.4 Surface area measurements of propane at 333K with 5 mm orifice plate	123
Table 6.5 Laminar burning velocity of propane at 333 K and atmospheric pressure with 5 mm orifice plates	124
Table 6.6 The temperature exponent of propane-air mixture with a range of equivalence ratios [98].....	124
Table 6.7 Laminar burning velocity of propane at 333 K and atmospheric pressure.....	125

Nomenclature

Latin letters

δ – Reaction zone thickness

U_1 – Laminar burning velocity

U_f, U_o – Flame speed

U_g – Unburned gas velocity

A_t – Cross-section area of the tube

A_f – Flame surface area

R – Inner radius of the spherical vessel

R – Spherical flame radius

P – Instantaneous chamber pressure

n_f – Number of moles of fuel

n_o – Number of moles of air

T_o – Initial temperature

P_o – Initial pressure

Greek letters

ϕ – Equivalence ratio

γ_u – Specific heat ratio

α – Temperature exponent

β – Pressure exponent

Abbreviations

DDT – Deflagration to detonation transition

LIF - Laser induced fluorescence

I.D – Internal diameter

LDV – Laser Doppler Velocimetry

1. Introduction

1.1 Overview

Combustion is the main source of power in the present world. A better understanding and knowledge of combustion technology is required for improvement in process and efficiency gains to take place. One of the goals of combustion research is to understand the mechanisms of ignition, flame propagation and energy release [1]. Nowadays energy is provided particularly through combustion processes, although there are attempts to develop alternative energy sources. Even with these efforts, combustion processes will remain the main source of power for the foreseeable future [2].

The present study investigates the combustion characteristics of gaseous (propane) and liquid (acetone) fuels within tubes. The study of laminar premixed flames has been central to research on premixed combustions, ever since it was recognized that flames propagate through a premixed fuel-air mixture at a characteristic rate [3]. A large number of experimental configurations have been used, which can roughly be divided into chambers and burners. In the case of burners the flame is fed by a constant flow- rate of mixtures, and the experimental issues occur when determining the surface area. In chambers, the volume is filled with the premixture and then ignited; and the flame is developed and propagates outward with the laminar flame speed.

The first propagation of premixed flames in tubes was performed in 1883 by Mallard and Le Chatelier, [4] using a horizontal tube that was open near to the ignition point and sealed at the far end. The measurement of flame propagation in tubes, was subsequently used by a number of researchers, to determine laminar burning rates, notably Coward and Hartwell [5], Gerstien et al. [6] and Guenoche [7]. However, there are essential problems with the tube method, owing to the interactions of gases with the boundaries, both at the end of the tube and with the tube walls. Additionally, a number of different experimental configurations have been employed, such as varying tube diameters, varying combinations of open and closed tubes and the use of orifice plates, located in the tube ends.

The flame in the tube is usually captured by filming its progress, using a high speed camera. The flame movement down the tube is faster than the laminar burning velocity. This is due to wall interactions and the expansion of the burned gases. The laminar burning velocity can be determined by accounting for these effects, as demonstrated by Coward and Payman [8].

$$U_l = (U_f - U_g) A_t / A_f \quad (1.1)$$

Where,

U_l – Laminar burning velocity, (m/s)

U_f – Flow flame speed, (m/s)

U_g – Unburned gas velocity, (m/s)

A_t – Cross-sectional area of the tube, (m²)

A_f – Flame surface area, (m²)

The tube method has a number of advantages which will be discussed in the next chapter.

In recent times the combustion of mixtures in the tubes has received attention by those interested in the deflagration to detonation transition (DDT) [9-10]. The overall mechanism of DDT can be described as follows. The flame forms and starts to propagate along the tube, the surface area increases, resulting in flame acceleration, which in turn results in a weak shock front propagation, ahead of the flame. These shocks combine and adiabatically compress the unburned mixture behind them, which leads to a thermal explosion and eventually a detonation [10-11].

The experiments in this study were performed in horizontal and vertical tubes at atmospheric and elevated temperature conditions, for a range of equivalence ratios. Experiments have concentrated on a tube that is open at both ends and using orifice plates fitted at both ends. The main focus of this work is on the flame shape, flame speed, unburned gas velocity, flame front area and the laminar burning velocity of premixed mixtures. The results have been compared with previous experimental and modelled studies.

The following provides a short background of the other aspects relating to the combustion characteristics required for further reading.

1.2 Flame characteristics

A flame can be defined as a subsonic combustion wave, driven by a self-propagating exothermic reaction. It is typically characterized by a localized reaction zone, separating reactants and products [12]. Flames are observed in two cases, a stationary flame, which is propagating into the gas flow from the burner, or a non-stationary flame, which travel in an initially quiescent mixture.

There are two types of flames; premixed flames and diffusion flames. In diffusion flames the reactants are initially separated and reaction occurs only at the interface between the fuel and oxidizer, where mixing and reaction both take place, which can also be laminar or turbulent. Premixed flames occur where the fuel and air are mixed before they are close to the flame area [1]. Premixed fuels flow up the burner tube at a rate which exceeds the normal burning velocity of the mixture. A separate combustion wave that moves subsonically is called a deflagration. If the combustion waves travel at supersonic speeds then they produce detonation and have a different propagation mechanism [12].

1.3 Definitions

1.3.1 Laminar burning velocity of premixed flame

The laminar burning velocity is a value for the speed of the unheated premixed gas just before entering the flame zone [13]. It is depend on the fuel concentration, temperature and pressure. The laminar burning velocity is affected by both flame temperature and radiation. Planar and stationary flame fronts are a good measure of laminar burning velocity of fuel-air mixtures, although this is very hard to achieve [14]. Techniques for measuring the laminar burning velocity for stationary and non- stationary flames are shown in the next chapter.

1.3.2 Flammability limits

If the quantity of fuel is increased in a fuel/oxidiser premixture, a point will be attained at which the mixture becomes flammable. The proportion of fuel at this point is termed the lower or lean flammability limit. The upper or rich flammability limit occurs when adding more fuel to the mixture and the mixture will no longer burn. The flammability limits for a mixture can be extended by increasing the initial temperature and pressure [1].

Flammability limits have been measured experimentally [12] for a number of gaseous fuels, at atmospheric pressure, by using a vertical tube (about 120 cm long and 5 cm diameter), as shown in the lower and the upper limits of propane (C_3H_8) which is approximately 0.51 and 2.83 respectively [12].

1.3.3 Ignition

Ignition sources can be divided into two types: homogenous ignition and point ignition. In the first type, ignition occurs at the same time for the whole mixture. If the heat of a homogenous mixture of reactants in the vessel is increased, a point is attained at which ignition occurs. This phenomenon is called the self-ignition or auto-ignition point [1]. The auto-ignition point is widely employed because it is associated with spark ignition. Spark ignition does not require an external source of energy, and is extremely reliable [12].

The second type point ignition, occurs when the flame develops near to the ignition supply, and then extends through the mixture's reactant [1].

1.4 Flame structure

Figure 1.1 provides further information about flame propagation, as given by Ragland and Bryden [15]. This includes the reactant and a temperature gradient, from the reaction zone to the burned mixtures. It is clear that, there are two zones within the flame. In the preheat zone, the gases temperature will be increased due to heat conduction. In the reaction zone the propagation is continued, with increased temperature, owing to chemical energy release [13]. Furthermore, in this zone, a visible flame area with thin layer δ appears.

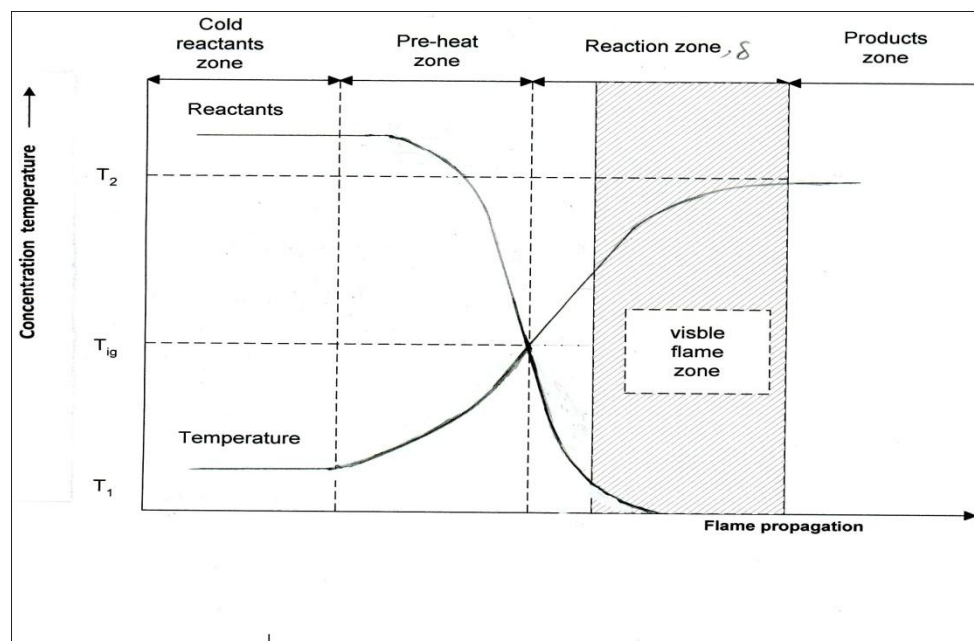


Figure 1.1 Laminar flame structure, showing preheat and reaction zones

1.5 Flame temperature

The flame temperature is the temperature of the products that are heated by the flame. For premixed flames, a well defined reactant composition enters the flame at a permanent temperature and pressure. As a result, it is feasible to determine the adiabatic flame temperature from the thermodynamic properties of the fuel mixture reactant. The adiabatic temperature of a general fuel-air mixture at $\phi = 1$ is more than 2000 K, whilst close to flammability limits, the obtained temperature is lowered from 1400 – 1500 K.

1.6 Motivation for the present work

Up until 40 years ago the laminar burning velocity was often found by measuring the speed at which a flame propagated down a tube. At the present time constant volume spherical and counterflow burners are arguably the two most popular in general use. Therefore, the motivation for the present investigation is to examine the use of premixed flames in tubes as a method of measuring the laminar burning velocity. The advantages are in simple geometry and the fact that it is a relatively easy rig to manufacture, which accounts for its historic popularity. In addition, most of the available data published using this method is at ambient temperature and pressure. The aim of the present study is to determine the flame speeds and laminar burning velocities of propane-air mixtures at ambient condition, with both tube ends open and with orifice plates at both ends of the tube. Moreover, is to determine the flame speed and the laminar burning velocities of propane and liquid fuel acetone-air mixtures at high temperature and ambient pressure.

1.7 The specific objectives

The specific objectives of the research are:-

- To establish and improve a tube rig, with a view to achieving laminar burning velocities of propane and acetone-air mixtures similar to published results with both ends open, creating different orifice plates and stabilising the apparatus vertically
- Investigate an improved processes by using a high speed camera up to 3000 fps to obtain clear and sensitive images of the flame as it propagates along the tube
- Develop and modify the rig for propane and acetone-air mixtures at elevated temperatures and atmospheric pressure
- Investigate the effect of temperature and gravity, on the flames mechanism, with respect of equivalence ratios
- Measure flame speed, unburned gas velocities, surface area of the flame and finally the laminar burning velocities

1.8 Structure of the thesis

This thesis is organized into 7 chapters that describe the research performed. The next chapter gives a brief literature review of the different techniques used to measure laminar burning velocities of fuel-air mixtures. A brief review of factors affecting the laminar burning velocities and the variety of fuels are discussed. In addition, the combustion properties, flammability limits and a brief review of gas fuel propane and liquid fuel acetone are presented in this chapter. Finally, analysis of the unburned gas velocity and LDV application are discussed.

Chapter 3 lays out the details of the experimental setup and the methodologies of the tube rig experiments which were used to measure the flame speed and the laminar burning velocities for propane and acetone-air mixtures at ambient pressure and temperature and at elevated temperature.

Chapter 4 discusses results from the tube experiments of propane-air mixtures with both ends open, at room temperature and at atmospheric pressure, for horizontal and vertical configurations of the rig.

Chapter 5 presents the results of propane-air mixtures at initial temperature and pressure, with orifice plates at both ends of 8, 5, 3, 1 mm and combination plates of 5/3 and 5/1 mm, for both horizontal and vertical positions. This chapter also discusses the results obtained for propane and acetone-air mixtures at elevated temperature 333 K with orifice plate of 5 mm, which took place at both ends of the tube. In addition, a comparison of flame speeds at ambient and high temperature is presented.

Chapter 6 shows the LDV measurements used to obtain the unburned gas velocity and hence the laminar burning velocities of propane-air mixture at room and high temperatures and atmospheric pressure with orifice plates of 5 mm which is taking place at both ends and combination plates of 5/3 mm.

In the final part, chapter 7 the conclusions and future work are presented.

2. Literature review

This chapter covers the combustion characteristics of premixed fuel/air mixtures, and the different techniques used to measure their laminar burning velocities, indicating the pros and cons of such techniques. The speed with which flames propagate down tubes is dependent not only on the laminar burning velocity, but also upon the ignition source, tube configuration, heat transfer and flame shape.

In this chapter different techniques and factors that have an effect on the laminar burning velocity are presented, followed by reviews of the fuels that have been used in this work.

2.1 Methods used to measure laminar burning velocity

Over several decades many researchers have tried to determine the laminar burning velocity experimentally and computationally. They have used a variety of experimental methods to achieve these measurements. A variety of models with alternative chemical kinetic mechanisms has also been used. Examples of experimental techniques include: - [12-13, 16-17]

1. Bunsen burner method
2. Constant volume explosion in a spherical bomb
3. Flat-flame burner method
4. Counterflow method
5. Flame propagation in tubes

2.1.1 *Bunsen burner method*

This is the oldest method of determining the laminar burning velocity and was first used in 1855 by Bunsen [13]. In this technique the mixture of fuel and air is premixed before flowing into the burner tube. The burning occurs at the top of the tube and produces a luminous conical premixed flame surrounded by a larger diffusion flame, as shown in Figure 2.1.

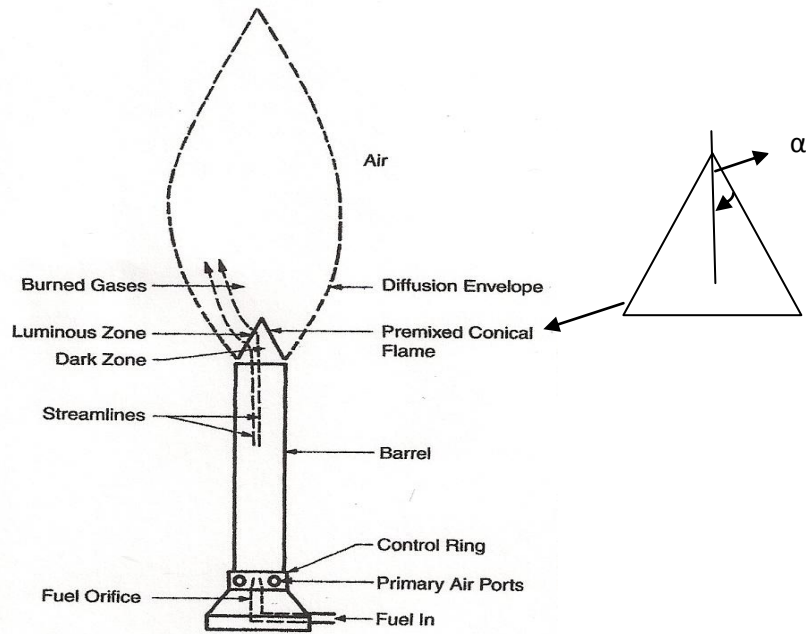


Figure 2.1 Schematic of a premixed laminar flame shown above a Bunsen burner [13]
 [“This material is reproduced with permission of John Wiley & Sons, Inc.”]

In this technique, the flame at the top of the burner is stabilised, as the burning velocity is equal to the incoming gas speed. As the flame is stationary it can be easily visualised and its area found. Shadowgraph, Schlieren and direct photography have been used to provide a more accurate capture of flame images. [18].

The determination of the laminar burning velocity of the Bunsen burner technique uses the following equation:-[19]

$$U_1 = U_f \sin \alpha \quad (2.1)$$

Where, α is the angle of the half cone angle

The advantage of this technique is that it uses inexpensive apparatus that is easy to measure and construct [13]. Indeed this is likely the reason why it is so commonly used. In addition the Bunsen burner is applicable for turbulent flames [20].

However, there are a number disadvantages, including [13]:

- As the flame is burning outside the tube there could be chemical interchange with the surrounding air which could have an effect on the equivalence ratio
- The wall quenching has clear effects on the flame speed, and is difficult to prevent
- Burner method requires a larger volume of gas than the tube or spherical bomb methods [18]

- With large tube diameters flashback can occurred

2.1.2 Constant volume explosion in a spherical Bomb

At the present time, this method is arguably the most popular in determining the laminar burning velocity [21-32]. Its advantages are that the flame requires no stabilisation so measurements can theoretically be performed for across the whole flammable range and that the flame does not come into contact with any walls so there are no heat losses to account for. There have been two difficulties with the technique, firstly the flame propagates outward from spark and therefore, a technique has been required to track the flame at relatively high speed, and secondly the flame speed was found not to be constant in the early stages of its growth.

Measurements of pressure rise in spherical vessels have been for a number of years. As the flame propagates the hot burned gases expand pushing the flame forward compressing unburned mixture. As the compression is relatively rapid it can be shown to be almost isentropic resulting in final pressures in the vessel up to 8 times the initial pressure. The use of pressure measurement was developed by Lewis et al. [33] and Foick et al. [34] for measuring laminar burning velocities of the flame. The mixture is ignited in the centre of the spherical vessel and, due to increases in both temperature and pressure; the expansion of burned gas pushes the unburned gas near to the wall of the vessel. Many researchers have used this technique to measure the laminar burning velocity of combustible mixtures, with a variety of fuels and operating conditions. A number of investigators have derived a formula for calculating the laminar burning velocity from the pressure record in the vessel. Lewis and Von Elbe [35] assumed that the mass fraction burned is proportional to the pressure of the combustion process, and derived the following relation:

$$U_1 = \left(1 - \frac{R^3 - r_b^3}{3P\gamma_u r_b^2} \frac{dp}{dr_b} \right) \frac{dr_b}{dt} \quad (2.2)$$

Where,

R – The sphere radius

r_b – The instantaneous flame radius

γ_u – The specific heat ratio of the unburned gas

p – The instantaneous chamber pressure

Metghalchi and Keck [22] measured the laminar burning velocity of propane-air mixtures for a pressure range of 0.4 to 40 atm and temperature range 298 to 750 K for an equivalence ratio of 0.8 to 1.5.

From Equation 2.2 it can be seen that it is necessary to know the flame radius as well as the pressure rise, this is challenging as the flame approaches the wall as it is difficult to arrange optical access. Furthermore Groff [36] demonstrated that the flame surface spontaneously wrinkled (became cellular) at elevated pressures. The cellularity is the result of hydrodynamic instabilities that become significant at high pressure with the result that the surface area is unknown and the burn rate cannot be accurately determined. As a result of these problems researchers became interested in measurements in the early stages of flame growth where there was no significant rise in the pressure. The first unstretched laminar burning velocities made in spherical bombs were by Dowdy et al. [37] for hydrogen-air flames. They used high speed schlieren photography to capture the flame progress. The flame speed increased as it expanded due to stretch effects. The stretch is well characterised in the case of a spherically expanding flame [38].

Verhelst et al. [39] studied the influence of equivalence ratios, temperatures and pressures on the laminar burning velocity of hydrogen-air mixture, at zero stretch rate. They used a spherical bomb and found that the unstretched laminar burning velocity increased with increase in temperature. However, the flame became more cellular, with an increase in pressure, due to diffusion thermal instabilities. The same approach has also been used to measure the laminar burning velocities of iso-octane-air mixtures at a free stretch, using twin flame kernels in an explosion spherical bomb [40].

Marley and Roberts [41] measured the unstretched laminar burning velocity of propane-air mixtures, at zero stretch, at normal temperature and pressure, using “high speed chemiluminescence imaging”, in a spherical bomb. Their results confirmed that the high speed imaging procedure provides more accurate results compared with the published [42-43], who those used shadowgraph and schlieren imaging techniques, respectively.

The main advantages of this method are: -[18]

- Small quantities of fuels are required.
- Negligible heat losses.

However, there are a number of disadvantages are:

- The effect of buoyancy caused deformation of the flame shape, particularly for slow flames, which increasing the cellular instabilities [14].

- Due to increased pressure, the burnt gas expands towards the walls and then both burned and unburned gases are heated by the compression, which is supposed to be adiabatic [18].
- The value of the laminar burning velocity measured by this method is shown to be a small increase with an increased amount of burnt mixture due to decreasing the curvature of the flame or the small losses close to the spark gap [44].

2.1.3 Flat-flame Burner method

Powling [45] have succeeded in running flat flames, with the burning velocity just balanced by the flow velocity of the gas. Figure 2.2 shows the apparatus of a flat-flame burner [13], the burner is around 6 cm in diameter and is jacketed by a stream of nitrogen. Within the burner is a metal matrix which produces a uniform velocity profile. The flame takes the form of a flat disc. Its stabilisation seems to be effected by a very slight divergence of the flow lines just above the burner. Without this the flame would either blow-off or strike-back and it would not be possible to stabilise it. The surface area of the flame can be measured and then the laminar burning velocity can be obtained, by dividing the volume flow rate of unburned gas by the surface area of the flame. Due to some unburned gas escaping at the flame edges, causing inaccuracies, this method depends heavily on the accuracy of flame area measurement. Moreover, the heat loss from the flame reduces the burning velocity and makes the method unreliable; as the flame is non-adiabatic. The flat flame was more recently developed by Van Maaren and Goey [46] using Laser Doppler Velocimetry, to measure the axial velocity shape of the flame, and study the effect of expansion and buoyancy on the burnt gas flow. Their results were in close agreement with the published data.

The only disadvantage of this method is that only it is hard to identify the rim of the flame and hence difficult to determine its area precisely [19].

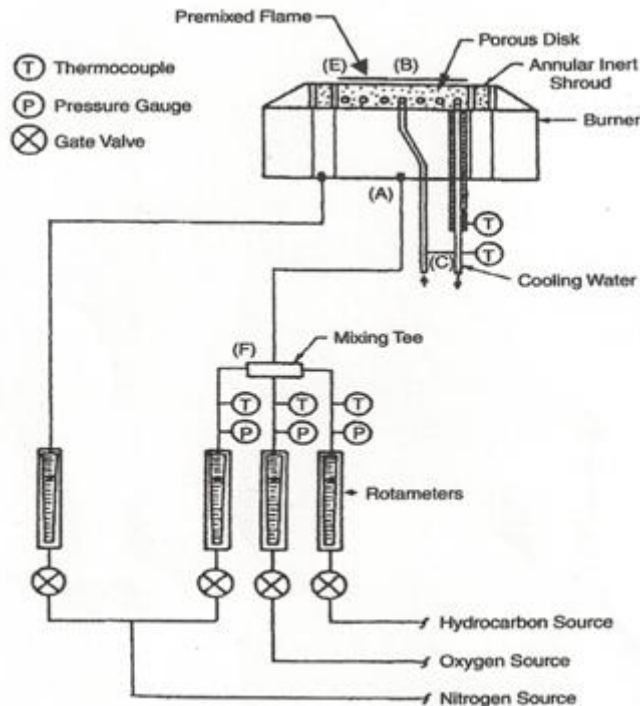


Figure 2.2 A flat-flame burner setup [13]

["This material is reproduced with permission of John Wiley & Sons, Inc"]

2.1.4 Counterflow (Stagnation) flame method

This method was developed by Yu et al.[47]. The flame was established in the stagnation area between two divergent fuel flows, as shown in the Figure 2.3. It can be seen that there are input jets above and below the stagnation area, to produce premixed mixtures in counterflow streams. The flame produced is symmetrical on both sides of the stagnation plane. They determined the laminar burning velocities of propane-air mixtures and methane-air mixtures, with and without adding small quantities of hydrogen, at the upstream boundary of the preheat zone. Their results showed that the laminar burning velocities for both propane and methane increased with the addition of hydrogen and might be in linear with stretch without hydrogen addition. As a result, the unstretched laminar flame speed can be obtained, by linearly extrapolating laminar burning velocities to the zero strain rate [48-49]. This method has become very popular within the combustion community in recent decades [50-55]. This technique has a number of advantages are:-[47]

- One-dimensional laminar flames are established.
- A flow is stabilised, so it can have negligible heat loss.

However, the main disadvantage of this method is that due to increasing the nozzle separation space, the flame becomes unstable, resulting in reduced accuracy for the laminar burning velocity of lean conditions [48].

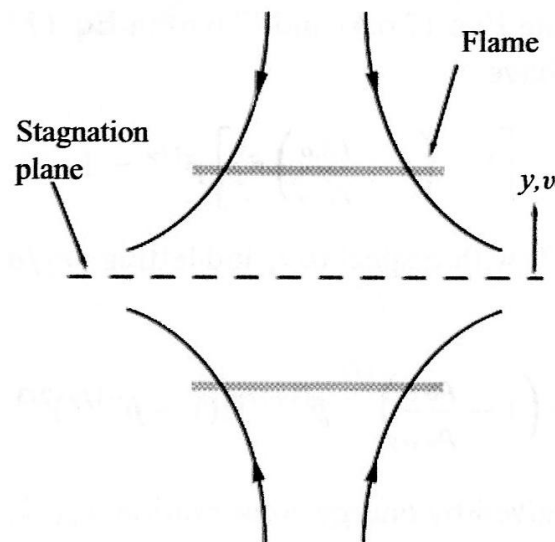


Figure 2.3 Schematic showing a counterflow configuration [14]

["This material is reproduced with permission of Cambridge University press."]

2.1.5 Flame propagating in tubes

The main advantages of this method relate to the very simple apparatus and ease of assembly. Nearly 130 years ago Mallard and Le Chatelier [4] studied the propagation of flames in the horizontal tubes, with ignition at the open end and propagation towards the closed end. They also studied the effect of the tube diameter, length and composition, on the flame speed. Wheeler [56] demonstrated that the speed of “uniform movement” of this flame in mixtures of methane and air was the normal speed of the propagation of the flame. He confirmed that the influence of diameter is very important to avoid wall quenching. His results confirmed that the speed of the flame in a tube with a 9 cm internal diameter was slightly higher than the speed in a tube with a 5 cm internal diameter. Moreover, he noted the period of the uniform travel increased with tube diameter and length. Using a tube 600 cm long and with a 5 cm internal diameter, he showed that the uniform travel for methane-air mixture extended over a distance of 150 cm, compared with Mallard and Le Chatelier’s [4] results who used the same

diameter of tube but only 100 cm long, demonstration's the uniform movement of the flame speed over the first half of the tube, i.e. the first 50 cm.

Coward and Hartwell [5] suggested a method for determining burning velocities by photographing the flame and computing its surface area and the movement of the flame through a horizontal cylindrical tube. As the pressure remained constant they suggested the following formula:-

$$U_l A_f = U_f A_t \quad (2.3)$$

Coward and Payman [8] then related the laminar burning velocity U_l to the linear observed flame speed U_f by equation (1.1).

Consequently, the surface area of the flame and the unburned gas velocity should also be determined with the flame speed of the flame down the tube. The surface area of the flame is obtained by photographing the flame and then fitting it to an appropriate function. The major difficulty with this method is that in horizontal tubes the flame is often non-symmetrical and takes on a "tilted shape".

The most extensive set of measurements are those made by Gerstein et al. [57] who determined the gas velocity and then the laminar burning velocity of a number of hydrocarbon fuels. They produced uniform movement by fitting small holes at each end of the tube to allow the pressure to stabilise. Photocells were used to detect the flame as it passed. Cooling by the walls was considered to be important, especially, for slower flames. Markstein [58] concluded that the use of larger diameter tubes would help to get rid of the serious effects created by the flame-wall interaction, but then the flame-front shape tends to become uneven, making it hard to measure. Over 90 years ago, Mason and Wheeler [59] examined the influence of convection currents on the flame speed of methane-air mixtures, for a flame tube placed in a vertical position, with a tube of 5 cm internal diameter and 5 m in length. They conclude that when ignited at the open end and closed at the other end, the flame speed travelled downward roughly the same as at the horizontal position, and noted that the convection effect on the horizontal tube position is lower than the vertical position. However, when ignited at the open end and with the tube open at both ends, they showed that the flame did not exceed downward, while when ignited at the bottom and directed upwards, the flame was very fast and then faster than the horizontal propagation. Maxworthy [60] also studied gravitational effects on the flame speed and flame shape, propagating through a long tube, in his study. Jarosinski et al. [61] and Strehlow et al. [62] observed the

effect of gravity on methane and propane-air mixtures, respectively. Hamins et al. [63] in 1987, performed an experiment using the tube method in vertical position for methane-air mixtures, which was ignited in the middle of the tube, to allow the flame to travel upwards and downwards. They also observed that the upward propagation for leaner and richer condition of the flames was faster than the downward propagation.

2.1.5.1 Unburned gas velocity

The unburned gas velocity U_g is the volumetric flow rate of the fuel-air mixture in advance of the flame [6]. Stevens [64] created an experiment to measure the unburned gas velocity from the growth of a soap bubble and the expansion was recorded by a camera. The volumetric rate was then measured and, as a result, the unburned gas velocity was recorded.

Gerstien et al.[6] used a soap bubble test to determine the unburned gas velocity, by fixing a small tube at the open end of the flame tube, which is facing downwards and found the gas velocity to be relatively small (10 % of the propagation rate). The unburned gas velocity has normally been acknowledged to be a possible influence on the propagation speed of flames down the tubes, but there have been few measurements of this. The speed will be strongly affected by the experimental configuration, as a flame propagating in a tube with both ends open is less than the tube closed at the end. The difficulty of measuring surface area and unburned gas velocity resulted in the abandonment of this technique for measuring burning velocity. Rallies and Garforth [65] mentioned this problem in their reviews and stated that “ it is doubtful whether the wall interaction effects can ever be adequately corrected for. On the whole, therefore, the technique appears to be inherently unsatisfactory”. Gerstien et al. [6] confirmed that the unburned gas velocity was roughly in linear proportion to the speed of the flame and consequently they stated the following equation :

$$U_g = 0.236 U_f - 10.47 \quad (2.4)$$

This equation illustrates that the unburned gas velocity would only have to be measured a few times.

Bradley and Hundy [66] have been measuring the unburned gas velocity using a hot-wire anemometer for methane-air mixture using a spherical bomb with a range of equivalence ratios. They confirmed that this method was appropriate for high temperatures and the laminar burning velocity increased roughly by 0.02 m/s, with increases to the initial temperature, by 10 K in the area of room temperature.

Andrews and Bradley [67] offered several methods to measure the unburned gas velocity directly. These methods are “particle tracking, micropitot tube probes and hot wire anemometry”. They confirmed that the gas velocity ahead of the flame front measured by particle tracking, leads to low laminar burning velocity values, compared with those which used Schlieren photograph measurements. However, this technique with smaller particles and increased temperatures, caused an error in the measurements of laminar burning velocity [67]. On the other hand, micropitot probes and hot wire anemometry are more accurate for measuring unburned gas velocity, owing to lower values and no dependence on flow rate, compared with the particle tracking method.

2.1.5.2 Reasons for the abandonment of tube method

Following the paper by Gerstien et al. [6] there were few further published studies of laminar burning velocities in tubes. Andrews and Bradley [67] pointed out that there was considerable uncertainty in the measurement of the flame area which is compounded by the non-symmetrical nature of the flame shape. This is thought to be due to buoyancy of the burned gases pushing the top of the flame forwards. Errors of up to 20 % in the measurement of the surface area have been quoted [68]. There is also concern about heat losses at the wall, Andrews and Bradley estimated the measured burning velocity might be 16 % lower than the actual value due to this. Rallis and Garforth reviewed burning velocity measurements in 1980 and conclude that wall effect could not be satisfactorily accounted for [65].

2.1.5.3 Reasons for the selection of cylindrical flames in tubes

The apparatus of the tube method compared with spherical vessel, is clearly far more portable. This therefore, allows the apparatus to be taken wherever it is required, as opposed to interested parties having to travel to the spherical bomb, due to its restrictive size. Because of the system's simplicity, it is also cheap to build and very easy to change. Also the flames shape, which is propagating through the tube, is fixed by the diameter of the tube. Therefore, the use of flames in thin tubes could hence to improve the precision of measurements of the laminar burning velocities. Moreover, the flames propagation in the tube with fitted orifice plates at both ends [6] is apparently uniform, so the burning velocity should not be affected by flow divergence or stretch, the only possibly errors are due to heat loss by the walls.

In many situations, an absolute and very accurate measurement of the burning velocity may not be necessary. In industrial situations, it may preferable that large number of comparative measurements be made. This may be a situation if fuel mixtures are to be tested. The relative

small size and simplicity of a tube rig seems to offer this potential. The small size of the rig may lend its self to be being easily heated so measurements at elevated temperatures may be made. However, the technique needs to be reviewed, using modern experimental techniques to both follow the flame progress and measure the gas velocity ahead of the flame.

2.2 Comparison of values of burning velocity

A comparison of the peak burning velocity measured by Gerstein et al. [6] and Davis and Law [69], are shown in figure 2.4 , for C1 to C7 normal alkanes. Davis and Law used a counterflow technique to determine the laminar burning velocities for a variety of hydrocarbon fuels C1 to C8, with a range of equivalence ratios and at ambient conditions of temperature and pressure. The same trends can be seen for both sets of measurements. Methane, having a relatively low burning velocity, a rapid jump in the burning velocity for ethane and a slow decrease in the burning velocity as the carbon chain is increased [69].

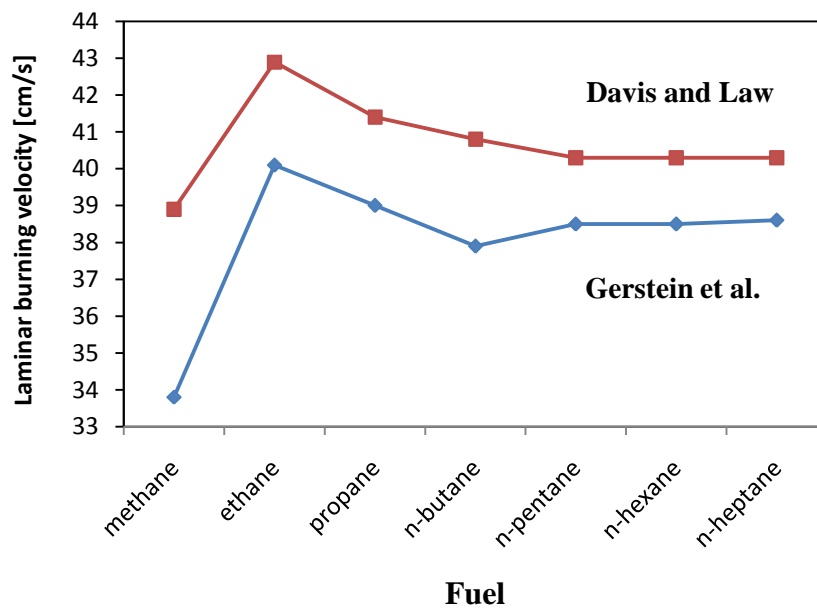


Figure 2.4 A comparison of reported laminar burning velocities at room temperature and atmospheric pressure

In addition, the tube method appears to produce low values of the laminar burning velocities, due to cooling by the walls, which reduces the observed flame speed below the true value [18]. The spherical bomb method is free from the errors peculiar to burners (e.g. quenching at burner rim and divergence of flow lines). Also the value of laminar burning velocity is a little low about 41.3 cm/s at equivalence ratio of 1.1 [70]. The probable reason caused either by

curvature of the flame front, or by the small heat loss near the centre, due to spark gap [44]. However, the flat flame technique cannot be affected by curvature of the flame surface; a short extrapolation back to zero heat extraction is necessary, but the inaccuracy thereby introduced should be minimal [44].

2.3 Factors affecting the laminar burning velocity

2.3.1 Equivalence ratio

The equivalence ratio ϕ is a function used to indicate the fuel -air composition of mixtures. It is the ratio of the quantity of fuel to oxidiser present, versus the quantity of fuel that would be present, under stoichiometric conditions.

$$\phi = \frac{(n_f/n_o)}{(n_f/n_o)_{\phi=1}} \quad (2.5)$$

Figure 2.5 illustrates the relationship between the equivalence ratio and the laminar burning velocity of propane fuel. At $\phi < 1$, the mixture is named ‘fuel lean’ and more air is present than is required for complete combustion. At equivalence ratio > 1 , the mixture is named ‘fuel rich’ and owing to the lack of oxygen in the fuel-air mixtures, incomplete combustion of the mixture takes place. As a result, the peak burning velocity occurs near ($\phi = 1$) as shown in the Figure 2.5.

At lean conditions, there is a greater quantity of nonreactive molecules, such as nitrogen present. Heating these nonreactive particles lowers the temperature of the flame, which therefore requires more energy and takes longer to reach ignition temperatures, hence slowing the rate of propagation of the flame [71]. At rich conditions, owing to incomplete combustion, a greater amount of radicals are produced in the flame front. The flow of these radicals increases the reactivity of the reactants and thus increases the burning velocity, such that it occurs at slightly rich ϕ .

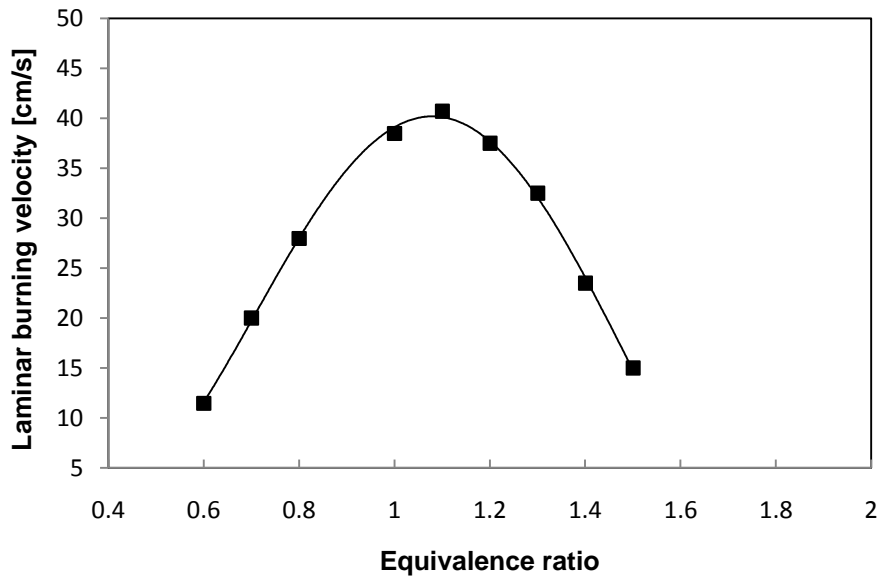


Figure 2.5 Effect of equivalence ratio on the laminar burning velocity of propane-air mixture at 300 K and 1 bar [72]

2.3.2 Temperature

Figure 2.6 shows the laminar burning velocities of different fuels when increasing unburned mixture temperatures. Increasing the temperature of the fuel moves the reactant temperature closer to the ignition point and therefore requires less energy input from the exothermic reaction. The same quantity of energy is released from the combustion reaction, hence raising the temperature of the flame [71].

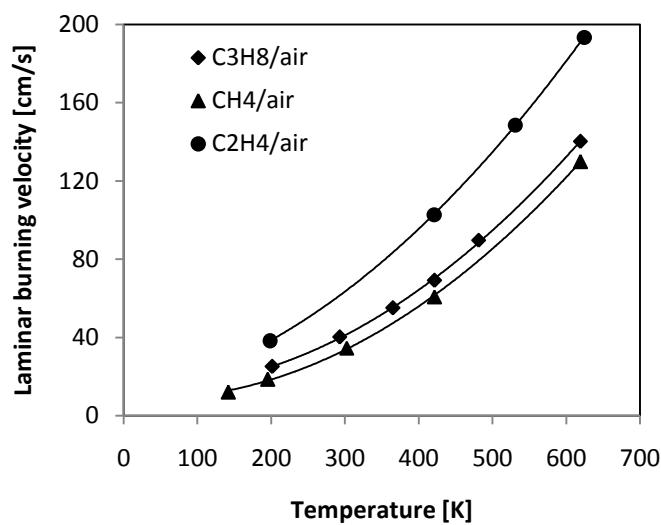


Figure 2.6 Relationship between unburned mixture temperatures and the laminar burning velocity for various fuels [13]

In the literature, a few studies determined the laminar burning velocities at elevated temperatures and pressures, and most of the present data is close to ambient conditions.

Metghalchi and Keck [22] measured the laminar burning velocity of propane-air mixtures up to 500 K, using a spherical bomb. At the same temperature range, Toshio [73] studied the influences of temperatures on the burning velocity of methane-air mixtures, by using the same technique (spherical bomb). He confirmed that the laminar burning velocity increased with the initial temperature of the mixtures. Farrell et al. [74] also used the same technique to determine the laminar burning velocities, and studied the effects of molecular structure for more than 40 hydrocarbon fuels at 450 K, and at a range of equivalence ratio from 0.6 to 1.4. Recently Domnina et al. [75] used experimental and computational techniques to determine the laminar burning velocity of propane-air mixtures, by spherical bomb and INSFLA package up to 423 K. The measured values were correlated using the power law relation, and they found this technique to be uncomplicated and reliable, even if their results were obtained of burning velocities over a limited range of initial temperatures and pressures.

2.3.3 Pressure

Figure 2.7 shows the influence of pressure on the laminar burning velocity, as can be seen, the laminar burning velocities decreases with increased pressure. This pressure rise causes the obvious reduction in the degree of “dissociation” of the hot mixtures, and then increases the rate of the reactants. The reduction in the concentration of radicals in the preheat zone makes the combustion of the fuel more difficult and slows the laminar burning velocity [76].

Hassan et al. [77] measured unstretched laminar burning velocities of methane-air mixtures in a spherical bomb, with a range of pressures from 0.5 to 4 atm, and at room temperature. They showed that an increased in pressures leads to an increase of Markstein numbers and decreases laminar burning velocities. Gu et al. [78] also determined laminar burning velocities of methane-air mixtures, with a range of pressures up to 10 atm. They noted the laminar burning velocity of CH₄-air mixtures at zero stretch increased with decreased pressures. However, they noted that, with a high pressure, the mixture flames were more unstable, particularly under the leaner conditions.

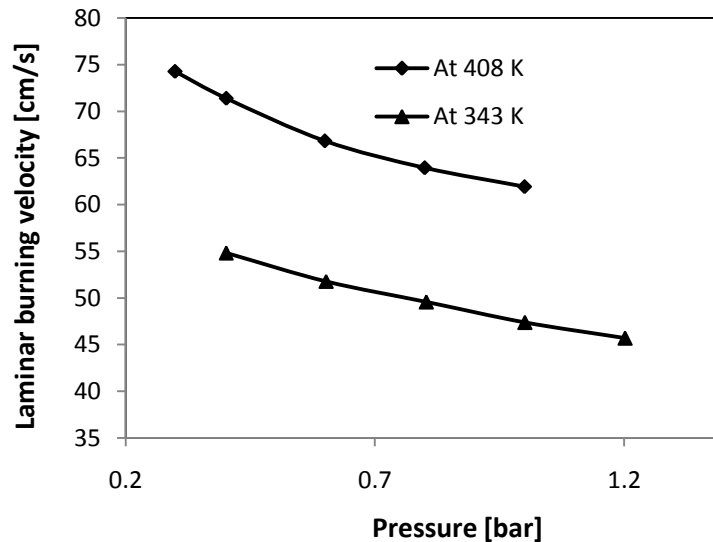


Figure 2.7 Effect of the laminar burning velocities on the pressure of propane-air mixture at $\phi = 0.89$, at a temperature of 343 and 408 K [75]

Kitagawa [79] studied the influence of pressure on the burning velocity of propane-air mixture by a spherical bomb with a range of pressure from 0.1 to 0.5 MPa. He observed that at higher pressures the cellular flame structure caused the flame to increase in speed.

Recently Tang et al. [80] used a spherical bomb at constant volume to measure laminar burning velocity of nitrogen diluted propane-air mixtures, with a range of pressures up to 7.5 atm and at high temperatures. They found the effect of nitrogen dilution was clearer at high pressure and that the mixture flame's instability increased with pressure. Their results were in good agreement with the previous work. Bradley et al. [81] obtained laminar burning velocities of ethanol-air mixtures up to 14 atm pressure and up to 393 K temperature, with a range of equivalence ratios. They also found that the influence of flame instability increased with pressure. Burbano et al. [82] measured the laminar burning velocities of syngas mixtures by using a burner at sub-atmospheric pressure. They observed that the laminar burning velocities decreased with increased pressure, in both lean and rich conditions. However, with decreased pressure, the flame thickness increased, which was causing the stability of the flames.

On the other hand, Tse et al. [83] investigated the laminar burning velocity at a maximum pressure of 60 atm. This was the only work that found the laminar burning velocity at operating pressure, similar to the internal combustion engine. Their results showed the determination of unstretched laminar burning velocity up to 20 atm, while cellular flames were observed for pressure higher than 20 atm.

2.4 Flammability limits

The study of flammability limits for fuel-air mixture is very significant, not only as a design parameter for safety against explosions and fire hazards, but also it is important to know for the design of combustion equipment. The flammability limits are a commonly used index for representing flammability of gas and vapors. One of the first “standard” methods for measuring flammability limits was published by the U.S Bureau of Mines, in Pittsburgh, in 1952 [76]. In this method, a vertical tube, closed at the upper end and open at the bottom next to the ignition point, is used. The reason for choosing this method is that the flames moving upwards have larger limits of flammability than for downward propagation. A number of researchers have used the tube method for measuring flammability limits [84-85]. Recently Schoor and Verplaetsen [86] determined the upper flammability limits of methane-hydrogen-air mixtures, using both spherical vessel bomb and tube techniques (following the European standard describe). They showed that the visual flammability standard used in the tube technique became higher than the pressure rise criterion in a spherical vessel technique, with an increased the initial temperature. They also found that the upper flammability limits of hydrogen fuel portions of 20 to 40 mol % increased with an increase in the tube diameter of up to 80 mm at room temperature and at atmospheric pressure. Moreover, large vessels [87] and rapid compression machines [88] have also been used to measure the flammability limits of different fuels. Shebeko et al. [89] measured the laminar burning velocities and flammability limits of gases (methane and hydrogen)-air mixtures at high temperatures and pressures. They showed that the flammability limits of mixtures increases with increased temperature and was decreased by increasing pressures. Cashdollar et al. [90] studied the flammability limits of propane-air mixtures by closed explosion chambers of various volumes, between 20 and 120 L. Their results showed the difficulties connected with turbulence, buoyancy and the ignitor force against chamber volume. Additionally, they confirmed the upper flammability limits of propane used in the tube method was slightly less than the 120 L in the closed chamber method, while the lower flammability limits was nearly the same.

2.5 Flame stretch in laminar flames

The concept of flame stretch is the fractional rate of increase of flame area with time, with unit of s^{-1} [76].

$$K = \frac{1}{A} \frac{dA}{dt} \quad (2.6)$$

Where, K is the Karlovitz stretch rate and A is the fractional rate of change of area. Flame stretch is considered to be a combined effect of flame curvature, flame motion and flow non-uniformity [53, 91].

The flame stretch rates in a spherical bomb can be determine by [92]:

$$K = \frac{2dr_f}{r_f dt} \quad (2.7)$$

And in a steady conical flame (Bunsen burner) by [92]:

$$K = \frac{-u_\infty \sin\theta}{2r_f} \quad (2.8)$$

Here, r_f is the flame radius at a given axial point in each case, u_∞ is the uniform upstream speed and θ is the angle at the top of a Bunsen burner flame.

Karlovitz et al. [93] noted that under the effect of a strong velocity gradient, which occurs in the boundary layer, the shearing forces stretches the flame, so that its surface area is always increasing. A flame is stable and will propagate provided that heat release (and free-radical production) within the flame volume exceeds losses. Because of the flame stretch, the heat balance is adversely affected, so that the reaction rate and burning velocity are decreased and the flame may even be extinguished, for mixtures with Lewis number $Le > 1$. For mixtures with $Le < 1$, the flame speed tends to increase with strain rate, due to local flame acceleration. Also, for mixture with $Le = 1$, the mass and heat transfer are in balance and the net effect on the flame speed is close to zero.

However, there are two stretch sources. First is the effect of flow non-uniformity along the flame surface. The second is the stretch, experienced through the flame movement and flame curvature. it is evident that flame curvature contributes to stretch, if it is in motion ($V \neq 0$) and flame propagation contributes to the stretch if the flame is curved [92]. Therefore, stationary spherical flames and propagating planar flames are unstretched. Also, the flow field strain can contribute to stretch, even if the flame is stationary and not curved.

Dowdy et al. [37] developed a new technique for measuring laminar burning velocity and the stretch effect of hydrogen-air mixtures. They used expanding spherical flames and compared their results with the modelling results. In their examinations, an expression for the time variation of the radius of an expanding spherical flame at constant pressure is derived as follows, with the flame stretch effect. The flame structure is assumed to be one-dimensional. Consequently, the analysis usually holds for great radii but is not applicable for small radii, where the quasi-1D assumption fails. They found the stretch factor by using equation 2.6.

Tseng et al. [94] investigated the influence of flame stretch on the laminar burning velocities of propane, methane, ethane and ethylene, using spherical flame. The maximum burning velocity of propane was 37 cm/s at equivalence ratio of 1.2. Markstein number was negative at $\phi \geq 1.4$, and the effect of stretch on the burning velocity was substantial, yielding Markstein number in the range of -2.5 to 7.2 .

The same technique used by Halter et al. [95] to study the effect of linear and nonlinear stretch on the flames of methane and iso-octane-air mixtures. The main reason for selecting these fuels was due to the reverse evolution in their Markstein length, with increased equivalence ratio. They observed that the considerable errors were at $\phi > 1.1$ for methane-air mixture, while iso-octane-air mixture at $\phi < 1$.

2.6 Propane

Propane is a three-carbon alkane, with the formula C_3H_8 , and has been commonly used as a fuel for many years. There are many researchers who use propane as a test fuel, to determine the laminar burning velocities by different techniques, for both experimental and computational [6, 22, 41, 72, 96].

In 1949 Andersen and Fein [97] determined the laminar burning velocity and flame temperature of propane-air mixtures, using the particle track method. Hassan et al. [42] performed experimental and computational tests to measure the laminar burning velocity of propane-air mixtures, using a spherical bomb with a range of equivalence ratios and pressures, from 0.5 to 4 atm and at room temperatures. They found that, with increased pressures, the flame is unstable. These results were in good agreement with the values presented by various researchers. Vagelopoulos and Egolopolus [49] also measured the laminar burning velocity of propane-air mixtures at room temperature and atmospheric pressure using the counterflow method. They used the LDV technique to measure the flow

speed directly and found that the values of laminar burning velocity are slightly lower than the results that were attained through “linear extrapolations”.

Recently, Razus et al. [75] measured the laminar burning velocity of a propane-air mixture up to an unburned mixture temperatures of 423 K, using a spherical vessel with central ignition. They compared their measurements with numerical computations by the INSFLA program, developed by Warnatz and Maas, [98-99] using a CH₄-C₄ mechanism based on chemical species. Their experimental results confirmed that the laminar burning velocity increased with increasing temperature and compared well with numerical computations.

Razus et al. [100] also investigated the effect of temperature and pressure on the explosion pressures of a spherical vessel propane-air mixture. They showed that the high explosion pressures occur at a fuel concentration higher than stoichiometry, at equivalence ratio 1.2 – 1.4 at constant temperature and pressure. The maximum explosion pressures were linear at the initial temperature. However, for all fuel mixtures the explosion times were decreased when the initial temperature was increased at the same equivalence ratio 1.2 – 1.4.

Akram et al [101] investigated the laminar burning velocity of a propane –air mixture at high temperatures of 370 – 650 K with various equivalence ratios of 0.7 – 1.3, using a planar flame in a divergent channel. Their results compared favourably with the experimental and numerical results obtained in the literature. They found a peak laminar burning velocity of pure propane-air mixture near to an equivalence ratio of 1.1 for room temperature and high temperature, with the lowest amount of temperature exponent. Figure 2.8 shows the laminar burning velocities of propane-air mixtures, from the literature, at room and high temperatures and at atmospheric pressure.

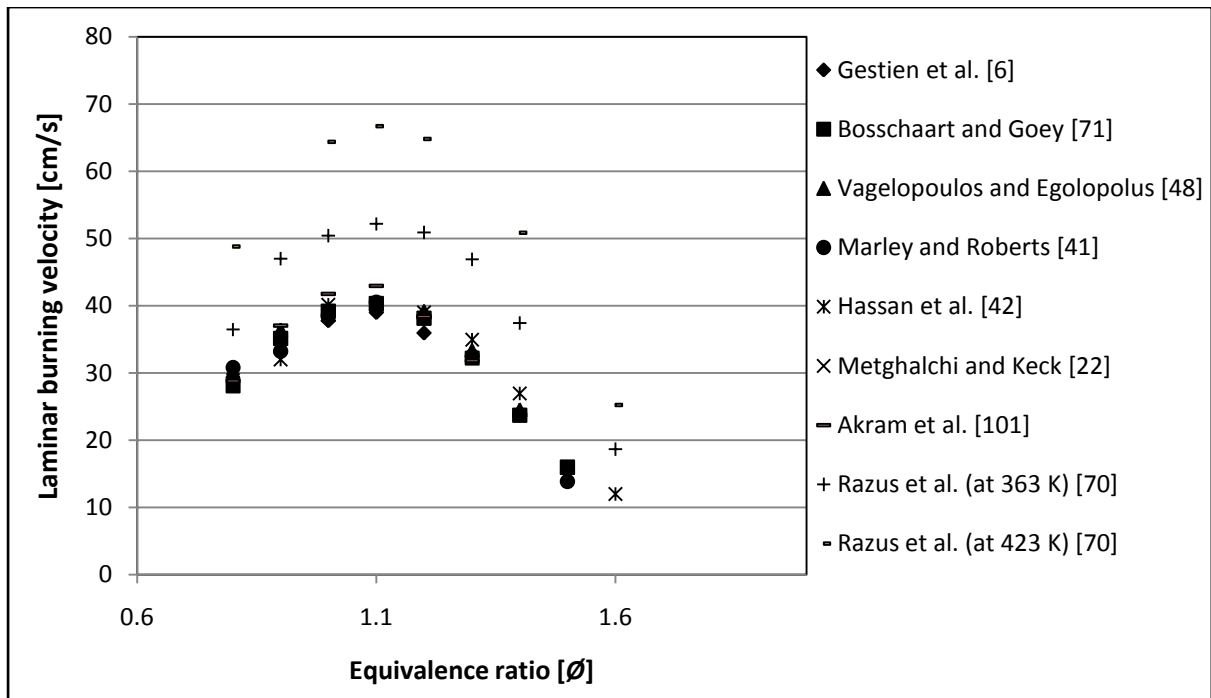


Figure 2.8 Laminar burning velocities of Propane-air mixtures from literature data at ambient and elevated temperatures and atmospheric pressure

2.7 Acetone

Acetone C_3H_6O is a significant reactant in the oxidation of hydrocarbons in flames and also in the atmosphere too. Acetone and acetaldehyde have been tested as a fluorescence tracer molecule and a strong signal of up to 550 nm has been observed [102]. Also, acetone was used to perform a number of experiments in laser induced fluorescence (LIF) measurements [102-104], LIF system have been employed to determined the concentration and the distribution of fuel in combustion processes.

Only a few sources have reported the laminar burning velocity of acetone-air mixtures as shown in the Table 2.1.

Table 2.1 Summary of previously experimental work for the laminar burning velocity of acetone-air mixture, for various methods

Source	ϕ	Temperature (K)	Pressure (atm)	Technique
Gibbs G and Calcote H - 1959	0.7 – 1.2	298	1	Bunsen [105]
Molkov V and Nekrasov V – 1981	0.4 – 8.5	296 – 520	1	Bomb [106]
Pichon S et al. - 2009	0.8 – 1.5	298	1	Bomb [107]
Burluka A et al. – 2010.	0.7 – 1.7	298	1	Bomb [108]
Chong T and Hochgreb S – 2011	0.8 – 1.4	298	1	Counterflow [109]
Nilsson E et al. - 2013	0.7 – 1.4	298 - 358	1	Heat flux [110]

The results of experiments performed to determine the laminar burning velocity of acetone-air mixtures using different methods, at 298 K and at atmospheric pressure, are plotted in Figure 2.9. These results were in contrasting values. Gibbs and Calcote [105] found a peak laminar burning velocity at $\phi = 0.93$ (44.4 cm/s) using a shadowgraph imaging of the Bunsen burner technique, with negligible flame stretch. Their study was performed in the laboratory, which increased the moisture content by 0.3 %, making measuring the chemical kinetic mechanism difficult, and then the effect on the values of flame speed were obtained [105]. Picone et al. [107] measured the laminar burning velocity of acetone-air, using a spherical bomb with Schlieren photography and the peak value was the lowest, about 35 cm/s at an equivalence ratio of 1.15. These results were nearly the same as those obtained by Burluka et al. [108] who used the same spherical bomb technique and with both Schlieren photography and pressure recording. The maximum flame speed was approximately 36 cm/s at $\phi = 1.1$ as shown in the Figure 2.9. Additionally, their results illustrated good agreement at the lean region, while at the rich region Burluka et al. gave higher values for laminar burning velocities. Recently, Chong and Hochgreb [109] and Nilsson et al. [110] using the counterflow and heat flux methods, respectively, gave appreciably higher values of laminar burning velocities at all equivalence ratios, as shown in Figure 2.9. They found a peak of laminar burning velocity at $\phi = 1.2$ (42.5 cm/s) and at 1.1 (38.4 cm/s) respectively. However the results obtained by Nilsson et al. [110] were close to those of Burluka et al. [108], except at the lean side, both used a spherical bomb method. The lower results were obtained by the

spherical bomb technique, due to flame stretch which affected the flame propagation and became non linear [110].

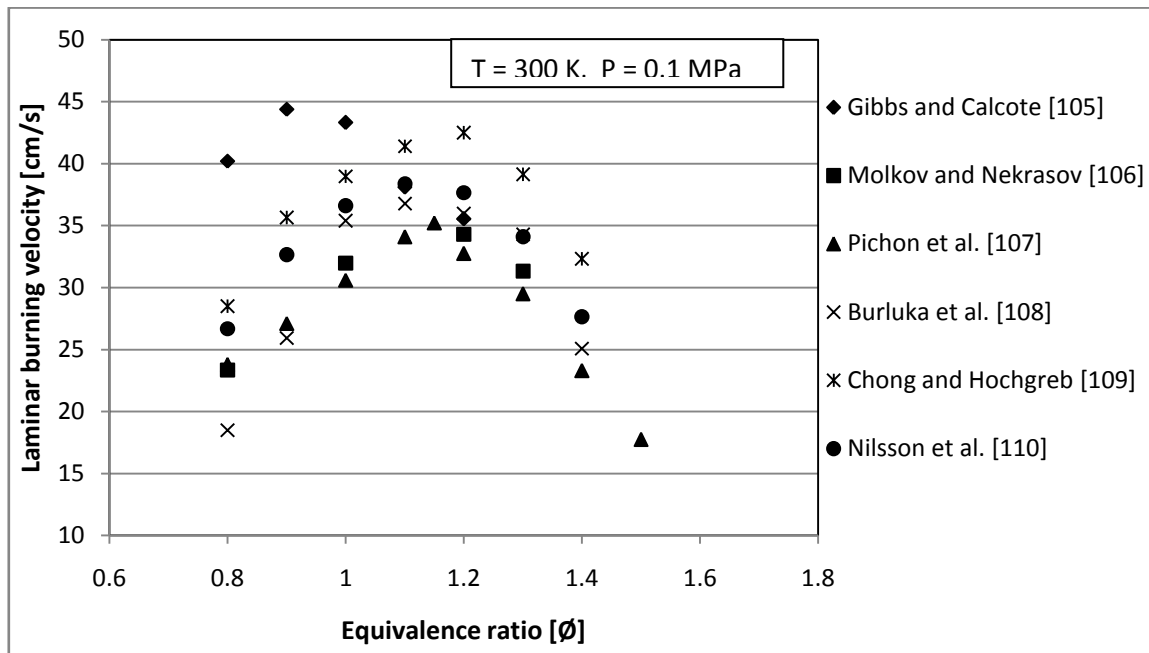


Figure 2.9 A comparison of laminar burning velocity values of acetone-air mixtures, from published data, at room temperature and atmospheric pressure

2.8 Flame surface area

The most important procedure to calculate the surface area of the flame has been developed by Coward and Hartwell [5]. They assumed that the surface area is roughly equivalent to that of a semi-ellipsoid. This shape is formed by an axis which is created from the line connecting the points where the flame contacts the top and the bottom walls of the tube as shown in the Figure 2.10 (b).

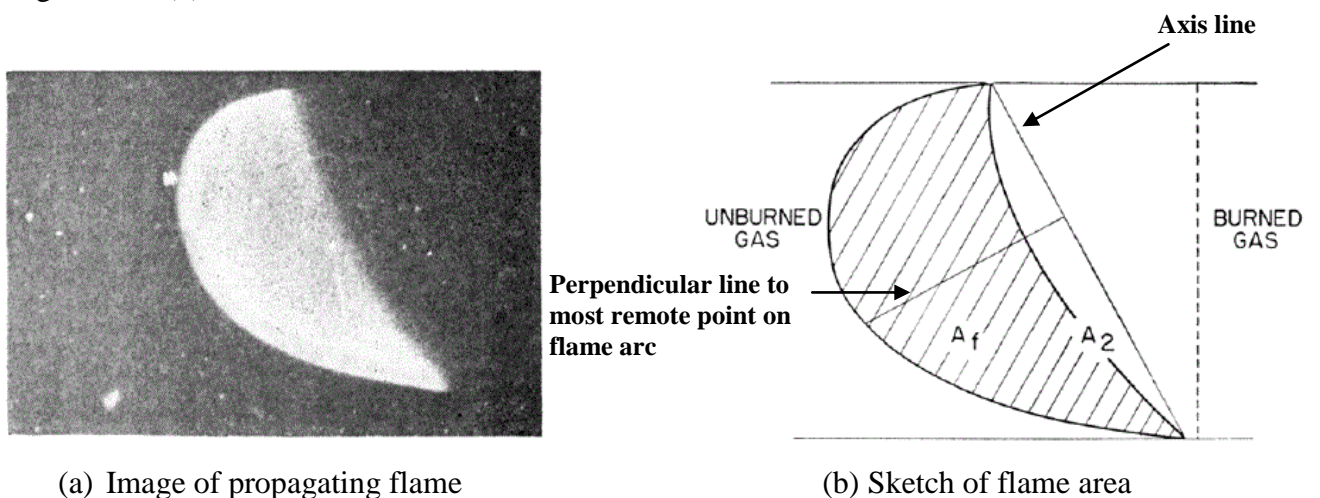


Figure 2.10 Imag and sketch flame areas [6]

They used the perpendicular distance between the axis line and a point on the flame front to determine the diameter of the flame.

Hoare and Linnett [111] enhanced the measuring of the flame area, by capturing two images of the flame, from in front and above as shown in the Figure 2.11 (a) and (b). This technique of using three dimensions, to measure the surface area, is more difficult, as it is not easy to transfer the two-dimensional image data to three-dimensional information.

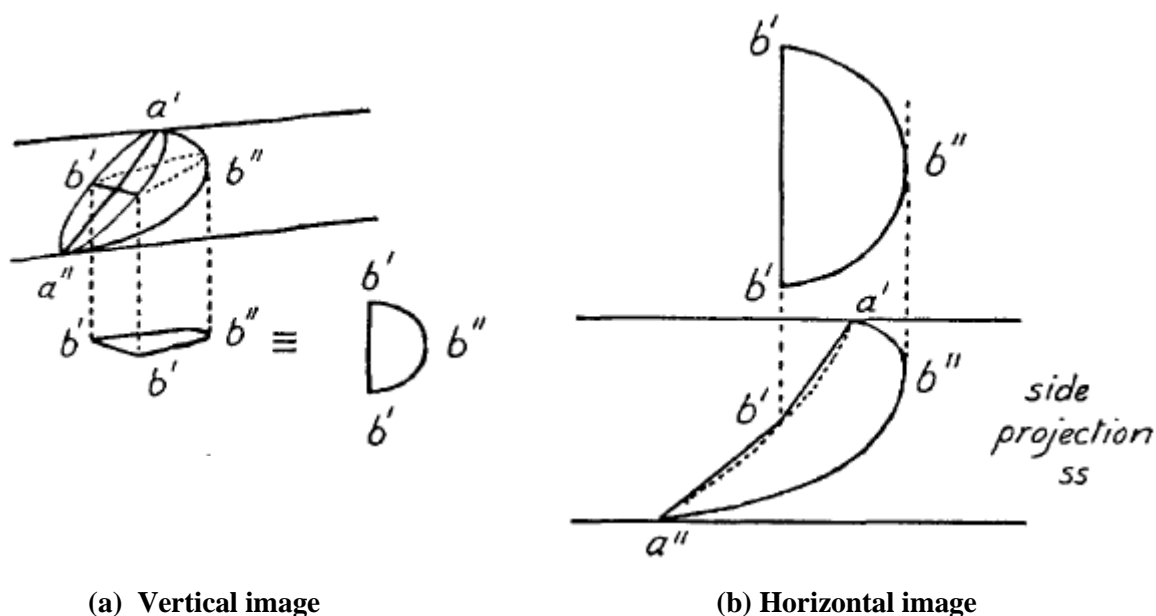


Figure 2.11 Vertical and horizontal images of flame shapes [111]

["This material is reproduced by permission of the Royal Society of Chemistry"]

Here, a' , a'' and b' are the back rim of the flame, while b'' is the extreme forward limit of the flame.

Figure 2.12 shows how Hoare and Linnett applied their theories to measuring the curvature of the flame. This technique of using the overhead image and computing the flame curvature, increased the precision of the measurements of the flame area, compared to the method which was used by Coward and Hartwell [18]. They divided the flame curvature into a number of sectors and each part became as a separate circle as shown in Figure 2.12a and then the radius was determined.

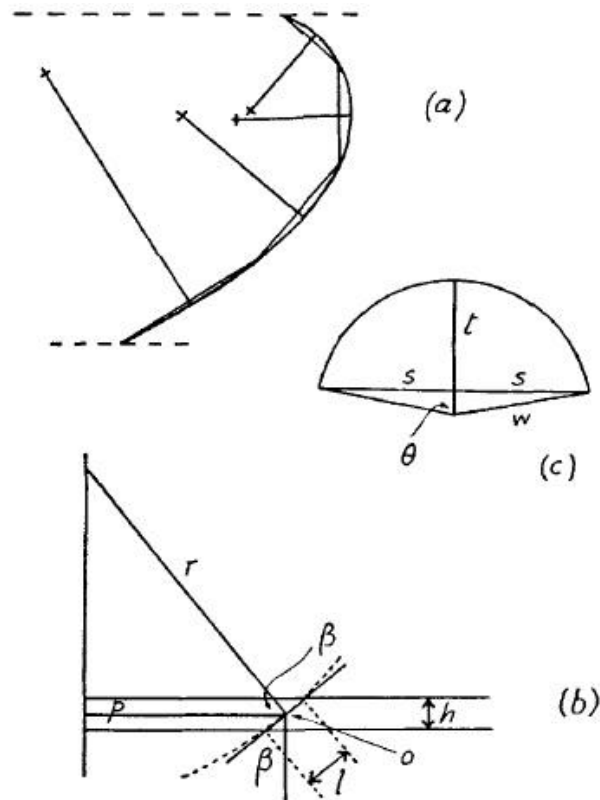


Figure 2.12 Flame curvature method [111]

["This material is reproduced by permission of the Royal Society of Chemistry"]

Here, β is the tangent angle makes with the vertical, p the distance horizontally from O to a point vertically below the centre of the circle and h is the length of the horizontal part of the flame and it is smaller than the distance of l and r .

However, due to a circular flame configuration, a Schlieren photography cannot be used in the tube method (unstationary flame) [18]. Consequently, photographs of the luminous zone were used in the current study.

2.9 Laser Doppler Velocimetry (LDV) application

Laser Doppler Velocimetry was developed by Yeh and Cummins in 1964 [112]. They measured the speed of dyes injected inside a circular tube. They used a beam directly, near to the test area and combined it with the scattered light at the beam splitter.

Foreman et al. [113] used the same technique for gas in a glass tube and the smoke was added to provide scattering particles. The speed obtained directly was not accurate; however, their results confirmed that the flow speed became more linear. Van Maaren and Goey [46] used the Laser Doppler Velocimetry to measure the gas velocity ahead of a methane-air mixture

stabilised as a flat flame above a matrix. They used the He-Ne laser with a beam splitter and obtained the flame speed by one component.

Laser Doppler Velocimetry has many applications, measuring blood and biological flow, which have a very low speed. Moreover in the study of combustion and flames, supersonic flow and environment studies which have a higher speed [114]. However, in internal combustion engines, with high temperatures and pressures, this system is very appropriate in understanding the flow mixing. In additionally, it is a good technique when used in turbulent flames, with high oscillations and correlations between varieties of properties. This system also has the ability to obtain the data from noisy signals which helps to make the complicated measurements easier to perform[114].

3 Experimental Apparatus

3.1 Original apparatus

The apparatus used in this work was loosely based on that of Gerstein et al. [6] who reporting burning velocity measurements in tubes for a number of hydrocarbons. Their rig was shorter than the tube measurements used in Sheffield in the 1920's and 1930's. The apparatus was designed and constructed by Phil Pennington [115] as part of an undergraduate project. The unique feature of the apparatus was that the fuel-air mixtures were made up and mixed in the rig; this was performed in a loop using fans to move the mixture around the tubes. In order to study the propagation of flames down the tube valves were used to isolate parts of the rig such that a straight length tube could be created.

A schematic of the experimental rig used in this study is illustrated in Figure 3.1. It consisted of copper tubes, connected to a 65 cm long quartz tube through which the propagation of flames could be observed. All the tubes had an inner diameter of 20 mm. Ignition was performed by a gas lighter which was directed through a hole on the rig.

Fuel gas was injected into the rig using a syringe via a septum, which sealed the contents of the pipe from atmospheric air. The fuel was then mixed with air in the rig using two 12V powered fans run for 3-4 minutes in order to create a homogeneous mixture. The fans were then switched off, and the mixture allowed settling for approximately one minute. The flame tube was then opened to the atmosphere at both ends by switching the three way valves to the reverse position. The gas was then ignited and a camera was set to capture the flame as it propagated through the quartz tube.

During mixing, the three-way valve was set to a position so the gas mixture looping through the rig is closed to atmospheric air.

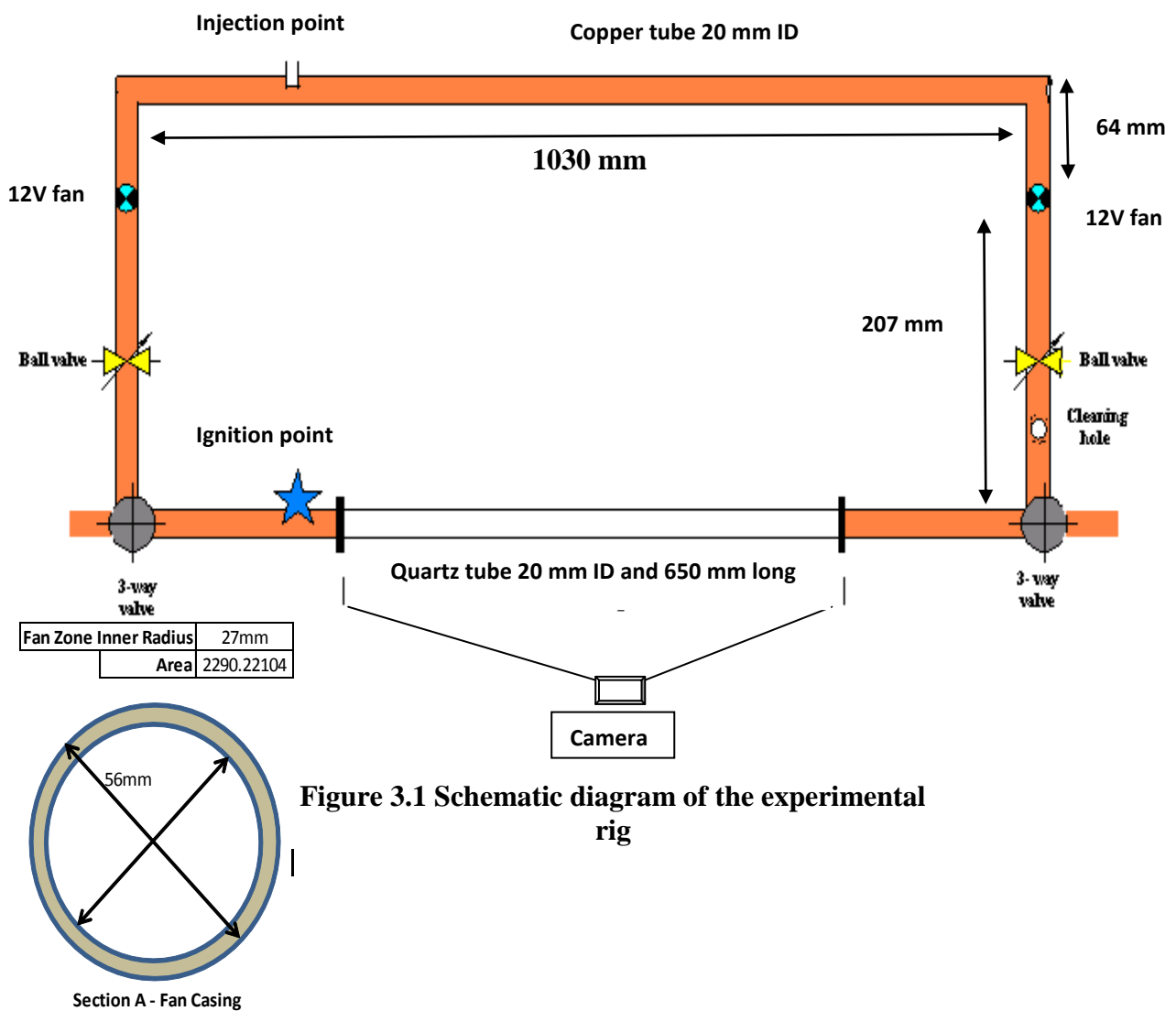


Figure 3.1 Schematic diagram of the experimental rig

3.2 Tubing

For successful measurements the flame propagation speed needs to be steady, the diameters and length of the tube have been shown to have an impact on the flame speed. Coward and Hartwell [116] conducted a series of experiments which analysed the effect of changing the tube diameter and found that as the diameter increases the flame velocity also increases, though at a decreasing rate. This can be seen in Figure 3.2.

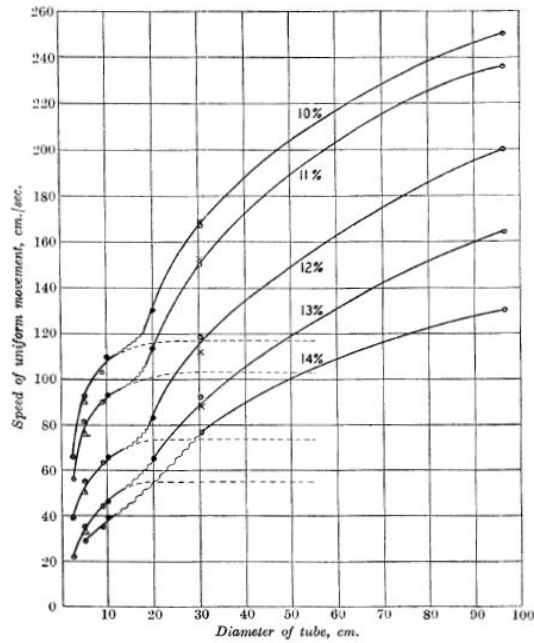


Figure 3.2 Effect on flame velocity by increasing the tube diameter [116]

Guénoche [7] presented results comparing the distance at which the flame speed reached its maximum value for different tube lengths, as seen in Figure 3.3. He published results for CO-air mixtures in tube closed at both ends with a diameter of 5 cm, showing that the surface area of the flame increased with tube length. The laminar burning velocity could only be found for a small length of the tube as the pressure increased as the flame approached the end of the tube. A constant velocity for CO-air flames was achieved in a tube of 225 cm. Although these results are for CO-air mixtures, but Borman and Ragland [71] stated that the flames of carbon monoxide are of a similar laminar burning velocity as propane. Therefore, it is likely that these two fuel types will reach a maximum velocity at a similar length down the tube. The quartz tubing in the original equipment is 65 cm long; the overall tube length is roughly 1 meter.

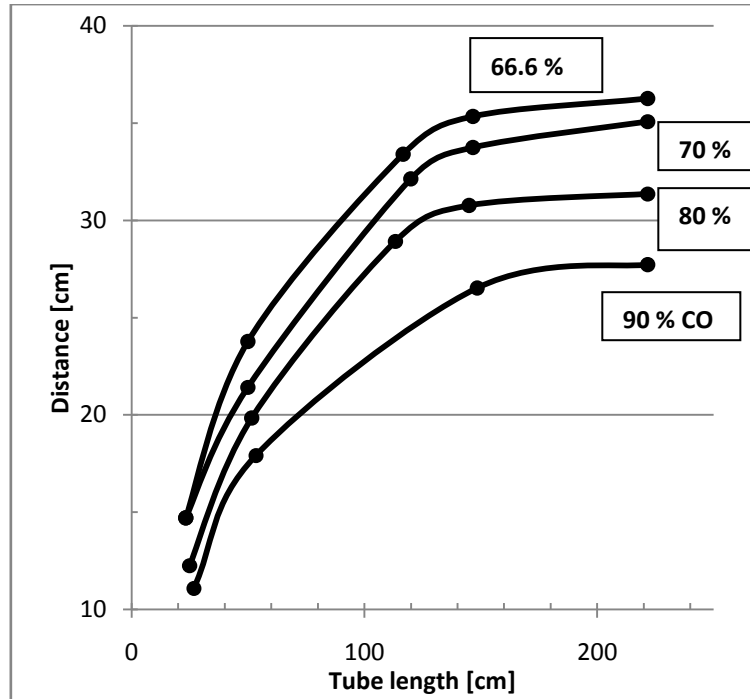
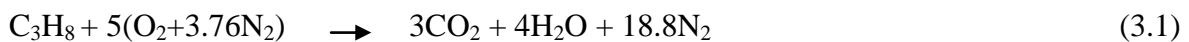


Figure 3.3 Distance to maximum velocity as overall tube length increase, tube with 5 cm diameter and closed at both ends [7]

Gerstien et al. [6, 57] used a tube with an I.D of 2.8 cm and a length of 58 cm and reported constant flame propagation. They used orifice plates in both ends to minimize oscillation in the tube. According to Akkerman [117], flame dynamic is almost entirely independent of tube length and Prandtl number but depends on the tube width which directly controls the Reynolds number.

3.3 Calculation of the required fuel volume

For these calculations it was assumed that the composition of air is 21 % Oxygen and 79 % Nitrogen therefore, for the complete combustion of propane at the stoichiometric condition:



The volume fuel-air ratio of stoichiometric reaction at ambient condition is therefore,

$$\text{Fuel}/\text{Air} = \frac{n_f}{n_o} = \frac{1}{5(1+3.76)} = \frac{1}{23.8} = 0.042 \quad (4.2 \text{ vol. \%}) \quad (3.2)$$

The flammability limits of propane in air are given in Table 3.1.

Table 3.1 Flammability limits of propane in the atmospheric air [71]

	Stoichiometric	Lean	Rich
Fuel-Air ratio (volume based)	0.042	0.021	0.105
Equivalence Ratio	1	0.5	2.5

To calculate the volume of propane required for stoichiometric combustion, the volume of the rig must be known. Numerical calculations were likely to be inaccurate due to difficulties in determining the inner dimensions of the two fan housings, pipe bends, three-way valves and the connections between components. The volume of the rig using numerical, calculations gave 1202 ml with possible tolerance of ± 32 ml due to assumptions in the measurements as shown in Appendix A.

To get a more accurate measurement, a water test was performed. This involved filling the apparatus with water. The rig is shown in Figure 3.1 placed in a vertical position, and the water poured into the rig through the top valve. Holes were placed in fan housings allow the discharge of air as well as to empty the water after the test was completed. The volume of water was measured by dividing the total weight of water by the density of water (1000 Kg/m^3). Results obtained are shown in Table 3.2.

Table 3.2 System volume measurements

Test-1 (ml)	Test-2 (ml)	Test-3 (ml)	Average
1203.6	1206.2	1201.1	1203.63

3.4 Igniter

Initially, a spark-plug was used to ignite the flame at the start of the experiment located at one end of the quartz tube. For later experiments, the spark igniter was replaced by a gas lighter to reduce flame oscillations. The method of ignition is shown in Figure 3.4; it was achieved by inserting the gas lighter into a port in the tube. Figure 3.5 compares the propagation of $\phi = 0.9$ propane-air flames with spark ignition and gas lighter ignition for a tube open at both ends and with 5 mm orifice plates fitted at both ends. It can be seen that the spark

ignited flame was faster than the gas lighter ignition in both cases. However, the orifice plates decreased the flame speed respective of the method of ignition. Shock waves from the spark ignition are thought to be the cause for this behaviour. The sensitivity of the flame propagation in tubes to the ignition type has also been observed by Wu et al. [10] who showed that, spark flames propagated much faster than those ignited using a hot wire.



Figure 3.4 Gas lighter ignition

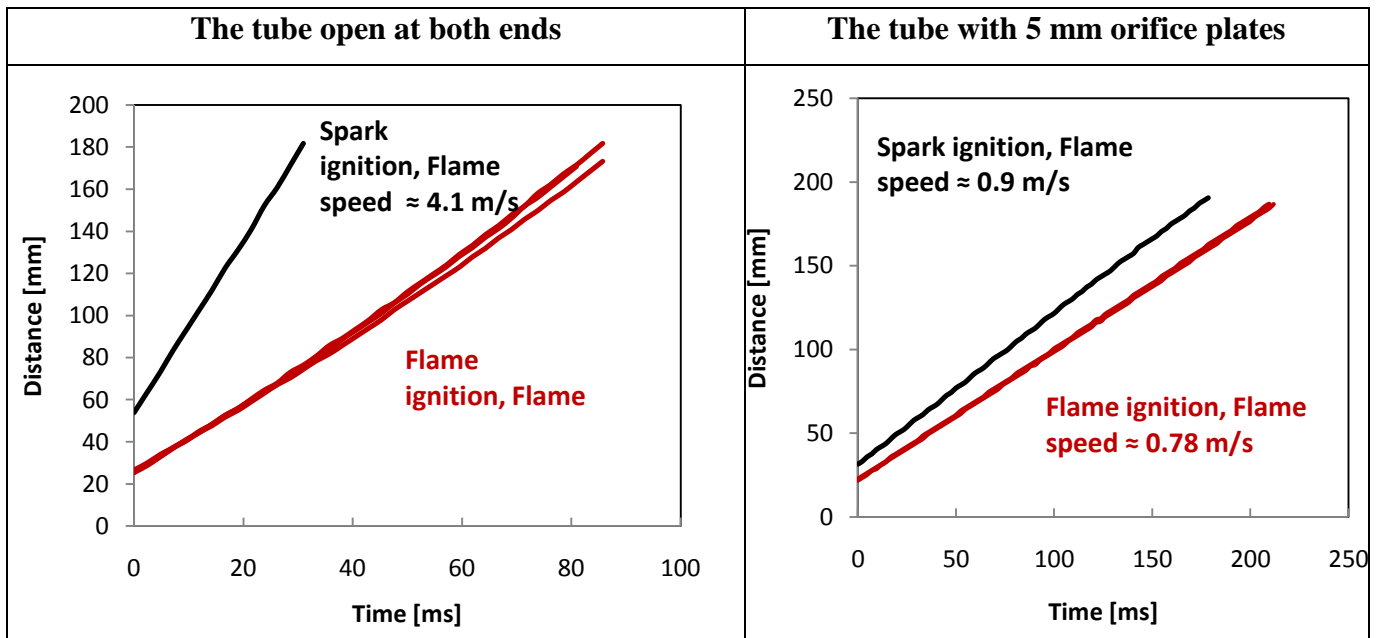


Figure 3.5 Effect of ignition source on the flame speed in the tube for a $\phi = 0.9$

3.5 Removal of remaining fuels and combustion products

It is necessary to clear the rig before the injection of fuel for a new experiment; this is to make sure the system is completely free of fuel and burning products from the previous experiment. In doing this, the plug of the cleaning hole was removed as shown in Figure 3.1 and compressed air was introduced into the system. The three-way valves were opened for 1 to 2 minutes to allow the compressed air to clean the system of burned and unburned fuels.

3.6 Orifice plates

Gerstein et al. [6] used an orifice plate at both ends of the tube to filter pressure waves and to increase the uniformity of the flame shape. Four sets of plates of sizes 8 mm, 5 mm, 3mm and 1 mm orifice diameter were manufactured from 1 mm thick brass as shown in Figure 3.6. Gerstien et al. [6] used an orifice plate of 8 mm diameter at the ignition end and 1.7 mm diameter at the other end in their tube. This would permit the hot expanded gases behind the flame to exhaust through the larger orifice compared to the cooler denser unburned gases a head of the flame [118].

Hoare and Linnett [111] suggested that the flame speeds was reduced with orifice plates as they resulted in an increase in pressure in the tube and hence a reduction of the burning velocity. Coward and Hartwell [5] and Wheeler [56] also used orifice plates for methane-air mixtures and showed that the flame had uniform movement and low relative speeds.

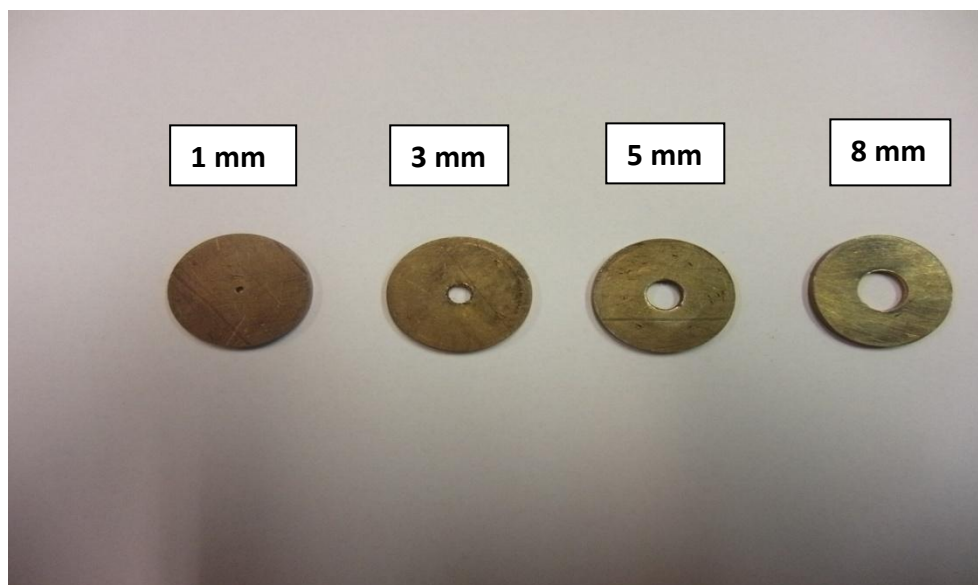


Figure 3.6 Four sets of orifice plates

3.7 Recording the flame

Many methods have been used to find the location of the flame front. Rallis and Garforth [65] summarized these methods as:

- 1- “Direct photography of the luminous flame”
- 2- “Shadow photography using a point source of light”
- 3- “Schlieren photography using either a coarse grating illuminated from behind or an optical system using lenses or mirrors”
- 4- “Interferometry”
- 5- “Particle track measurements-photographic or laser Doppler”
- 6- “Ionization gaps”
- 7- “Temperature measurement”

In this work, direct photography was used. High speed digital photograph was used to capture the flames at 420 fps (frames per second) using a Casio EX-FH100. The image resolution was 224×168 pixels. This allowed for clear, colour images of the flame to be captured. The experimental procedure and the speed of the flame were calculated as detailed in Appendix B.

On the other hand high speed camera (Phantom V210-black and white) operating at 3000 fps framing rate with an image resolution of 1280×200 was used to capture the flame image with high oscillations with both ends opened as this gave clear and sensitive images.

3.8 Flame speed processing

Figure 3.7 shows images at different steps of the processing for $\phi = 1$ with 5 mm orifice plates.

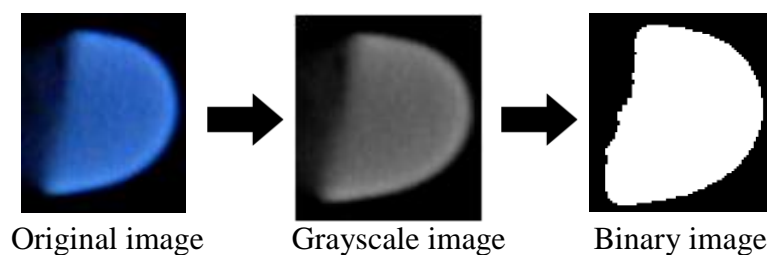


Figure 3.7 Images at different step of the process

These processes require a technique called ‘Thresholding’ in Corel Paint Shop software. Initially, the colour original image was converted into grayscale and the threshold applied. As a result, a binary image (black and white) was obtained. A function called ‘batch process’ in Corel Paint Shop was used to perform in a large number of images in one go. An example of the procedure is demonstrated in Appendix B.

Finally, to find the position of each frame along the tube and the flame coordinates of the flame front, a small programme developed by Dr. Rob Woolley was used by transferring the binary images (EPS image) into this program.

3.9 Unburned gas velocity measurements

3.9.1 Laser Doppler Velocimetry (LDV) specification

In order to obtain a laminar burning velocity it was necessary to know the velocity of the gas a head of the flame. Laser Doppler Velocimetry (LDV) is used to do this. Its main advantage is that is an optical technique and hence did not interfere with the flame in the tube [114, 119]. Other advantages are that it does not need calibration and has good spatial and temporal resolution [114].

The basic apparatus of the LDV system is shown in Figure 3.8; it consists of a transmitting optics including a beam splitter and a focusing lens, a continuous wave laser, a signal processor and a receiving optics and data analysis system [120]. The flow to be measured must be “seeded” with small particles that will scattered light from the laser beams into the receiving optics.

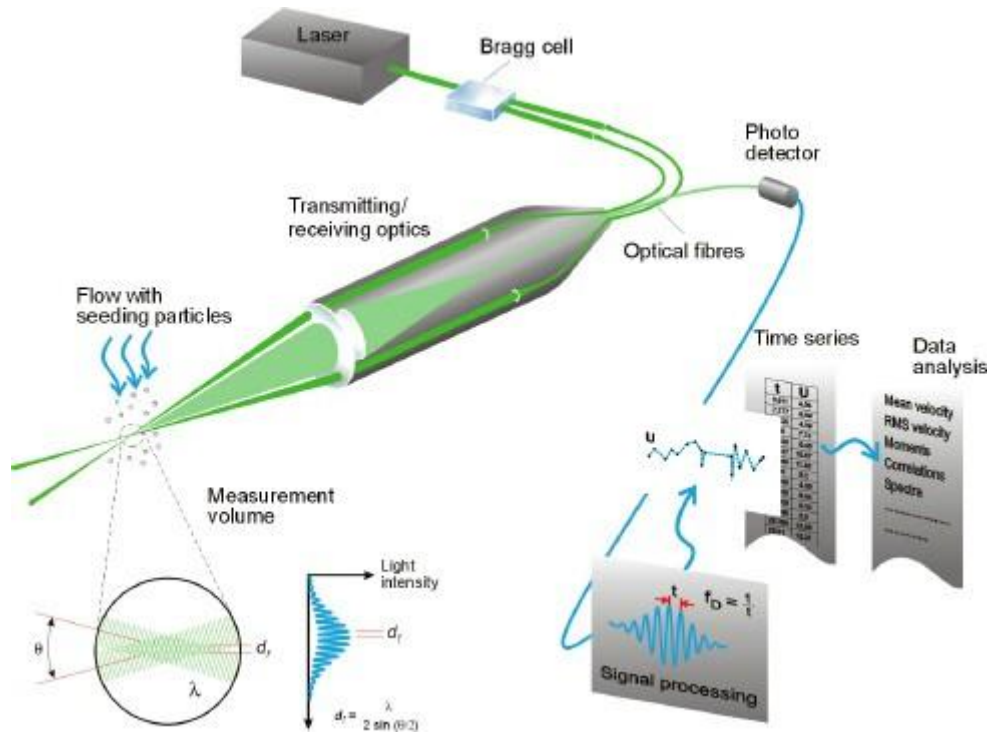


Figure 3.8 LDV equipments [121]

3.9.2 The measuring volume

A laser beams are split into two and the two parallel branches are focused at a point of interest within the flow field. At the point of intersection, fringes of light (alternating lines of light and darkness) will be produced due to the wave interaction of the beams. Particles crossing that fringe pattern will scatter the light with a frequency which is directly proportional to the particle velocity (Doppler frequency). This signal is received by a photo-detector and then further processed [119]. The fringe distance d_f is defined by the wavelength of the laser light (λ) and the angle between the beams (θ) as can be seen in figure 3.8:

$$d_f = \frac{\lambda}{2 \sin\left(\frac{\theta}{2}\right)} \quad (3.3)$$

Filters (high and low pass) remove everything but the required wavelength from the photo-detector signal [120]. This eliminates both the low frequency pedestal component and high frequency noise from the Doppler component.

The probe volume was produced by the intersecting laser beam, as shown in Figure 3.8. It should be created with small shape as possible to allow measuring velocities at a point in the flow field. The probe volume is kept as small as possible so that only one particle crosses the fringe sample at the same time. If two particles are in the control volume simultaneously a random super position of Doppler frequencies can result, dropping the signal due to destructive interference of the two signals [120].

3.9.3 Signal processing

The photo-detector converts the variable light intensity from the scatter photons to an electrical signal proportional to the light flux. The signal output from the photo-detector can be decomposed to low frequency (pedestal) output caused by the particle passing through the focused Gaussian-intensity laser beam. The Doppler frequency f_D , has a regular sinusoidal pattern and a high frequency noise [120].

The Doppler frequencies are filtered and amplified in the signal processor, which concluded f_D for each particle, often by frequency analysis. The fringe spacing d_f provides information about the distance travelled by the particle. The Doppler frequency f_D gives information about the time:

$$t = 1/f_D \quad (3.4)$$

Hence the velocity equals distance divided by time:

$$V = d_f * f_D \quad (3.5)$$

3.9.4 Seeding particles

Gases must be seeded. The seeding particles can be a solid powder or fluid. In this study liquid atomizer was used to generate olive oil particles. The six-jet atomizer type TSI 9306 fitted with a pressure gage and regulators to control the pressure as shown in Figure 3.9, and has an orifice diameter of 0.04 cm for each particle atomizer jet [122]. The liquid level in the reservoir should be less than a half to avoid that the atomizer becoming inundated [122]. The regulator and the dilution air valve should be closed just before connecting the compressed air. The atomizer outlet was connected to the top of the enclosure using a flexible tube. the regulator pressure was set to 25 psi, as this level is recommended [122], and connected to a

continuous source of compressed air. In this study, one atomizer jet was used, and a seeding time of about 10 to 15 seconds used for each test.



Figure 3.9 The Six-Jet atomizer

3.9.5 Set up of the LDV

An LDV measurement performed simultaneously with high speed imaging used Casio camera at 420 fps. A schematic of the experiment and an example of image from the camera are shown in Figure 3.10.

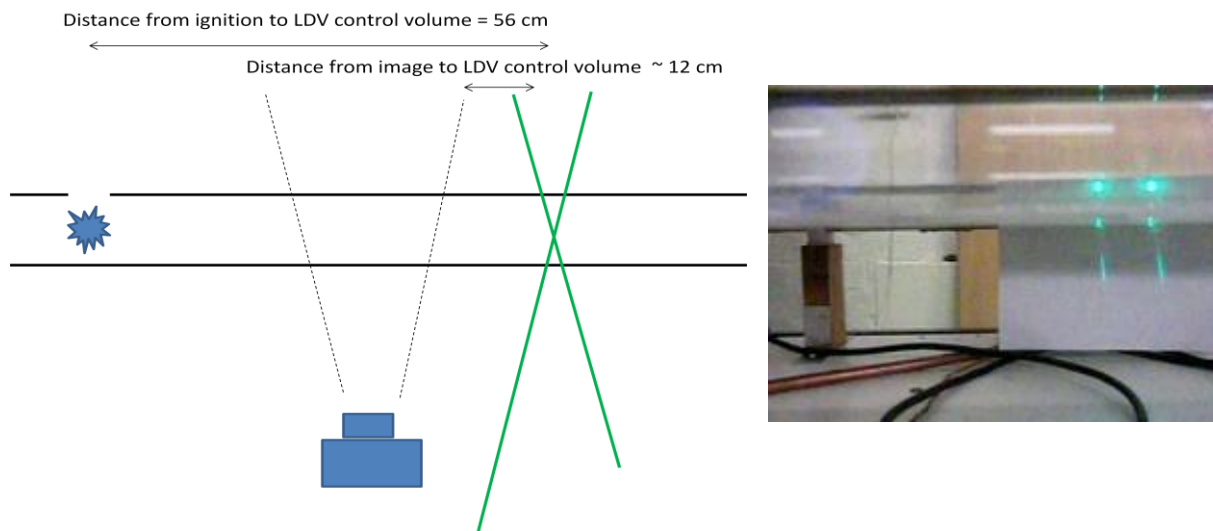


Figure 3.10 A schematic of the experimental set up

The flame can be observed in the first part of the tube, using successive flame images the flame speed could be determined.

The LDV and high speed images were synchronised by blocking off the LDV beams for a few seconds before the ignition. This was observed on the images and also resulted in a lost of LDV signal. This can be seen below in Figure 3.11.

Before ignition the gas velocity in the tube can be seen to have a mean of zero. High seeding concentrations were used to ensure a continuous measurement signal. The flame speed was measured from the video file. The velocity ahead of the flame was determined from the LDV.

The LDV experiment procedure and the data collection are detailed in Appendix C.

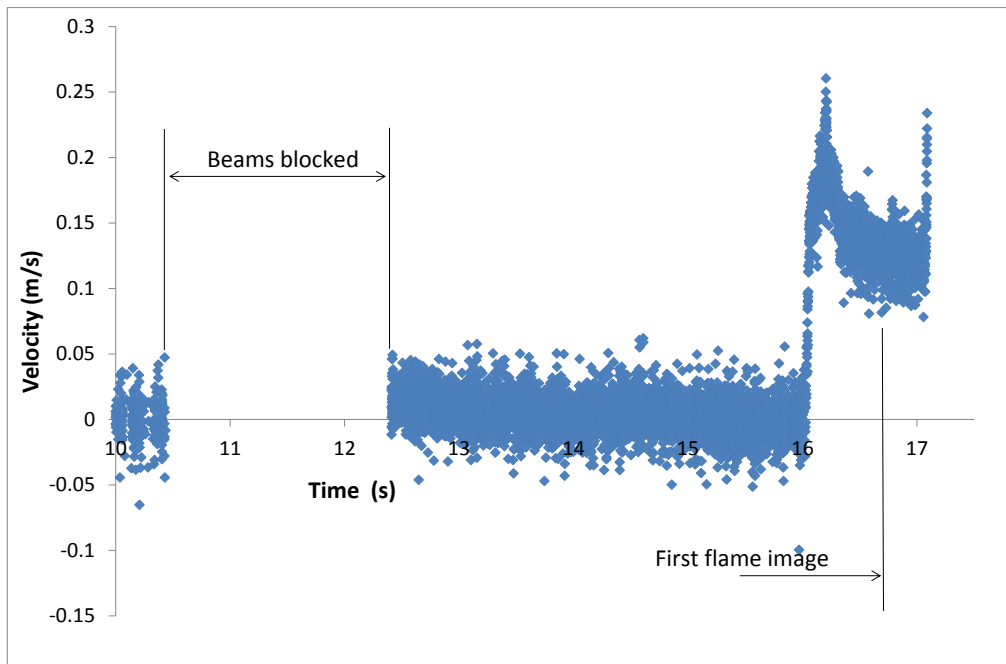


Figure 3.11 Velocity measured by the LDV system

3.10 High temperature measurements

This method was used in the preparation of high temperature testing for both propane and the acetone. The rig was modified as shown in the Figure 3.12.

For heating the system, silicone rubber heating tape type HTWC102-010 possessing a length of 3050 mm and a width of 25 mm. Type K thermocouples were added to the rig as follows:- heater, fuel input, before left valve, left quartz tube, right quartz tube, after right valve and room temperature respectively. The rig was heated to 333 K. The heating time from room temperature was approximately 90 minutes and the temperature was captured and plotted on a computer. The average temperature from all thermocouples was taken and can be found in Appendix D.

Acetone was injected into the rig using (250 micron) syringe as shown in the Figure 3.13.

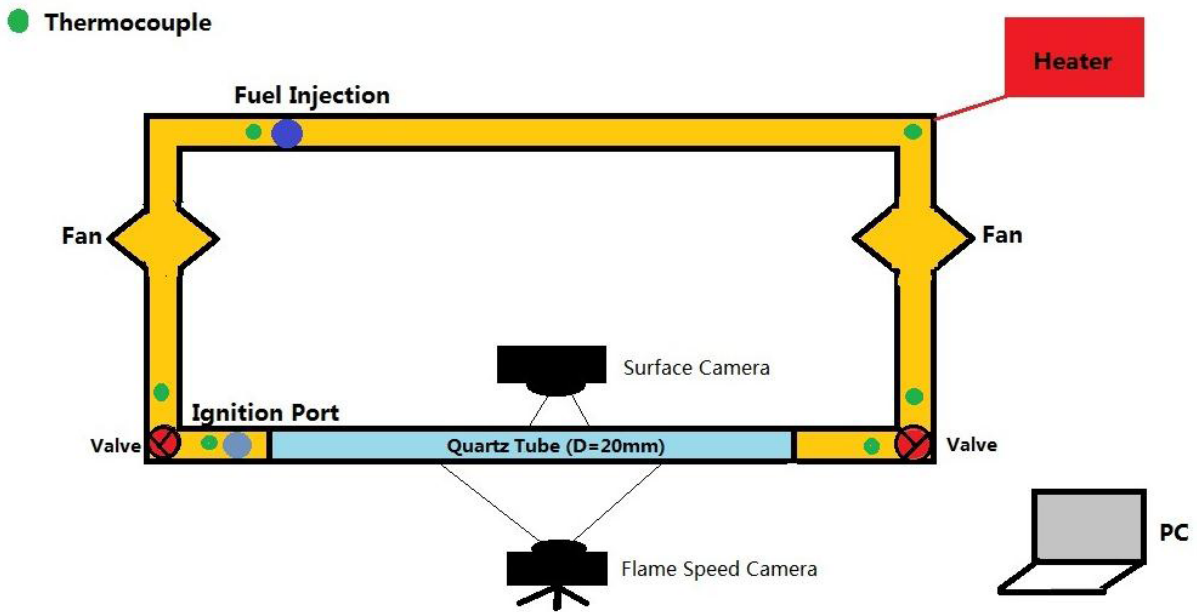


Figure 3.12 Experimental apparatus at 333 K



Figure 3.13 Syringe of liquid fuel

For experiments at high temperatures for both gas (propane) and liquid (acetone), fuel tests were conducted with orifice plates of 5 mm and each equivalence ratio was repeated 3 times. Fuel volumes were calculated as shown in Appendix E.

For liquid fuel the amount of acetone necessary to make the required fuel-air mixture was calculated and then injected into the system, as shown in Appendix F. The mass and volume of fuel were calculated at room temperature based on the assumption of a perfect gas for fuel vapours.

3.11 Measurement errors

- The errors encountered during the measurements may be due to some small error in the scale, trapped air bubbles in the system which were intended to prevent the addition of more water in the measurements, and overload water in the input holes. These errors are supposed to generate unevenness of + 35 ml and -55 ml. This gives the total volume of the system as 1203.63_{-55}^{+35} ml, which equates to a change in percentage of around -2.91 % to 4.57 %
- The errors were generated by the syringe ranges between ± 0.1 ml or $\pm 0.25\%$. However, this does not influence the accuracy of the equivalence ratio
- The errors generated due to leaking of mixtures through fitting and piping connections is around -1.0 ml, or -2.5 %. This value was estimated from comparing the data after sealing was achieved
- The sum of the errors described above, for the equivalence ratios ranges from -5.66 % to 4.82 %
- Reference temperatures in this work that are average by six thermocouples' record, have a low uncertainty of ± 1 K for room temperatures, whereas a high uncertainty of - 2.2 to + 12 K for 333 K
- Thresholding process of the images generates 1 or 2 pixels errors for each frame since the adjusted flame image is usually chosen from one in the middle of the tube

- Due to lower pixels (224×168) of the images, the flame speed has a maximum deviation of about ± 0.01 m/s if the total flame propagating along the tube has about ± 2 mm error
- The variation in flame speeds for horizontal propagation in the tube at open both ends is shown in Appendix G. It is due to the process of converting the flame into a digital image in pixel. This caused errors of ± 0.06 m/s in flame speed for each frame
- The difference in flame speeds for upward propagation in the tube at open both ends is shown in Appendix H. It is due to the process of converting the flame into a digital image in pixel. This caused errors of ± 0.4 m/s in flame speed for each frame
- The difference in flame speeds is shown in Appendix I. It is due to the process of converting the flame into a digital image in pixel. This caused errors of -0.08 to $+0.11$ m/s for each frame for propane with an orifice plate of 5 mm at both ends of the tube
- The difference in flame speeds is shown in Appendix J. It is due to the process of converting the flame into a digital image in pixel. This caused errors of -0.053 to $+0.136$ m/s for each frame for propane with an orifice plate of 5 mm at both ends of the tube at a high temperature of 333 K
- The difference in flame speeds is shown in Appendix K. It is due to the process of converting the flame into a digital image in pixel. This caused errors of -0.13 to $+0.13$ m/s for each frame of acetone with an orifice plate of 5 mm at both ends of the tube at a high temperature of 333 K
- A sum of the errors produced in flame speed is -0.73 m/s to $+0.85$ m/s
- There were small errors mainly relating to the time sync of the camera and the LDV, this errors are about 0.01s
- The variations due to curvature flame measurements errors are ± 0.02 mm (2 %), for the results of orifice plates of 5 mm at both ends of the tube at normal temperature and pressure, while the variations of the same orifice plates at high temperature of 333 K and atmospheric pressure are about 0.03 mm (3 %)
- The measurements of flame surface area give average potential variations of ± 6 % for the configurations of 5 mm plates at both ends and combination of 5/3 mm plates. However, the measurements of flame surface area at 333 K and normal pressure with 5 mm plates at both ends, give errors of -7 to $+12$ %
- The average variations of the unburned gas velocity for the experiments of 5 mm and 5/3 mm plates were 2.1 and 2.7 %, respectively

- The total errors in the calculation of the laminar burning velocity were 6 % for the experiments of 5 mm plates at both ends and combination of 5 mm neat to the ignition point and 3 mm at the far end.

4 Results of Flame propagation in a tube at open both ends

Experiments of propane /air mixture flames for the tube at open both ends are presented here. The experiments were performed at 300 K and 1 atm, the equivalence ratio (ϕ) was varied from 0.8 to 1.6. This configuration has been noted to be prone to flame vibration by previous researchers and has not been used to determine burning velocities [7]. Theoretically the gas velocity ahead and behind the flame should be small, as the burned and unburned gases are free to exhaust from both ends of the tube.

4.1 Results of horizontal tube with open both ends to atmosphere

Images of the flame, approximately half way along the quartz tube, are shown in Figure 4.1. These images were captured using the colour Casio EX-FH100 digital camera. Mixtures leaner than $\phi = 0.8$ could not be ignited, despite the reported lean flammability limit of premixed propane mixtures being at $\phi = 0.69$ at 1 bar and 300 K [41]. For $\phi = 0.8$ to 1, the flame propagated down the tube as a semi-ellipsoid that was slightly tipped towards the unburned mixture, as shown in Figure 4.1(a). This ‘tipping’ of the flame has been observed by a number of previous workers [5, 18], it is generally attributed to the (lack of) influence of gravity on the hot (less dense) combustion products tilting the flame forwards at the upper part of the tube. Viscous forces have an influence near the wall, as well as heat transfer from flame to wall, causing the curvature of the flame [3, 60]. The overall flame shape is the result of the no slip condition at the walls, in addition to heat transfer from the reaction zone to the wall. For $\phi = 1.1$ to 1.3 the flames initially had a ‘conventional’ convex (relative to the unburned mixture) elliptical shape, but the flame length was shorter than seen in the leaner flames, as shown in Figure 4.1(b). As the flame progresses down the tube it can then be seen to shorten and then elongate, with an associated increase in flame speed. Fresh unburned mixture and flame appear to be drawn into the burning mixture down the centre line of the tube. When the flame was oscillating it was not possible to distinguish the detailed flame structure, as the local flame speed was so fast that the camera image became blurred. The $\phi = 1.4$ and 1.5 flames generally propagated in a steady manner. These flames were more elongated, with long tails at the bottom of the tube. Some oscillatory behaviour was observed towards the end of the tube for $\phi = 1.4$. At $\phi = 1.6$ flames, propagated in a roughly tilted semi-ellipsoid shape and cellular structures were observed in the second part of the tube, as indicated in Figure 4.1(c) for 1.6 (b).

In the case where the tube is open at both ends, flame propagation was unstable and oscillatory for equivalence ratios around stoichiometric, where burning rate was highest.

(a)

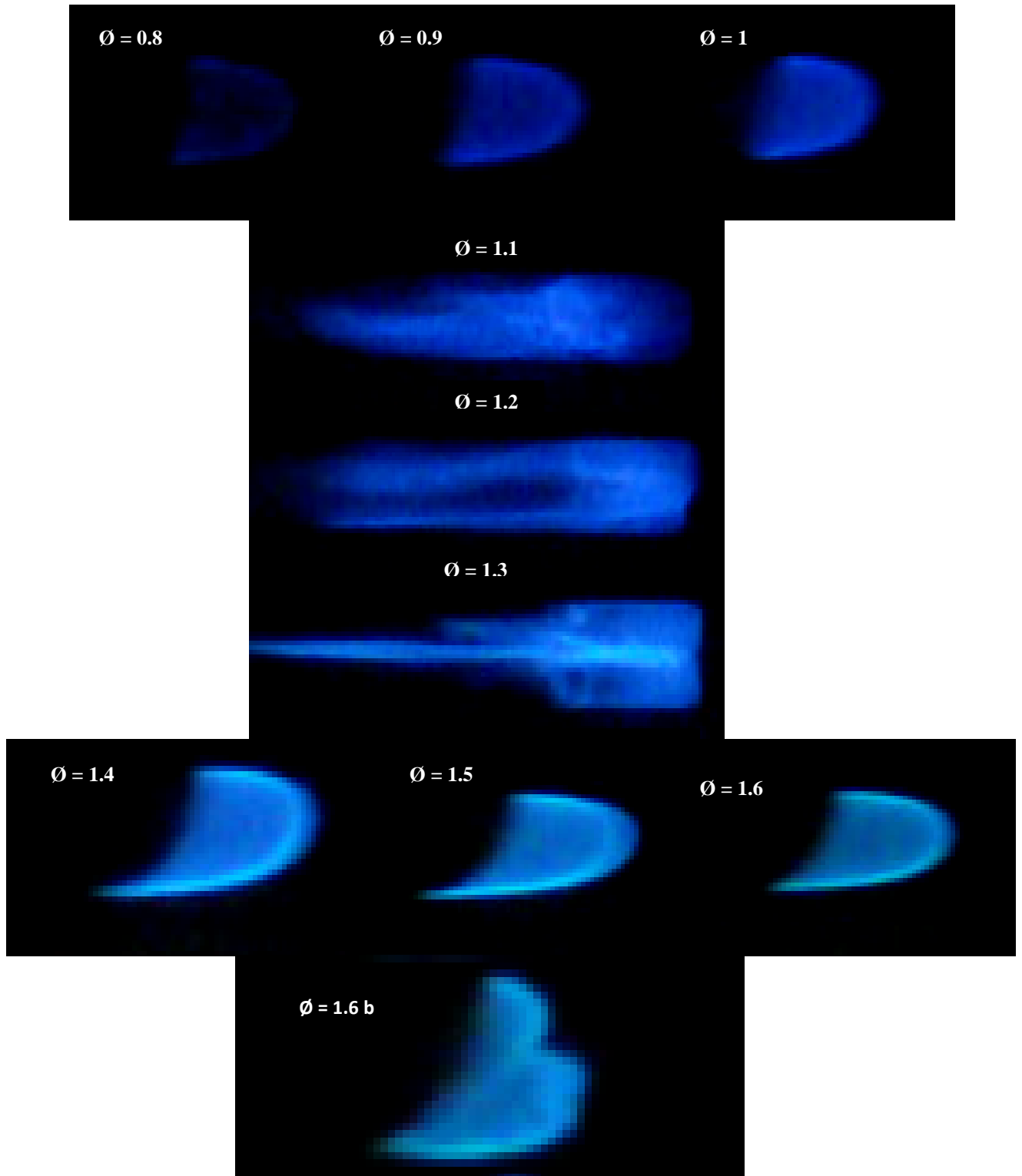


Figure 4.1 (a) Images of flames propagating down tube

(b)

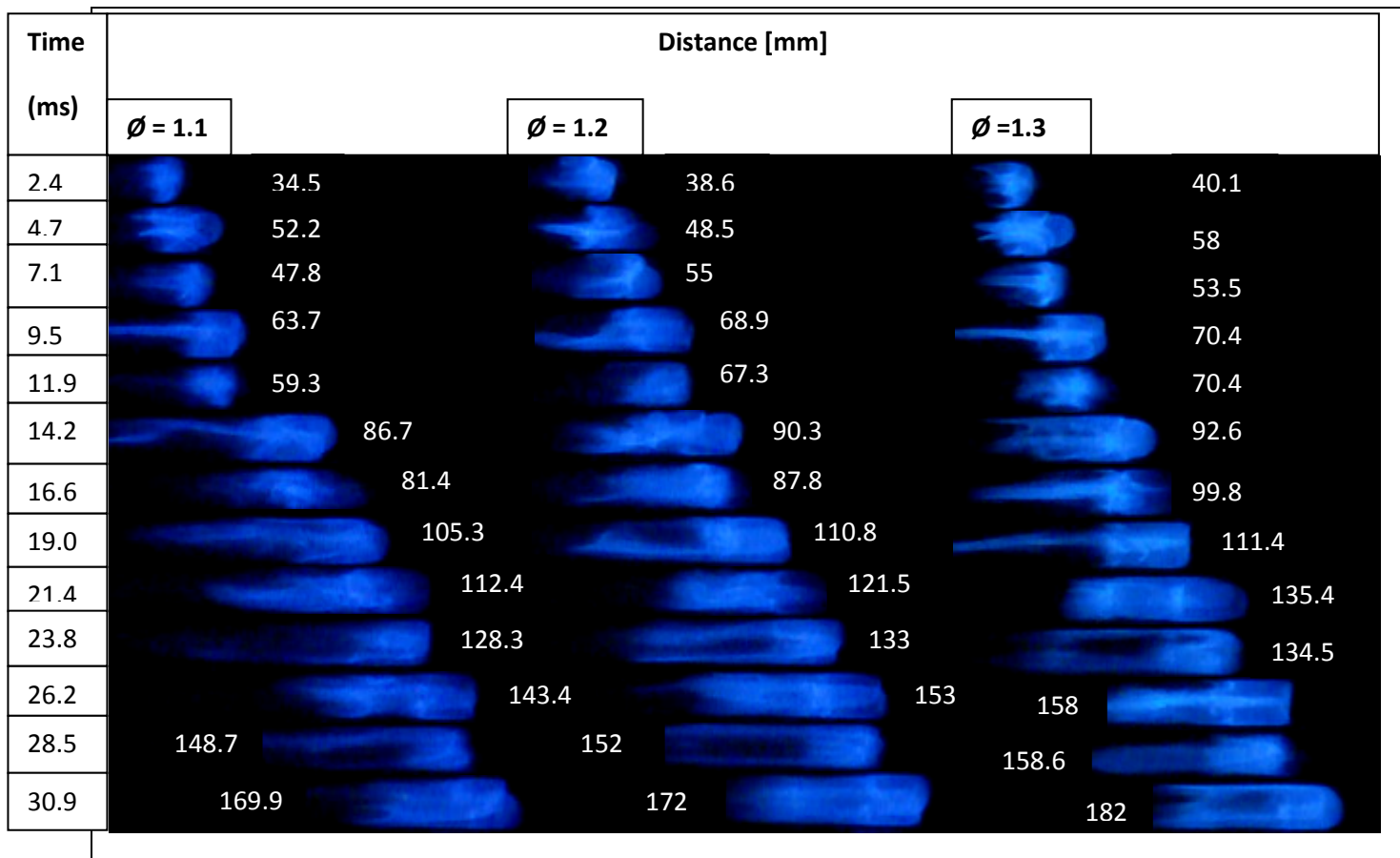
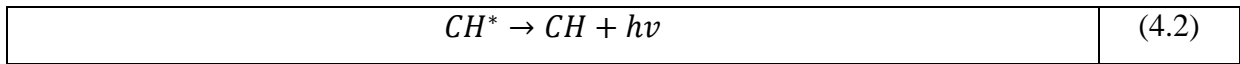
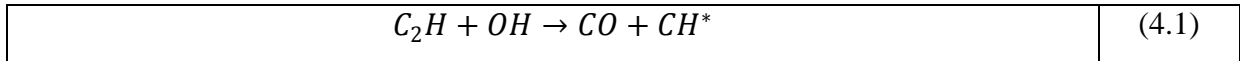


Figure 4.1 (b) Images of flame propagating down tub

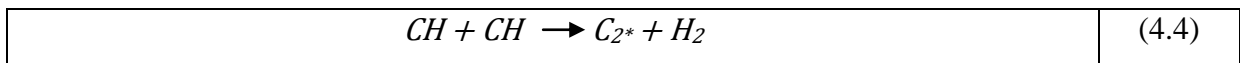
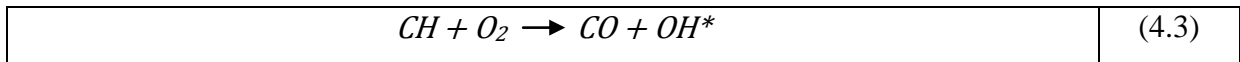
$\varnothing = 1.6 \text{ b (c)}$		
Frame	Time (ms)	Distance (mm)
24	57.1	121.7
25	59.5	125.1
26	61.9	126
27	64.3	131.1
28	66.6	131.1
29	69	138
30	71.4	137.1
31	73.8	143.1
32	76.2	144.8
33	78.6	150.8
34	81	154.3
35	83.3	157.7
36	85.7	162.8
37	88.1	163.7
38	90.5	169.7
39	92.8	170.5
40	95.2	176.5

Figure 4.1 (c) Images of flames propagating down tubes, at different equivalence ratios, and a framing rate of 420 fps. Tube opens at both ends

The Casio EX-FH100 is a colour camera, therefore differences in both the brightness and colour of the flames can be observed. The blue colour seen in all these flames is a result of emission of light associated with a specific reaction involving the CH radical [123-124]. When a chemical reaction leads directly to the formation of an atom or a molecule in an electronically excited state, from which radiation may occur, then we may have a light emission out of all proportion to that to be expected from thermal emission. This phenomenon is referred to as chemiluminescence. The important emitting species here are the radicals of CH, which are formed by a strongly exothermic reaction, as shown in equation (4.1).



Two other emission reactions are also important in premixed flame, involving OH and C₂:



The emission species of the OH* radical is an intermediate reaction in hydrocarbon oxidation. In the reaction zone, highly excited OH* radicals are formed by the strongly exothermic reaction. The chemical process of recombination of O and H atoms modifies the spectrum of OH*, but this would not normally be regarded as a case of chemiluminescence. There is also the possibility of indirect chemiluminescence, in which excited molecules formed by chemical reaction, pass on their excitation, by collision, to other species, from which abnormally high emission results. Here again, there are varying degrees of effect, according to whether the active molecules are in some unusually excited metastable form, or merely possess rather more than a fair share of vibrational energy [44].

In equation (4.2), light is emitted at 431.5 nm [35] in the blue range of the visible spectrum. Other chemiluminescence reaction associated with OH (342.8 nm) and C₂ (swan bands) with a head at 473.7 nm [125]. The C₂ emission occurs primarily in rich mixtures and due to decreased oxygen concentration, the flame colour changes to green from the violet-blue characteristic of CH radiation. However with decreased oxygen, density of C₂ radiation reaches a peak and then falls, which is generally due to the decreasing of free radical concentration in the reaction zone [35].

The CH* chemiluminescence versus equivalence ratios, is shown in Figure 4.2 [126]. As can be seen, the maximum CH* chemiluminescence at approximately $\phi = 1.1$, while stoichiometric conditions appears on the lean side. These results confirm that CH* chemiluminescence is not a linear function of fuel flow-rate [126].

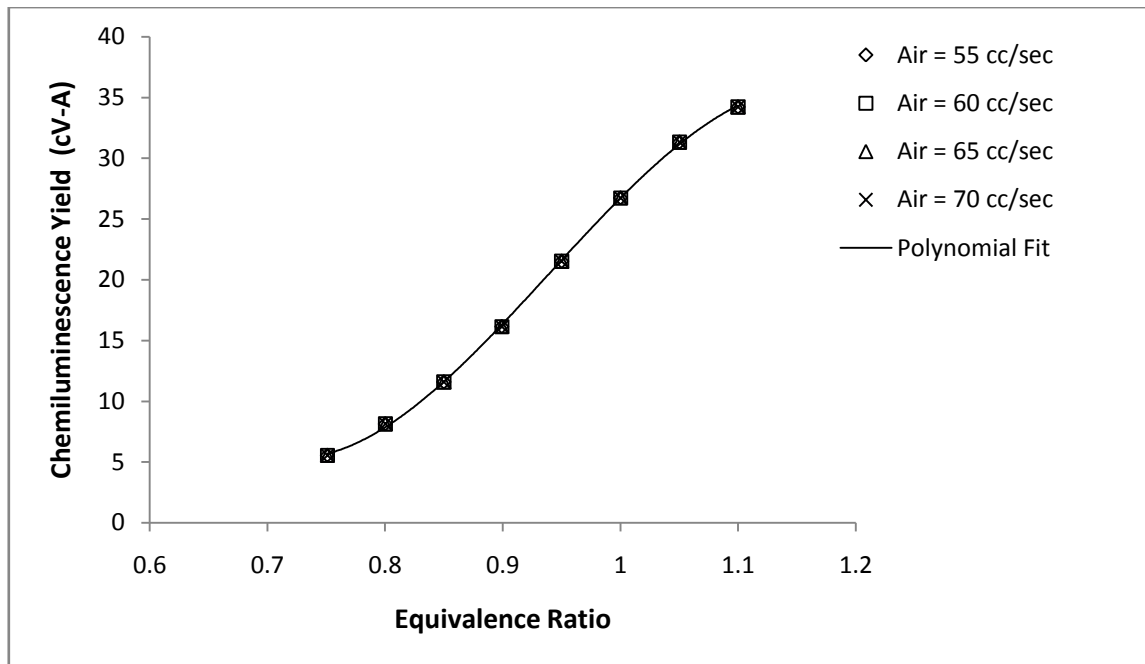


Figure 4.2 Normalized CH* chemiluminescence yield as a function of equivalence ratio [126]

Shown in Figure 4.3 are plots of the leading edge of the flame against time, for the flames shown in Figure 4.1. At least 5 flames were captured for each equivalence ratio. For $\phi = 0.8$ to 1, the flame propagated down the tube in a constant velocity resulting in a linear plot. At $\phi = 1.1$ to 1.3 oscillations occurred with an associated acceleration as the flame propagated down the tube, as shown in Figure 4.1 (b). All three equivalence ratios exhibit roughly the same trend down the tube, as shown in Figure 4.3. The flames were not filmed at a sufficient framing rate to obtain the frequency of oscillation, or obtain a clear idea about how the flame was propagated. There also appears to be some motion blur, indication some periods of very high propagation rate. As the mixture became richer (equivalence ratio $\phi = 1.4$ to 1.6) the magnitude of the flame oscillation diminished.

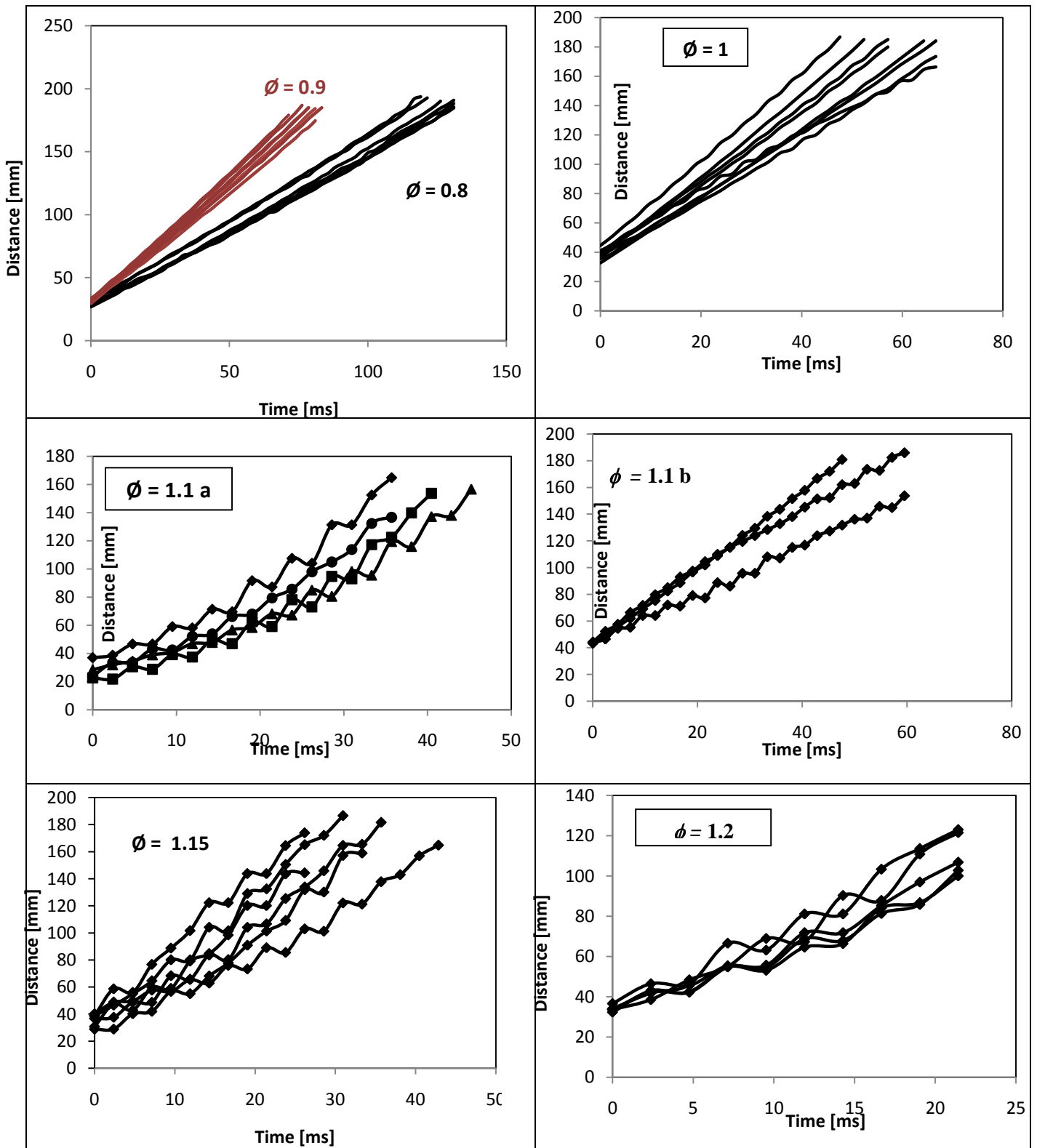


Figure 4.3 Flame distance against time for tube open at both ends

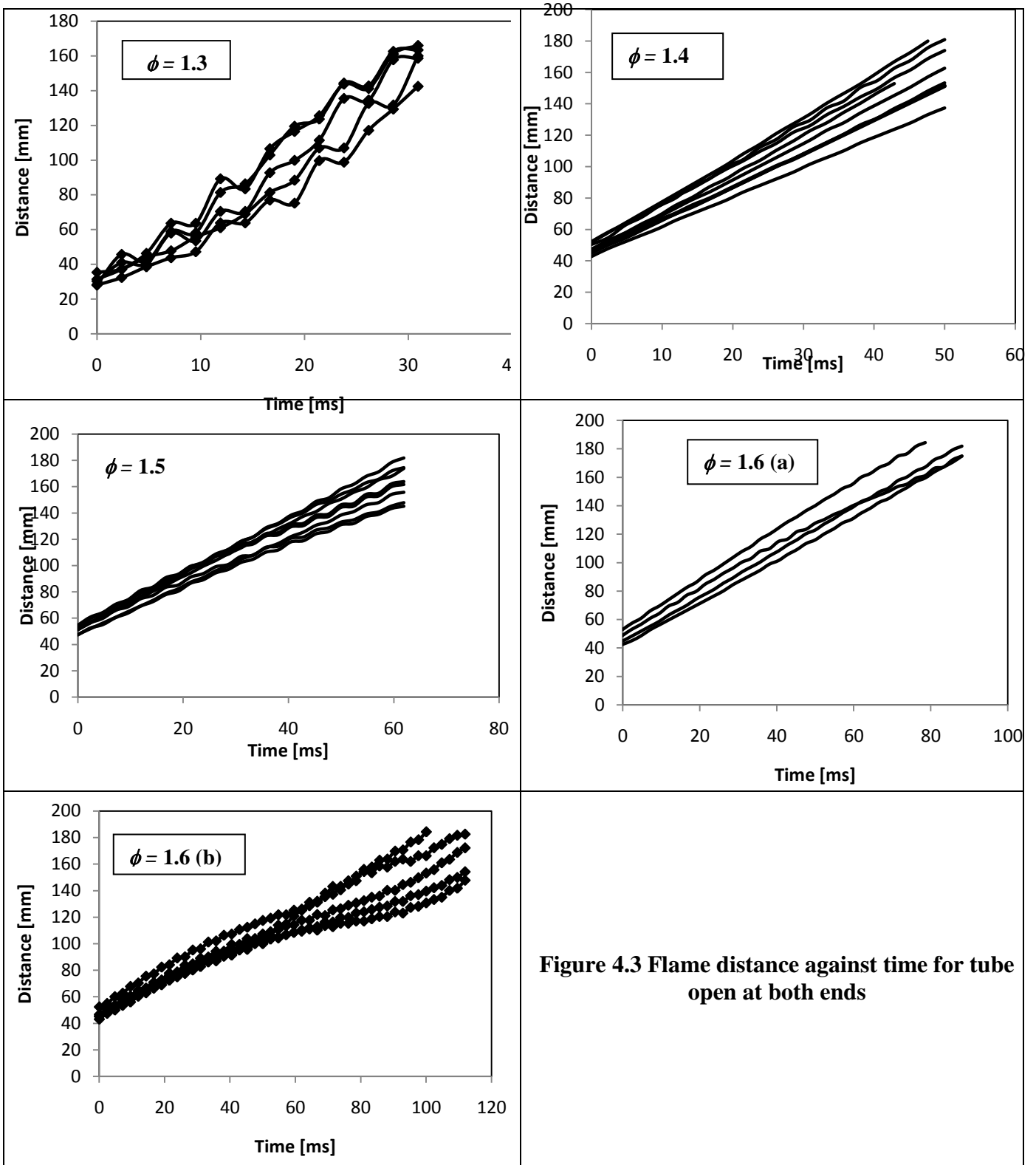


Figure 4.3 Flame distance against time for tube open at both ends

Table 4.1 Observed flame speeds for a tube open at both ends. Data are the averages from eight tests

ϕ	0.8	0.9	1	1.1	1.15	1.2	1.3	1.4	1.5	1.6
Average flame speed, U_f (m/s)	1.29	1.93	2.34	3.24	4.50	4.32	3.98	2.35	1.87	1.25
Correlation coefficient R	0.999	0.999	0.999	0.973	0.979	0.961	0.987	0.999	0.999	0.999
Standard deviation of the fit (m/s)	0.11	0.08	0.30	0.63	0.37	0.30	0.32	0.26	0.21	0.26

Figure .4.4 illustrates the flame speed plotted against equivalence ratio obtained with a linear least squares fit through the data. The flame speed increases with an equivalence ratio reaching a maximum value of $\phi = 1.15$, whereupon the average flame speed was 4.5 m/s, and then falls as the mixture became richer, as shown in Table 4.1. Also shown are the fitting parameters, correlation coefficient and standard deviation of the fit. It can see that R-squared values for the linearity flame speed were much higher than the disturbed flames, by about 3.8 %. The maximum flame speed in this study is nearly the same with previous work was performed by Mallard [127] on the same rig with the tube at open both ends, which was about 4.4 m/s. The wall cooling of the tube has no significantly affect on the flame speeds when the tube diameter is adequately large, for this reason, the quantity of heat dissipated from the burning gases by the walls of the tube, is proportionate to the circumference of the tube [128].

The ignition point should be positioned at or within 3 or 4 cm, of the open end of the tube. If the ignition point is some considerable distance within the tube, the flame travels in both directions from the point of ignition, and the disturbance caused by the flame moving towards the open end impacts the flame moving towards the closed end [128].

Mason and Wheeler [128] employed tube of 5 cm diameter and 5.2 m long, and the ignition point was placed in two cases, 4 and 17 cm from the open end of the tube. Their results showed that flame speed with point of ignition at 4 cm at the open end of the tube was higher than the case when the ignition point was at 17 cm from the open end of the tube, by about 5 %. This increased in the flame speed, due to drag acting on the flame, which was travelling towards the open end.

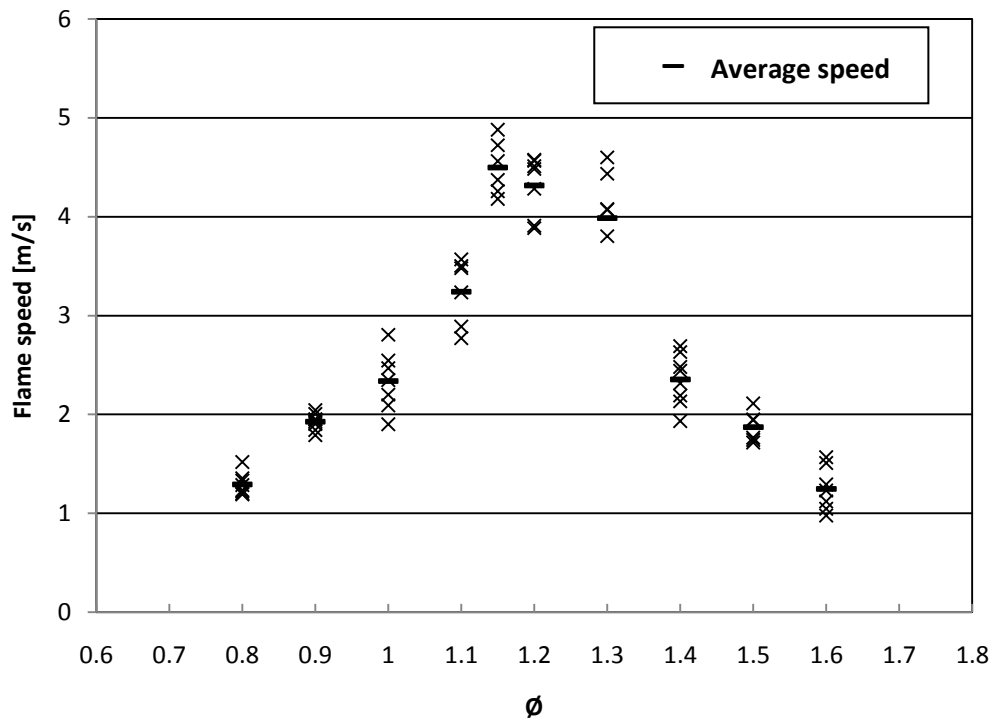


Figure 4.4 Variations in flame speed (obtained from a linear fit), with equivalence ratio, for a tube at open both ends

4.1.1 Reasons for the performance of the flame

This part will discuss the performance of the flame as demonstrated during the experiments.

- **Light emission from flame**

Almost all combustion phenomena result in light emission. Studies of flames can be used to acquire this information. If a flame were to be at thermodynamic equilibrium then the hot gases would emit the continuous radiation predicted by the Planck radiation law for the applicable flame temperature [2]. For a real black body, the emissivity is equal to 1 for all wavelengths. In flames, the emissivity is close to zero for most values of wavelengths but may reach fairly high values, near 1, for a limited number of emission bands, the strongest of which are in the infra-red. Even for visible regions, in which the radiation is owing to

emission from solid carbon particles, the emissivity varies to some extent with wavelength. [44]. Band spectra in the near infrared are owing to changes of vibrational and rotational energy of the molecules only, while spectra in the far infrared are due to changes of rotational energy only. Non-equilibrium distributions in the OH band system arise in rotational and vibrational excitations. High rotational temperatures for OH* in hydrocarbon-oxygen mixture flame is, as a result of the reaction shown in equation 4.3. Also, the effective rotational temperature of OH is very high, increasing from approximately 5400 K at atmospheric pressure to near 10,000 K at low pressure; this effect is best interpreted as direct chemiluminescence [44].

- ***Failure to ignite lean conditions***

A gas lighter could not ignite the fuel-air mixtures with an equivalence ratio lower than 0.8. Von Lavante and Strehlow [129] studied the extinction mechanism of methane-air mixture at different tube diameters, in a vertical position. They found that a heat loss through the walls had a small effect on flame extinction. Flame stretch was the main probable reason for flame extinction [129]. Moreover a diffusion in the front flame have caused this extinction, but it is played a significant role in enhanced propagation of the flame rather than cause its extinction [129]. In addition, as mixtures of methane-hydrogen-air with a different internal diameter (6 – 50 mm), the lean flammability limit decreased with a smaller internal diameter [130-131] this may be due to the stronger combined effect of diffusion and flame stretch in a small diameter tube, for Lewis number lower than one ($Le < 1$). For this reason tube diameters bigger than 50 mm were chosen as typical, because it causes a small change in the flammability limit [76]. For these reasons it would not be expected that the same flammability could be achieved in this Figure compared to the quoted values for larger tubes.

- ***Oscillatory behaviour of flames***

Complex oscillatory flames occurred most notably, in fuel rich conditions, particularly for equivalence ratios from 1.1 to 1.3. Wheeler [56] studied the ‘uniform movement’ of methane-air mixtures in long glass tubes with 5 cm internal diameter. He reported that these variations are continuous throughout the flame tube, with the flame moving towards the direction of travel at times, an example can be seen from frames 7 and 8 in the Figure 4.1 for the

equivalence ratio of 1.3. Also, he recorded that the unsteady flame may be "extinguished" by high oscillations, due to the mixing of burnt and unburnt gases and then the speed will be higher than the steady travelling flame. Ellis and Wheeler [132] reported ignition of 10 % of carbon monoxide-air mixtures, when cylindrical tube of 2.5 cm internal diameter and 20.3 cm long, where closed at both ends. During ignition at one end of the tube, the flames had a hemispherical shape near the ignition point and then became small and changed inside-out due to cooling by the tube walls. These changes led to increases in the speed of the flame, as shown in Figure 4.5. [“This Figure is reproduced by permission of the Royal Society of Chemistry”]



Figure 4.5 Photographs of flame shape propagation down the tube at close both ends

[132]

Ellis and Wheeler [132] used a cylindrical tube, 2 cm internal diameter and 40 cm long, for the same portion of carbon monoxide-air mixture. They showed that when ignited at the one end of the tube, the flames took an elongated shapes and the pressure was observed owing to the increase of the surface area of the flame. Coward and Hartwell [5] suggested that the burning rate may become higher with an increased diffusion of mass and heat, due to the creation of great turbulent eddies, leading to increased surface area of the flames. The propagation of flames in tubes has received some interest in recent years, as a modelling study. The problem is important for understanding DDT, flame hazards and also miniaturised combustion devices. For large Lewis number, flames (not the case in this work), Cui et al. [133] found that the flame created a pulsating mode and that it was subject to short periods of dynamic burning, followed by longer periods, where burning intensity was low. Violent flame folding has been observed in models of flame-acoustic resonance, for a flame travelling along an open-ended tube, towards a closed end [134]. Qualitatively, a number of descriptions of the flame behaviour are similar to those observed in the experiments performed here. Rayleigh-Taylor instability was observed and the formation of ‘blobs’ of burnt matter being pushed into the fuel-air mixture. Akkerman et al. [135] studied flame oscillations in tubes numerically, and they noted that with increased diameter of the tube, the oscillations became stronger. The burning rate and the surface area of flame had minimal dependence on the tube diameter. These results are in good agreement with previous results

found experimentally [136]. They examined the problem of open-ended tubes and demonstrated a self induced flame oscillation, where by the flame performs a concave to convex transition, accompanied by acceleration of the flame connected to the convex shape. Whilst the mechanism that builds the oscillations is likely to be different in these experiments results and the modelling studies, it is still significant to note that the acceleration of the flame is associated with a convex shape and also periodic changes in the burning rate and these have both been observed here.

The same investigation conducted by Fleifil et al. [137] found a fluctuation in the area of the flame, observed through the formation of a ring of unburned gas, between the leading edge of the flame and the tube wall. The pressure generated in the flow caused some ringing, which influenced the burning velocity. Also they observed that the phase of the area perturbation depended on the burning velocity, not on the velocity perturbation. As well, they observed that the burning velocity decreased as the phase lag increased. Similar behaviour was also noted by Gerstein [138] who suggested that these variations are formed due to the build up of pressure in the tube. Rallis and Garforth [65] proposed that these oscillations may be generated by the action of acoustic waves, which propagate down the tube and are then reflected back.

- ***Semi-Ellipsoid Shape in Non-Disturbed Flames***

For comparison purposes, the flame shapes of those flames that propagate in a uniform and linear way are shown in Figure 4.1.

Hoare and Linnet [111] used Bernoulli's theorem and found that the pressure increases behind the flame front. They also showed that, in the unburned gas, the pressure in the centre of the tube would be bigger than at the axis, due to the unburned gas flowing away from the flame front. For these reasons, flames are moving faster at the centre down the tube than along the tube axis, consequently resulting in the characteristic flame shape.

In their review, Rallis and Garforth [65] focused on the wall interaction effects, which result in heat transfer from the flame. They proposed that the heat is released by radiation, from the burned to unburned gases, and to the flame tube walls, during the combustion process, accompanied by conduction from the hot gases to the tube walls [60]. Nonslip at the tube walls is the reason for the flame curvature and leads the flame acceleration to become

uniform travel, due to the friction effect. This acceleration, with nonslip at the tube walls, will be increased by thermal expansion of the burning and decreases with the Reynolds number of the stream [60].

- *Flame tip*

The behaviour of flame tip has been discussed by Coward and Hartwell [5]. They demonstrated that this behaviour occurred due to convection upwards, of the hot combustion products causing a small amount of gas movement in and about the flame.

Hoare and Linnet[111] also noted that the convection will affect the front of the flame. In the case of slow flames, part of the flame will bend towards the top of the tube. However, with faster flame convection becomes ‘outweighed’ by the factors tending to make the flame hemispherical, and so the flame appears approximately symmetrical, about the tube walls.

- *Cellular flame*

Cellular flames have been widely observed in spherically expanding flames [36] and on flat flame burners [58]. In both cases the expected smooth flame sheet splits up into small distinct ‘cells’. The cell size, and hence their number has been shown to be a function of fuel type, equivalence ratio and pressure [58]. This phenomenon is widely attributed to thermo-diffusive and hydrodynamic instabilities. The hydrodynamic instability occurs due to variations in the density of the unburned gas. When there is a flow of gas ahead of the flame accompanied by a density variation in the unburned mixture, then the velocity of the gas must change (due to conservation of mass). This feeds back to the flame, resulting in ridges and dimples in the flame sheet. However, the thermodynamic instability is generally stabilised by thermo diffusive processes in the reaction front of the flame. If the diffusion of heat from the burned zone into the burned gas is dominant, where there are dimples or ridges in the flame sheet, heat is conducted from the flame into the unburned gas increasing the local reaction rate and smoothing out the flame. At certain air/fuel ratios, the diffusion of the unburned deficient reactant into the flame may be significant for flame propagation. In this case the fuel has to diffuse over a larger area resulting in an increase in the local equivalence ratio and a reduction in the local burn rate. In the limit this can lead to flame quenching. Where the flame is convex to the unburned mixture, these processes result in the local equivalence ratio becoming richer and a comparable decrease in the burn rate. In Figure 4.1 the periodic

appearance of a cell can be observed. In this situation, the size of the cells appears to be about half the diameter of the flame tube. The appearance of cellular flames can be 'predicted' using Lewis or Markstein numbers.

4.2 Results of upwards and downwards propagation in a vertical tube position open at both ends

A photograph of the experimental apparatus in the vertical position is shown in Figure 4.6. These experiments were performed to investigate the interaction between flame shape, flame speed and the influence of gravity on the flames.

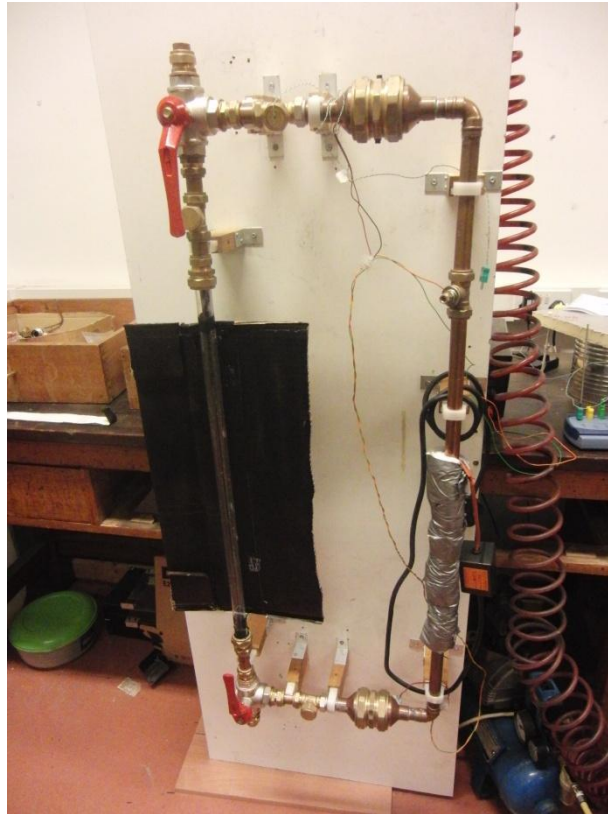


Figure 4.6 Vertical position

4.2.1 Results of upwards propagation in a vertical position with open both ends to atmosphere

Photographs of a propane-air flames propagating upwards for equivalence ratios of 0.8 to 1.6 are shown in Figure 4.7. The $\phi = 0.8$ and 0.9 flames had similar semi-ellipsoid symmetrical shapes. For $\phi = 1$, also, a semi-ellipsoid flame, but shorter than the lean cases, was observed. For $1 < \phi < 1.4$ the flames propagating upwardly were subject to violent oscillations and the flame took on an elongated shape as shown in figure 4.8, 4.9 and 4.10. At $\phi > 1.4$ the flame propagation became more stable and the flames are smooth but tilted.

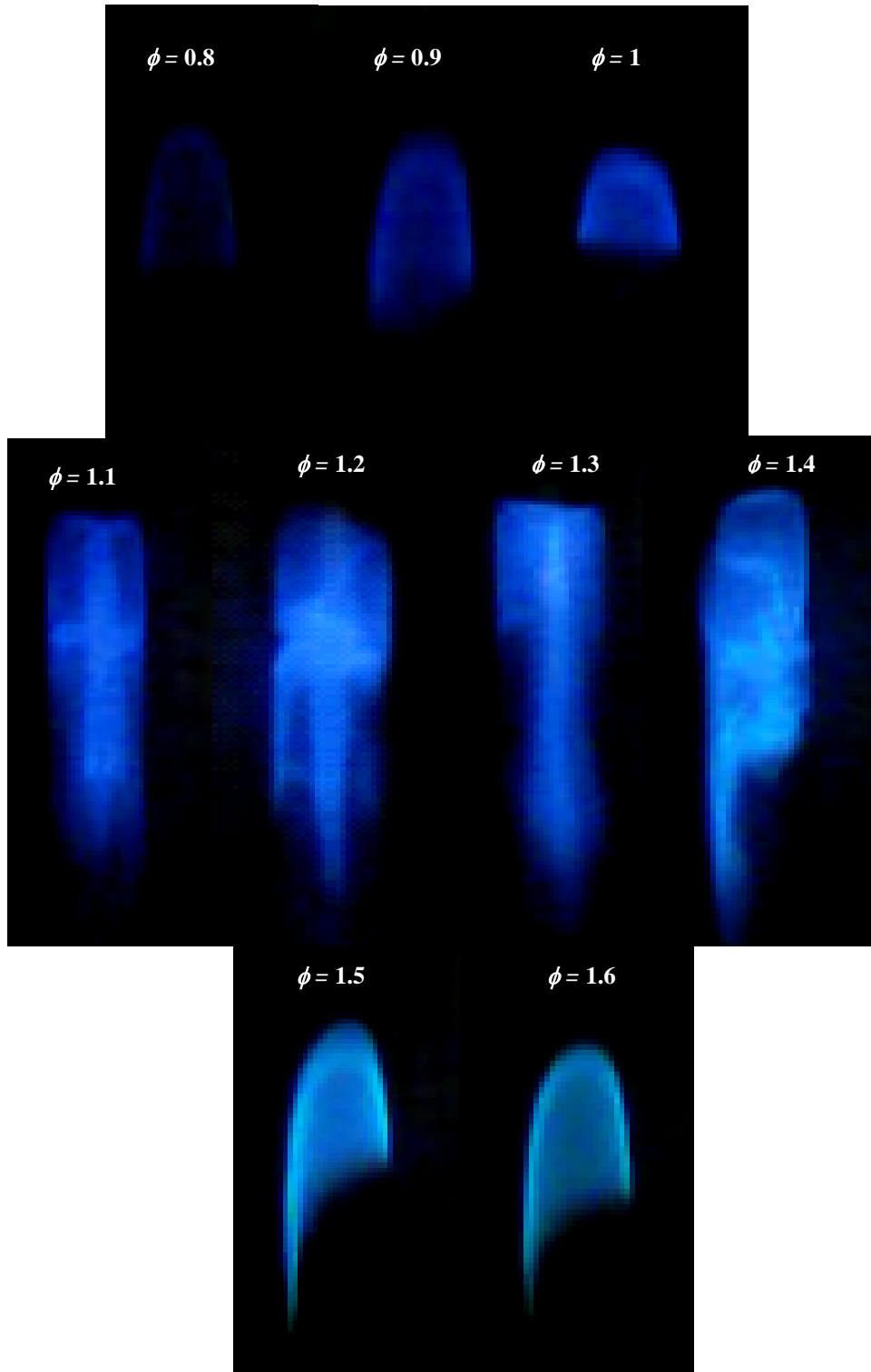


Figure 4.7 Flame shapes propagating upwards in a vertical tube with a 20 mm ID

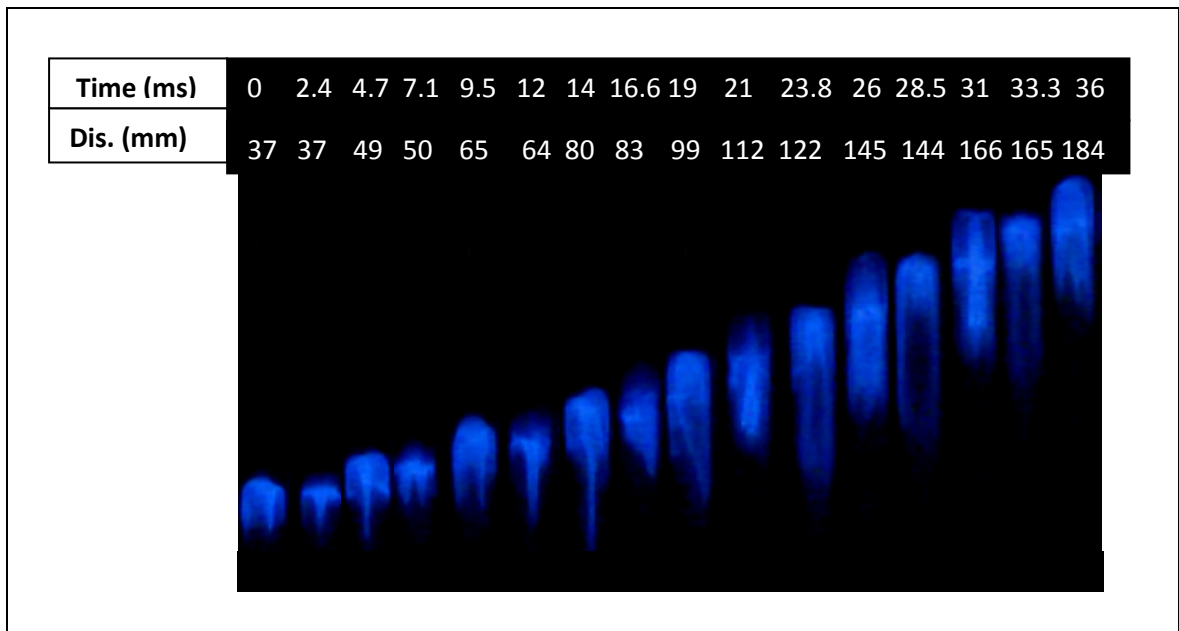


Figure 4.8 Images of non-uniform flames propagating upwards, at mixtures equivalence ratio 1.1

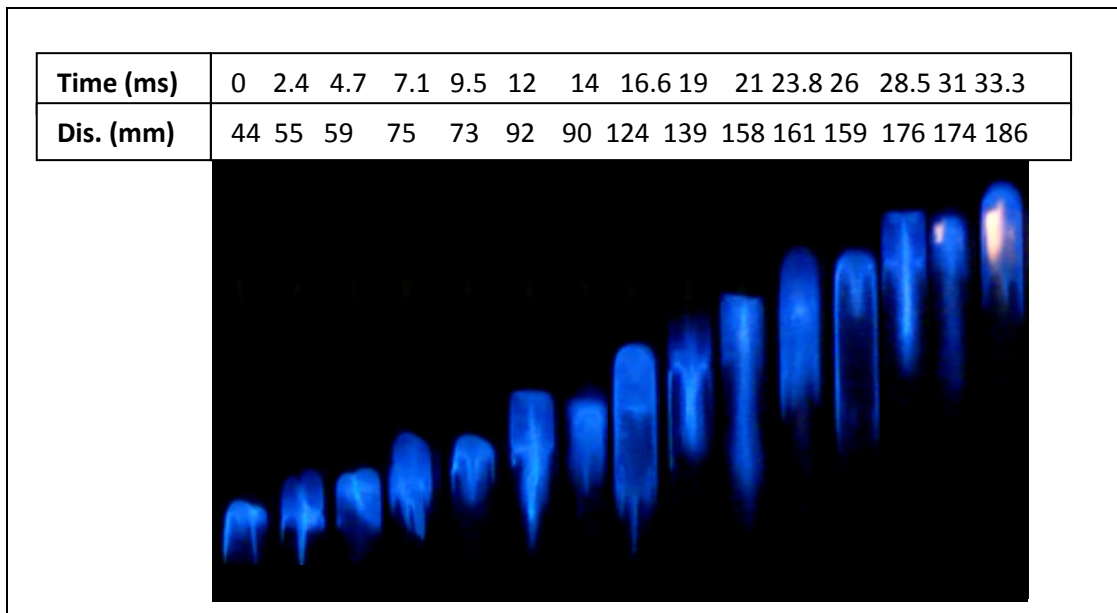


Figure 4.9 Images of non-uniform flames propagating upwards, at mixture equivalence ratio 1.3

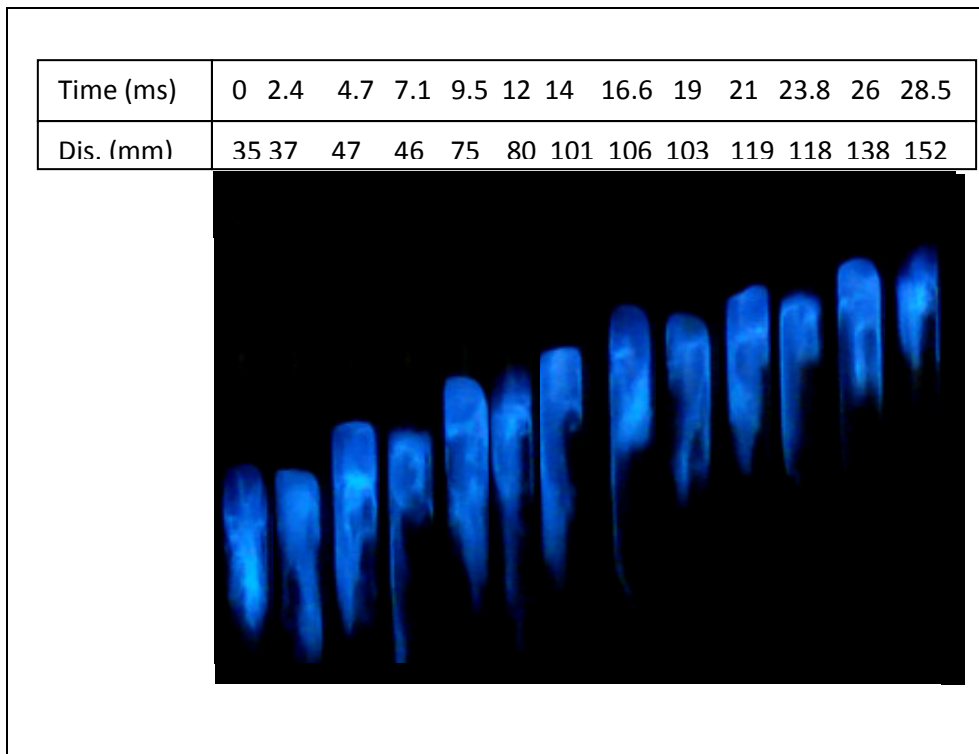


Figure 4.10 Images of non-uniform flames propagating upwards, at mixture equivalence ratio 1.4

These oscillations appear to be associated with acoustic vibrations of the gas column. In non-detonable mixtures the coincidence of regions of combustion wave vibration with the antinodes of the gas column is readily observed, and the wave resumes its uniform movement after passing through the antinodes. The reproducibility of the velocity of uniform movement can be insured only, by maintaining carefully controlled conditions at the mouth of the tube, particularly by igniting not too far from the open end [128]. This suggests that the thrust pressure is not necessarily distributed symmetrically around the shape analogous to that observed on stationary flames. That the combustion wave is sensitive to forces acting on the gas flow is evidenced by the effect of gravity on the speed of uniform movement.

The movement of a combustion wave in a tube open on both ends, propagating upwards, grows initially, from a steady shape to a rather flat shape, extending over the tube cross section about halfway along the tube, as shown in Figure 4.11 for frames of 21 and 28.5 ms. In this process, much of the unburned gas is pushed forward, but this mass is ultimately redistributed over the entire volume, and then a further burning takes place. Viscous drag at the wall causes the speed to be greatest in the centre of flame. The flame progresses symmetrically for the first 30 cm of the tube and then the oscillations are arise, due to the rapidity of flame motion [35].

The effect of gas oscillations on combustion waves has been studied by Markstein [139] by means of high-speed motion photography and pressure recordings. Vibratory movement, taking place in wide tubes, more than 9 cm diameter, after a period of uniform movement of flame was found to be accompanied by periodically appearing and disappearing wrinkles in the combustion wave, the wrinkles formed a cell structure similar in appearance to spontaneously formed cells. The size of the cells was found to be related primarily to the amplitude and frequency of oscillations, whereas in spontaneous cell formation the size is governed by mixture composition. With increasing amplitude the cells grew in size, until only a few remained over the tube cross section [139]. Markstein's observations led to confirmation that the oscillation increased the burning rate, and vice versa. For either concave or convex curvature of flame, the assumed relationship postulates an increase or decrease of burning velocity, depending on the choice of the proportionality factor, between burning velocity and reciprocal radius. In particular, it was found that gravity has a decreasing marked effect, as the burning velocity increases, and that for a negligible effect of gravity there should exist a minimum cell for any mixture. The existence of non-cellular flames would thus be interpreted to mean that in such mixtures the minimum cell size is large compared with the significant dimension of apparatus. At low burning velocities, gravity would influence the occurrence of cell structure depending on the direction of flame propagation. However, in upward propagation the cells would be of size smaller than in zero gravitation propagation [139].

Flame distances against time for equivalence ratios of 0.9 to 1.6 are plotted in Figure 4.11. For $\phi = 0.9$ and 1 the flame steadily traversed the length of the quartz tube. At ($\phi = 1.1, 1.2, 1.3$ and 1.4) the flames were non-uniform and began with high accelerating achieve, albeit oscillatory propagation rate down all the tube with a quasi stable for an equivalence ratio of 1.3. For $\phi = 1.5$ and 1.6 , the flame was stable and uniform, as shown in the Figure 4.11.

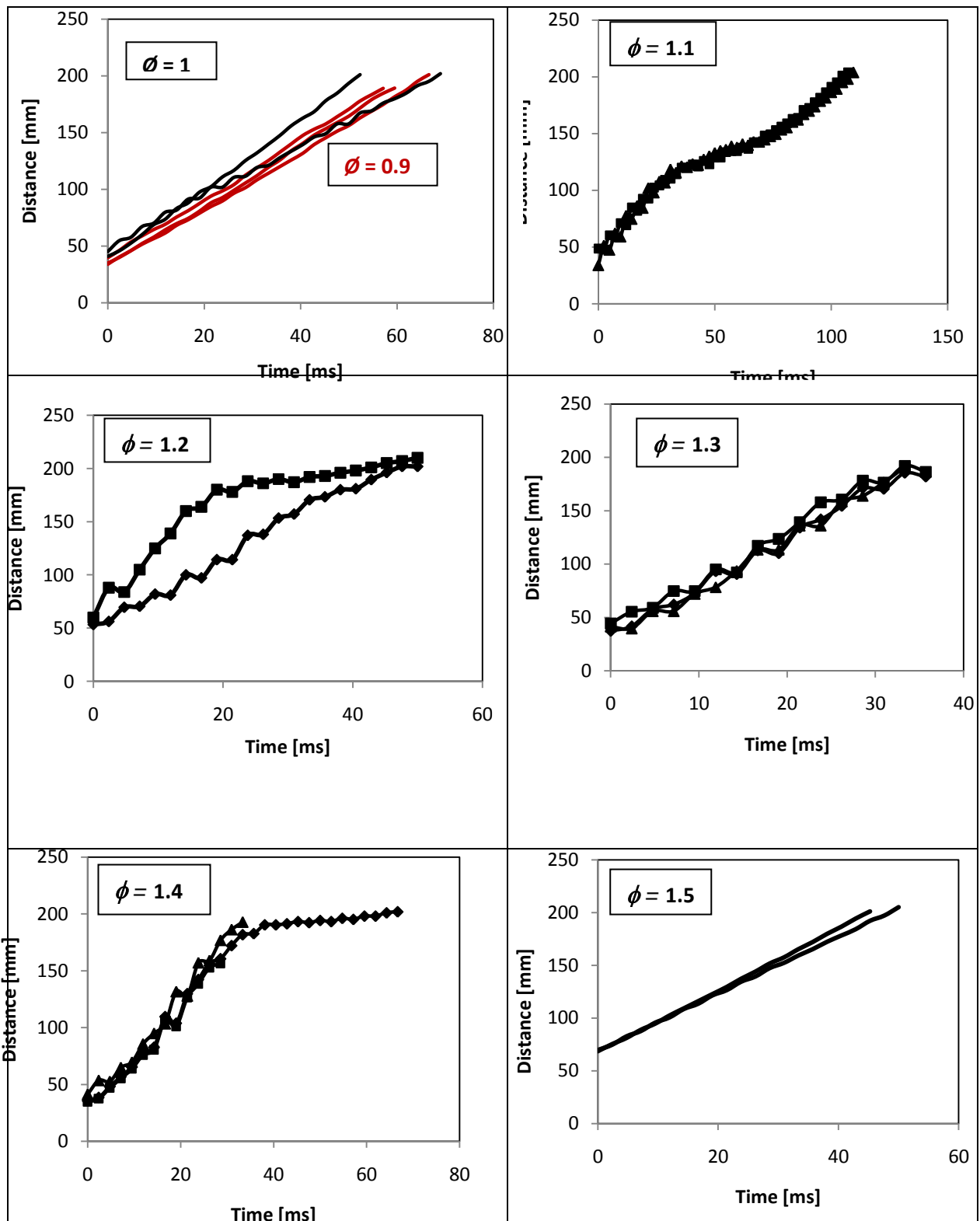
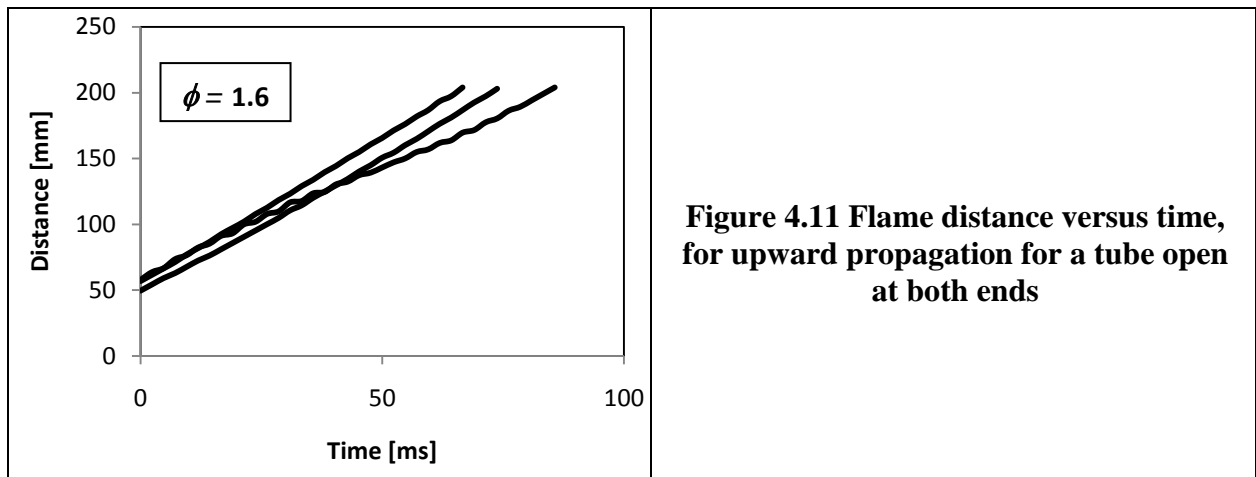


Figure 4.11 Flame distance versus time, for upward propagation for a tube open at both ends



For $\phi = 0.8$ the image appeared very weak at all attempts of repetition as shown in Figure 4.7. As a result, the image processing was unable to produce ‘clean’ images from each flame image could be obtained. An example of a processed flame shape is shown in Figure 4.12.

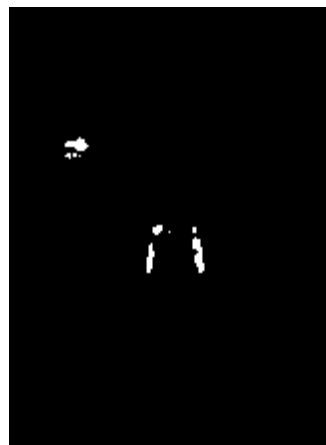


Figure 4.12 Flame propagation upward with an equivalence ratio of 0.8 at open both ends, processed by Corel Paint Shop application

The flame speed for upward propagating flames in a tube open at both ends are given in Table 4.2, with correlation coefficient and standard deviation from the fit. Shown in Figure 4.13 are the variation and the average of flame speed with equivalence ratios. It is seen the speed of the flames increase with ϕ to a maximum value at $\phi = 1.3$, where the average speed is 4.43 m/s as shown in the Table 4.2.

In vertical tubes the speed is fastest for upward and slowest for downward propagation. The speed also increases with increasing tube diameter, indicating that the ratio of combustion wave area to tube cross section increases. In non-detonable mixtures, the movement of the flame is found to remain fairly uniform over a considerable length of the tube, but beyond a critical tube diameter of 10 cm, the flow becomes turbulent [128].

Table 4.2 Flame speed variation of upward propagation

ϕ	0.8	0.9	1	1.1	1.2	1.3	1.4	1.5	1.6
Average flame speed, U_f (m/s)	-	2.58	3.1	3.58	3.78	4.43	3.65	2.89	1.98
Correlation coefficient R	-	0.999	0.997					0.999	0.999
Standard deviation of the fit (m/s)	-	0.08	0.74					0.17	0.28

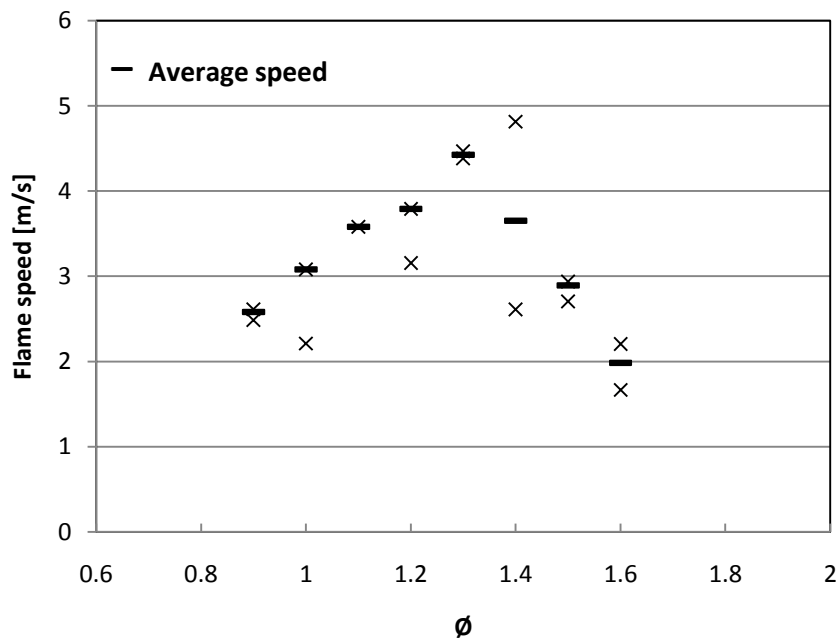


Figure 4.13 Equivalence ratio against flame speed of upward propagation at open both ends

A comparison of Table 4.1, for horizontal propagating flames with Table 4.2, for upward flame propagation, shows that the upward propagation was faster than horizontal propagation, by about 16 %, as shown in the Figure 4.14, except at an equivalence ratio $\phi = 1.2$, the observed flame speed appeared low on the vertical position. Also the peak value for flame speed was (4.4 m/s) at $\phi = 1.3$, against (4.5 m/s) at $\phi = 1.15$ for horizontal propagate flames.

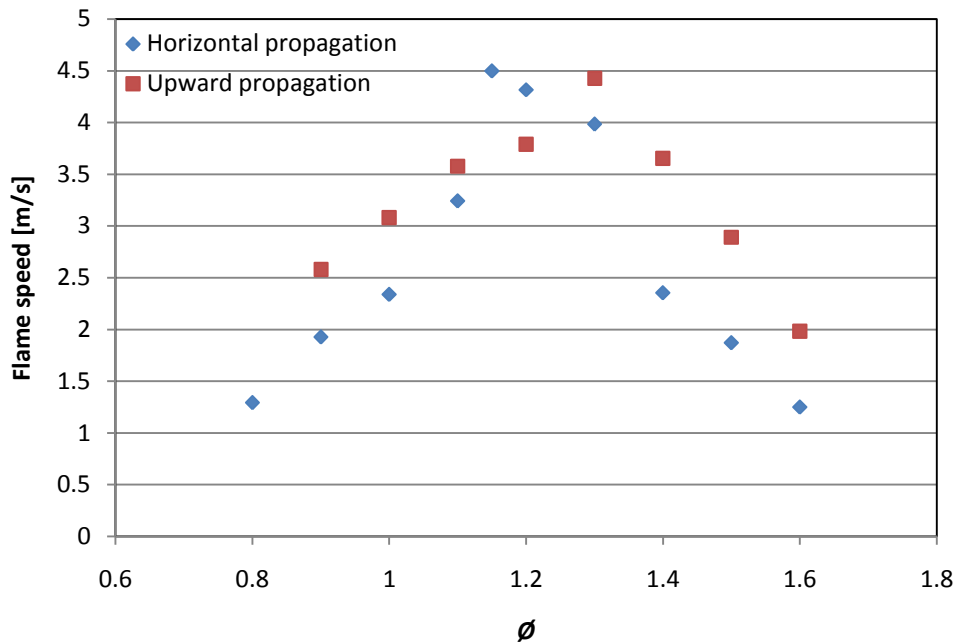


Figure 4.14 A comparison flame speed of horizontal and upward propagation in a tube open at both ends

4.2.2 Results of downward wards propagation in a vertical position with open both ends to atmosphere

There were a number of experiments conducted, with different equivalence ratios for downward propagation in a tube open at both ends. They were unsuccessful, due either because the mixture failed to ignite or the flame propagated down 25 cm of the length of the quartz tube and was then extinguishing. However, further attempts were made, by using a long gas lighter to get ignition at both the end of the tube and from inside, through the

ignition point, but this proved to be ineffective and indicates that the influence of buoyancy on the flame was occurring, due to increased heat loss and hence the failure of this experiment [62]. Also the flame is extinguished in a tube when the two mechanisms that allow flame propagation, diffusion of species and of heat are affected. This means that the two mechanisms are strongly dependent on the effective Lewis number of the deficient species. If the Lewis number is less than unity, the flame extinguishes because the rate of stretch is so large that the chemical reactions cannot go to completion. However, if it is greater than unity, extinguishment is not caused by the chemical reactions being incomplete but instead must be caused by a stretch mechanism. smaller tube leads to increase in surface area and subsequent increase in volumetric heat loss [35]. However it was found experimentally, that an increase in temperature would decrease the quenching distance. The probable reason for this that the heat losses are decreased with respect to heat release and species are not as readily deactivated [16].

4.3 Results of a horizontal tube with open both ends to the atmosphere, using high speed camera with a rating of 3000 fps.

Images of the flames roughly half way along the quartz tube under rich conditions, with high oscillations for equivalence ratios of (1.1, 1.2 and 1.3), are shown in Figure 4.15. These images were captured using the black and white camera type Phantom V210. The Figure shows that the same configurations were captured by the digital camera with a frame rate of 420 fps. The difference being that the flames are clearer. For equivalence ratios of 1.1 and 1.2, the flames were stable near to the ignition point, with a semi-ellipsoid shape and then became very short in the middle of the tube and then as can be seen, took on an elongated shape, towards the end of the tube. The flame midpoint began with mean velocities of 1.8 m/s, before accelerating and reaching a peak mean flame speed of 4.3 m/s as shown in Figure 4.4, corresponding with the maximum oscillation. The frequency of the oscillations throughout the accelerating region was found to be approximately 200 Hz. The propane is previously known to be a higher energy fuel than methane, and in this case the pressure wave produced by the combustion is also more active. The effect of the waves on the flame has been studied [59], and also the relationship between the vibration and oscillatory behaviour observed. The peak velocities are approximately 10 times higher than the laminar burning velocity. At $\phi = 1.3$ the flame shape is more clear than the configuration shapes captured by the digital camera at 420 fps. As due to speed of the flame, the colour camera images were blurred. The flame shape, with equivalence ratio 1.3, started with a semi-ellipsoid shape and elongated tail and then became deformed. The probable reason cause of this phenomenon is the interaction of the flame with the tube walls, and the mixture stream [135]. Initially starting with a convex shape and then the concave shape developed, with a couple of small humps, as shown in the Figure 4.15 for frame number 9 of $\phi = 1.2$ and frames 5 and 6 of $\phi = 1.3$. This behaviour is clearly demonstrated by the flame propagated equivalence ratio of 1.2, where the flame was stable initially and then backwards in the direction of the burned gases and produced a twin hump, as shown in the Figure 4.15, for $\phi = 1.2$. In the ninth frame of the sequence of equivalence ratio of 1.3, the front flame is roughly planar. However, there exists a long tail into burned gas which suggests the occurrence of a Rayleigh-Taylor instability, induced by a pressure gradient travelling from unburned to burned gases [140]. The oscillations were much stronger using the widener tube diameter and decreased by reducing the diameter of the tube, which increased the burning rate of mixtures [134]. However with increased burning rate, a flame front generates a larger quantity of gas per unit time. This

case occurred in the tube which closed at one end and open at the other. In this study, a tube which is open at both ends, most of the gas produced travels backwards and, as a result, the flame front acceleration is discontinued [135].

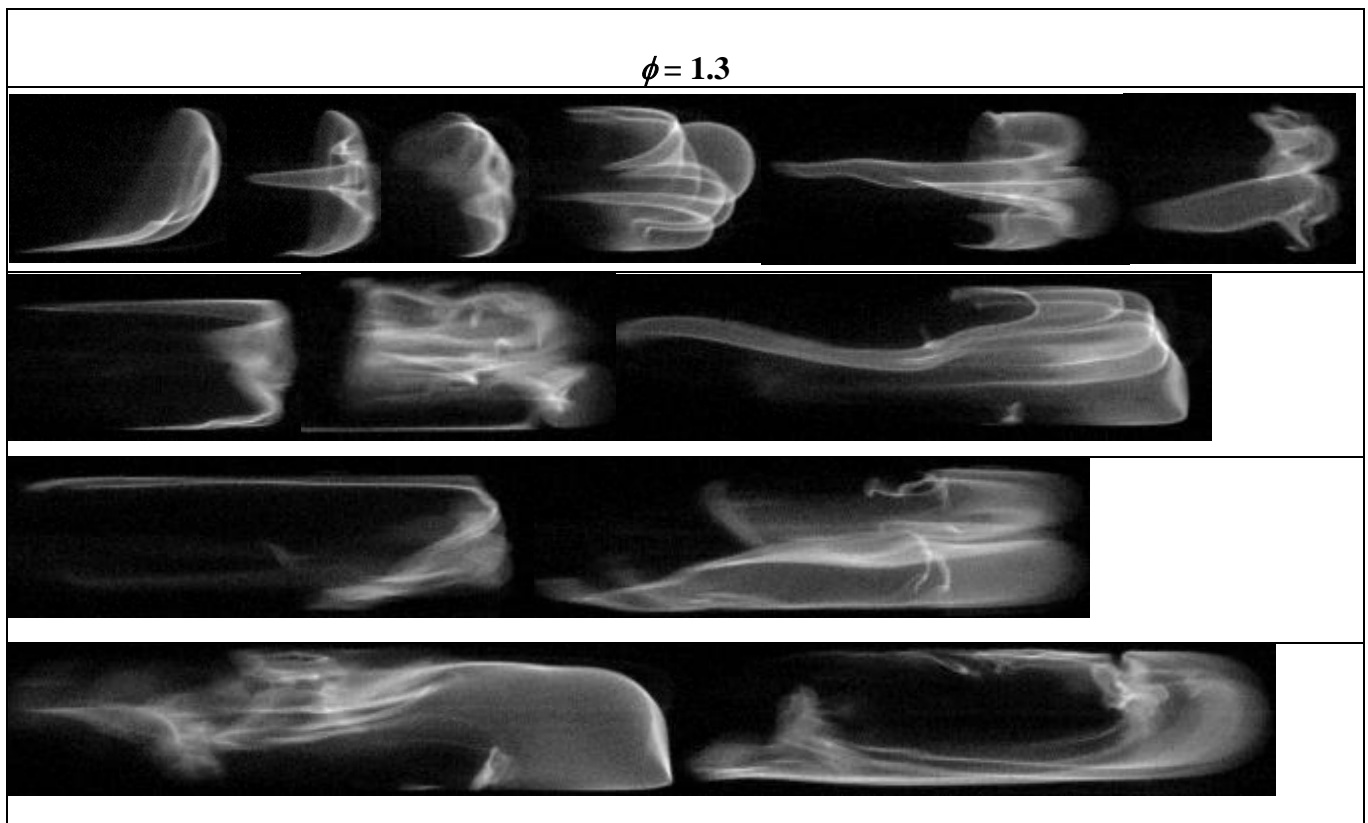
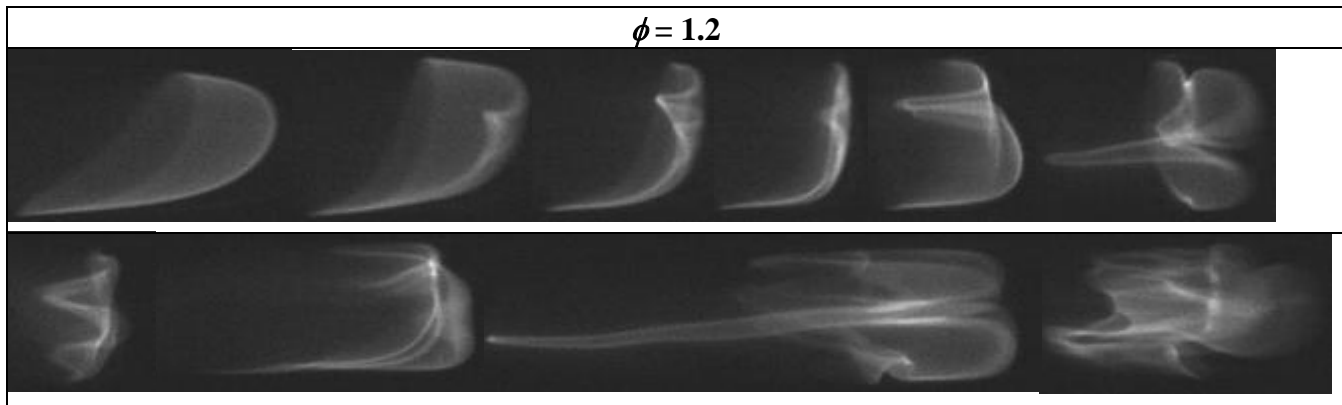
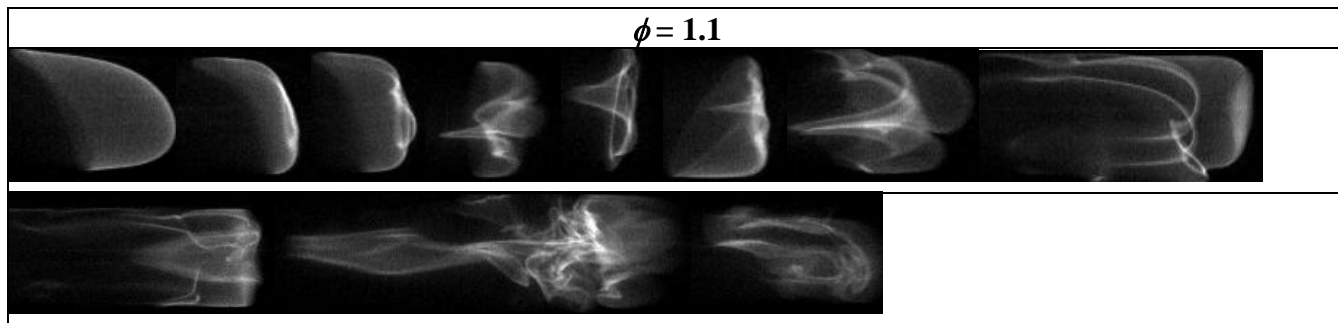


Figure 4.15 Consecutive images of flame propagating down tubes. A framing rate 3000 fps was used

Figure 4.16 shows plots of the leading edge of the flame versus time, for equivalence ratios (1.1, 1.2 and 1.3) of flames in Figure 4.15. At least 3 flames were captured for each equivalence ratio. It is clear that the all equivalence ratios have approximately the same trend down the tube, with quasi stable and non-linear flames.

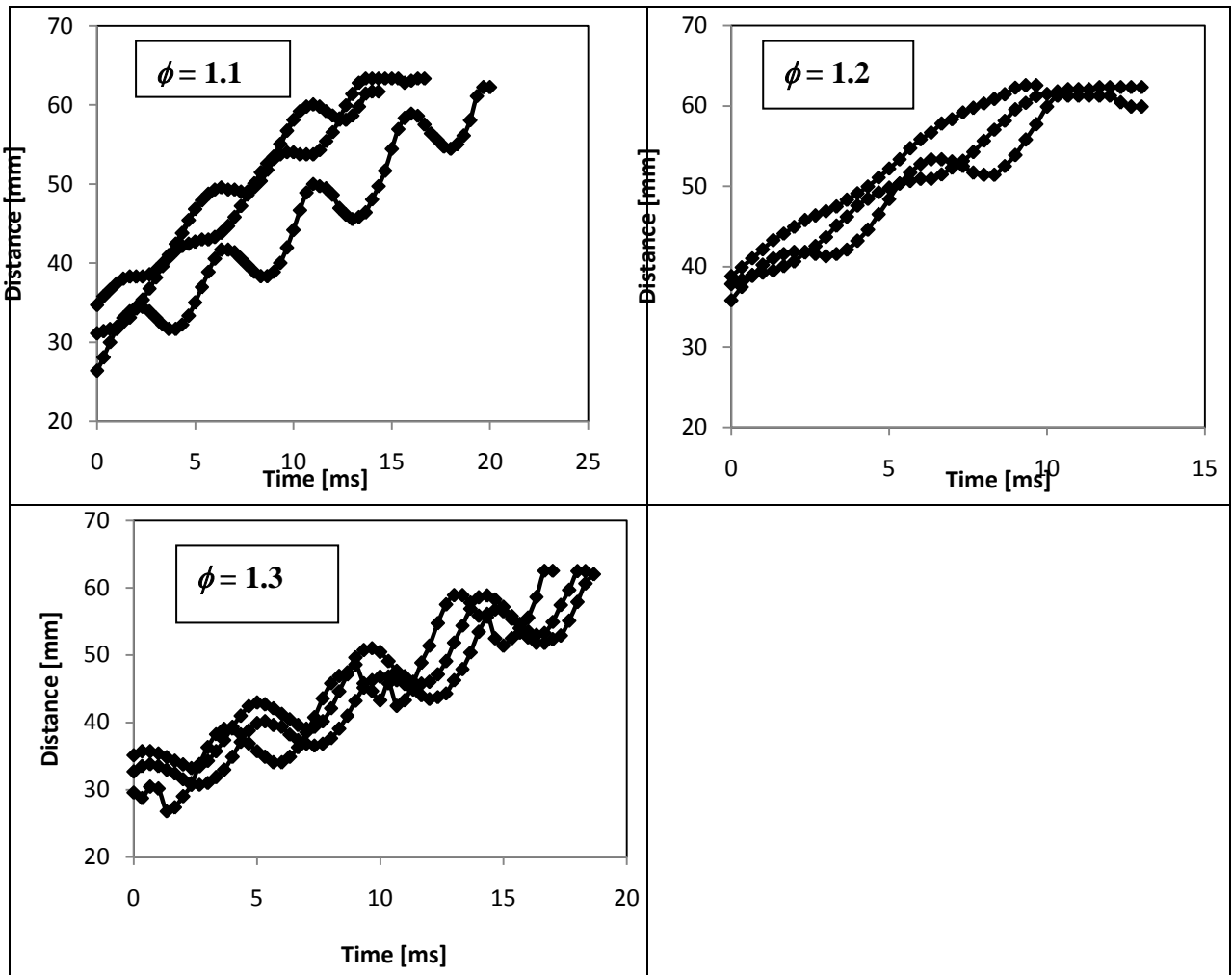


Figure 4.16 Flame distance versus time for tube open at both ends, a frame rate of 3000 fps

5 Results of flame propagation with orifice plates at both ends

In Chapter 3 the problems of pressure disturbances and resulting interaction with the flame were observed. For this reason orifice plates were placed at the ends of the tube, to absorb the pressure waves, with the result that flame propagation became more uniform.

Gerstein et al. [6] used orifice plates to increase the uniformity in their tests. They found that fitting an orifice plate near to the ignition point decreased the pressure waves in the tube [67]. In this work experiments were conducted using matched orifice plates of 8mm, 5mm, 3mm and 1mm. In addition, combinations were used by placing the larger plates at the ignition point and the smaller plates at the end towards which the flame propagated. The reason for placing a larger orifice plate at the ignition point of the flame tube has been attributed to the high temperature and velocity of the burned gas, which must be released to avoid a build up of pressure [118]. The combined configurations tested were 5mm/3mm and 5mm/1mm.

5.1 Results of horizontal tube with orifice plates at both ends

Figure 5.1 shows representative images of flames of different equivalence ratio for orifice plates of 8, 5, 3 and 1 mm. For 8 mm, flames were stable for equivalence ratios of 0.8 to 1. At large equivalence ratios their propagation was steadily until ~40 cm from the point of ignition where the flames became oscillatory as the holes were widened too much, as a result the orifices must not have had enough structure to absorb the pressure waves, as shown in Figure 5.2 for $\phi = 1.3$. The flames were initially tilted, then became more semi-ellipsoid in the second half of the tube (for example see frame 67). For orifice plates of 5mm, 3mm and 1mm the flames were all roughly the same; tipped semi-ellipsoids and propagated steadily for all equivalence ratios. The only exception was $\phi = 1.6$ with orifice plates of 3 mm where the flames were steady and tilted with a slightly longer tail. The flames with smallest orifice plate of 1 mm size again were tipped and semi-ellipsoid for equivalence ratios of 0.9 to 1.2. However, at $\phi = 1.3$ the flames became elongated and titled. For $\phi = 1.4, 1.5$ and 1.6 the flames lengthened, were tilted and had thin flame fronts.

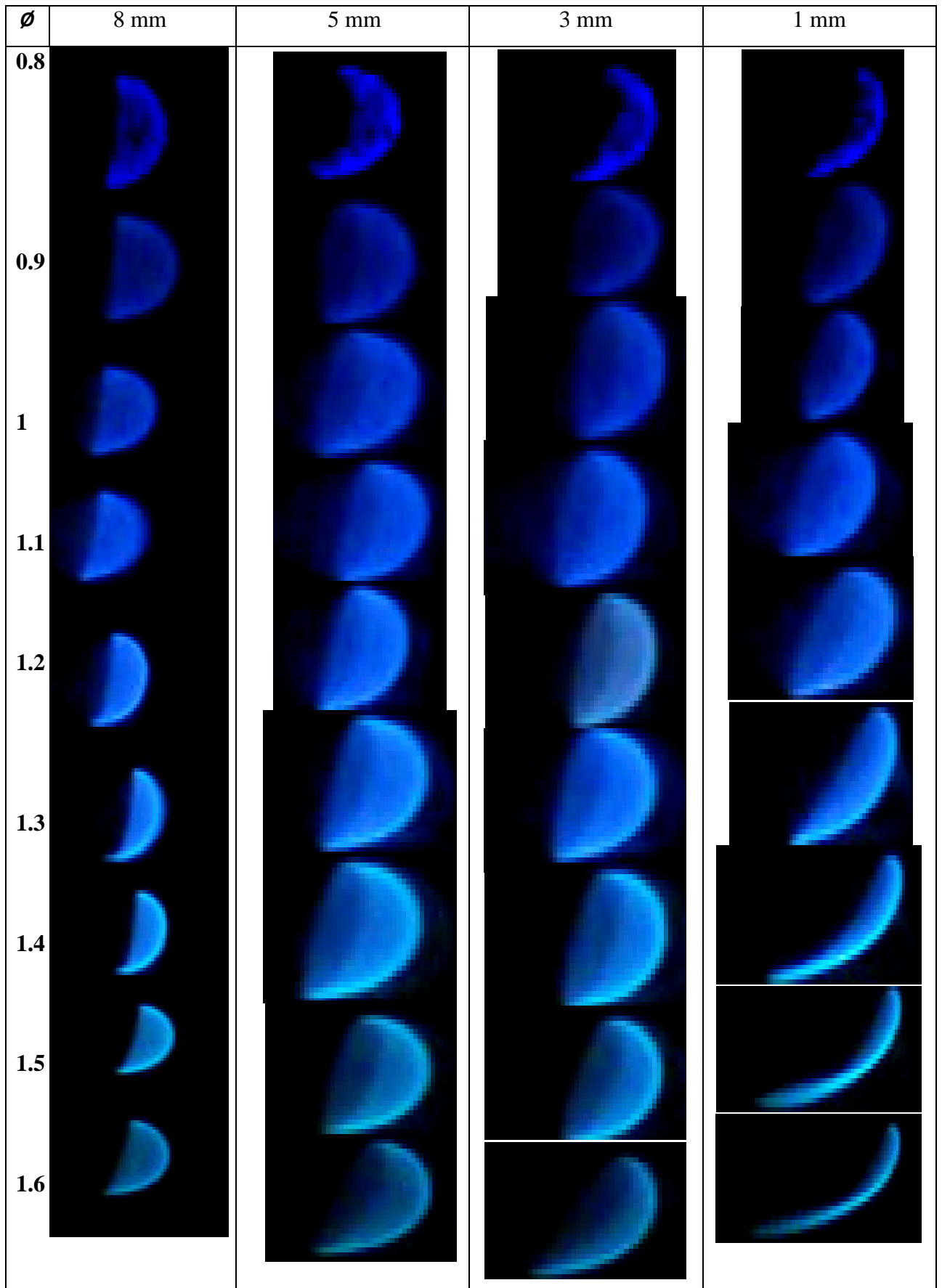


Figure 5.1 Flame shape across equivalence ratios of 8, 5, 3 and 1 mm orifice plates

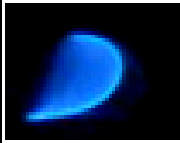
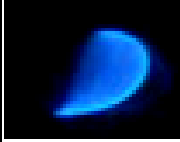
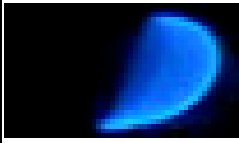
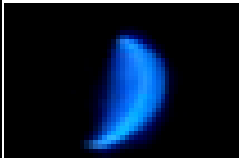
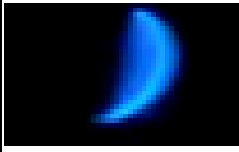
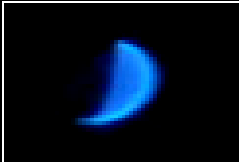
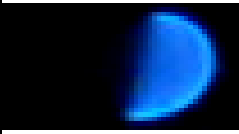
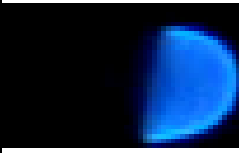
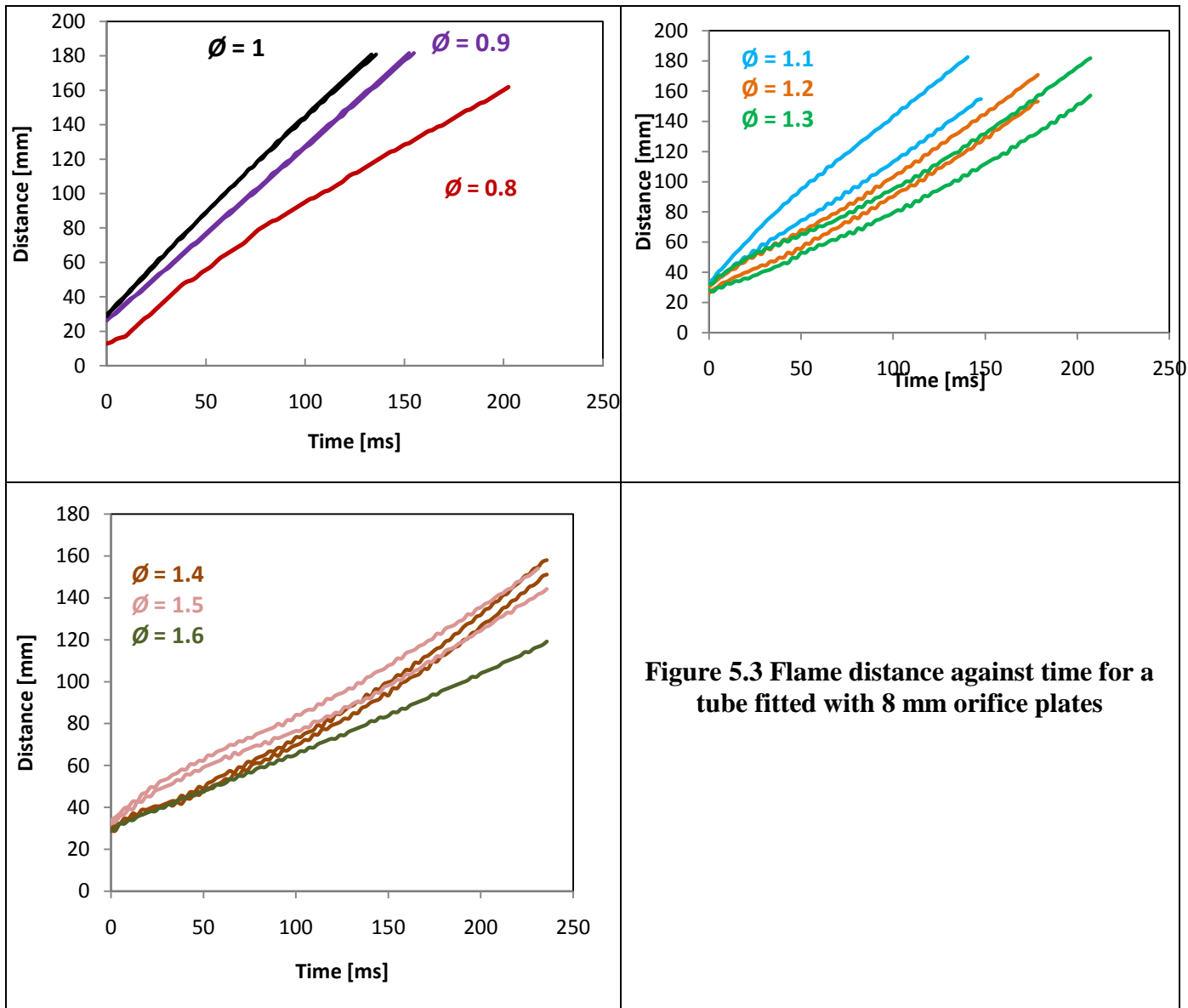
Frame	Images
1	
3	
5	
29	
31	
33	
65	
67	

Figure 5.2 Images of flame propagation down tube with orifice plates of 8 mm at both ends. Mixture equivalence ratio = 1.3

Flame distance against time plots and presented in Figure 5.3 for the two repetitions of each equivalence ratio, for orifice plates of 8 mm. For $\phi = 0.9 - 1$ and 1.6 the flames moved with a constant velocity, resulting in straight lines; however the flames of $\phi = 1.1$ to 1.5 did not propagate at a constant velocity, as shown in the Figure 5.3. This resulted in lower correlation coefficients and higher deviations as shown in Table 5.1.



Distance against time plots for orifice plates of 5, 3 and 1 mm are presented in Figures 5.4, 5.5 and 5.6. The flames generally propagated at constant speed resulting in linear plots. Tables 5.2, 5.3 and 5.4 confirm this.

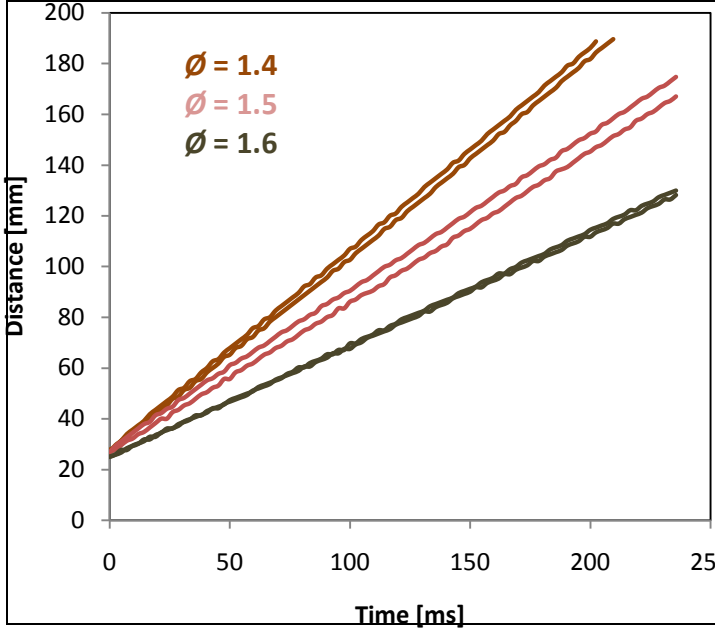
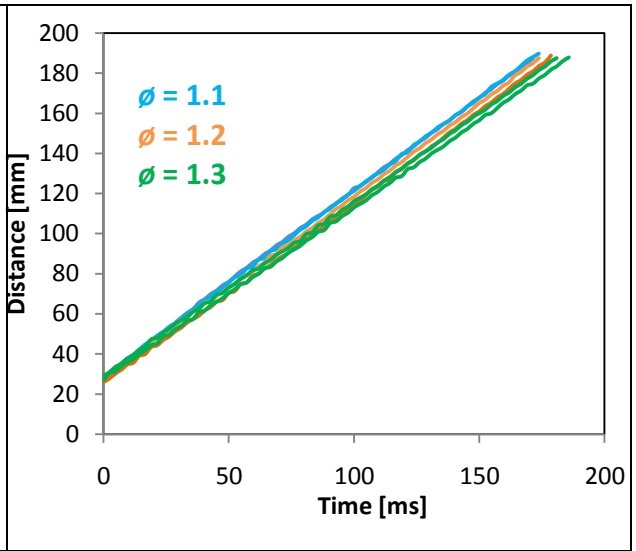
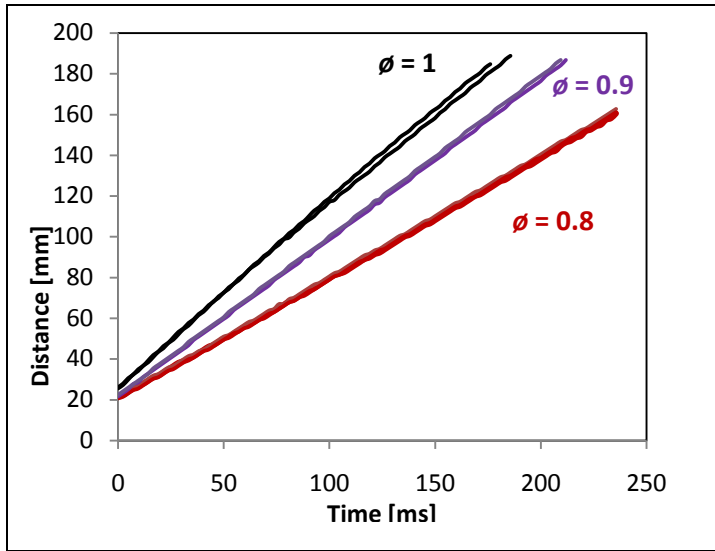


Figure 5.4 Flame distance against time for a tube fitted with 5 mm orifice plates

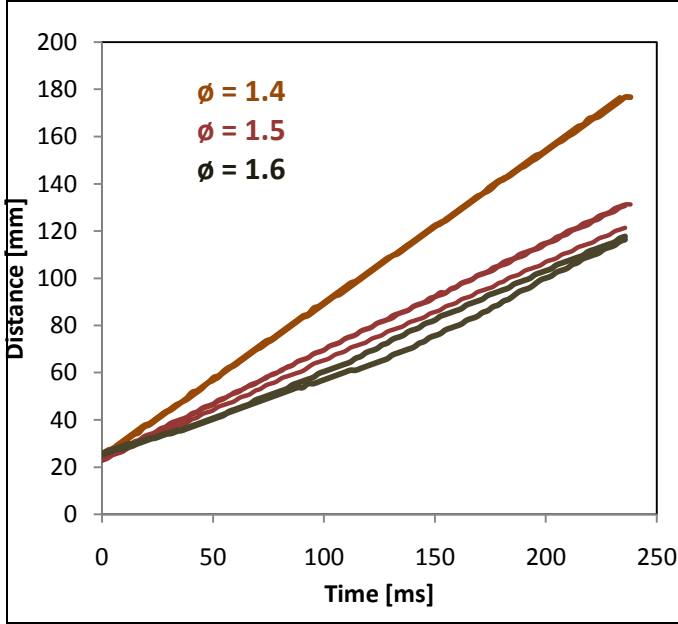
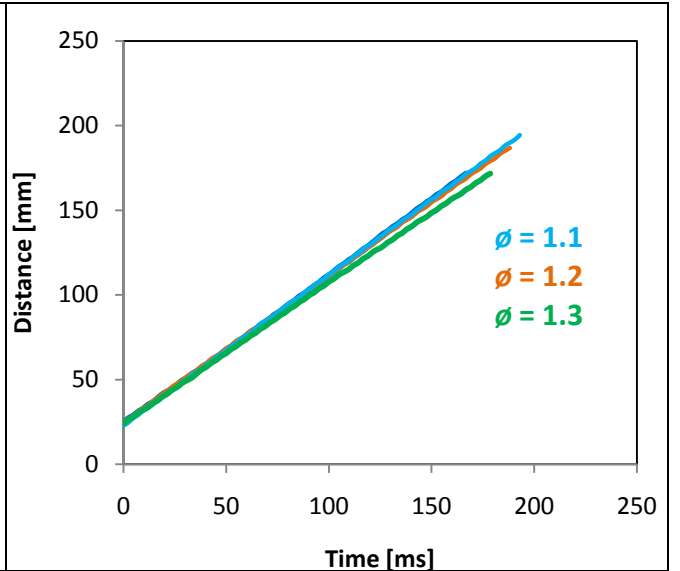
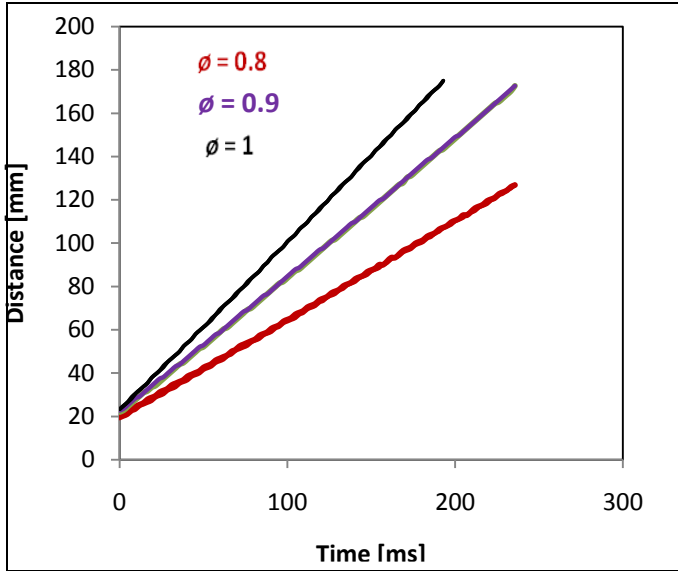


Figure 5.5 Flame distance against time for a tube fitted with 3 mm orifice plates

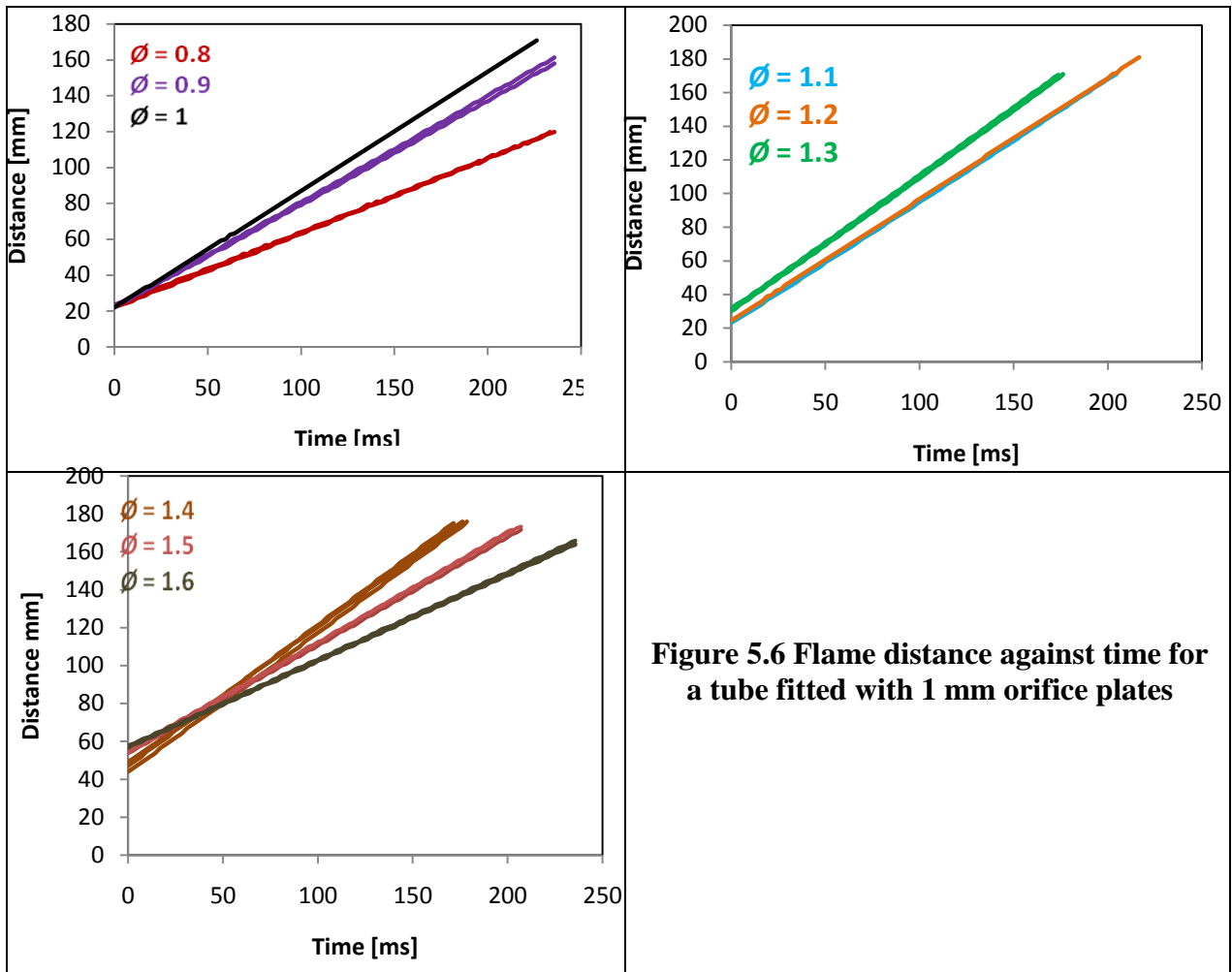


Figure 5.6 Flame distance against time for a tube fitted with 1 mm orifice plates

Figure 5.7 shows the shape of flame propagation for equivalence ratio ranges, from 0.8 to 1.6, with orifice plates of 5/3 and 5/1 mm. For 5/3 mm orifice plates, the flames were tilted for equivalence ratios from 0.8 to 1.5, whilst $\phi = 1.6$ was tilted with an elongated and thin flame front. At all equivalence ratios, the flame shapes were similar to those of the experiments performed using orifice plates of 3 mm at both ends of the tube.

However, for 5/1 mm orifice plates, the equivalence ratios of 0.8 to 1.2 the flames were more tilted but roughly hemispherical. For equivalence ratios 1.3 to 1.6 the flames were increasing tilted forward and very elongated with thin flame fronts.

From the observation in the experiments, the flame shape reported for orifice plates of 5/1 mm was similar to those with 1 mm orifice plates.

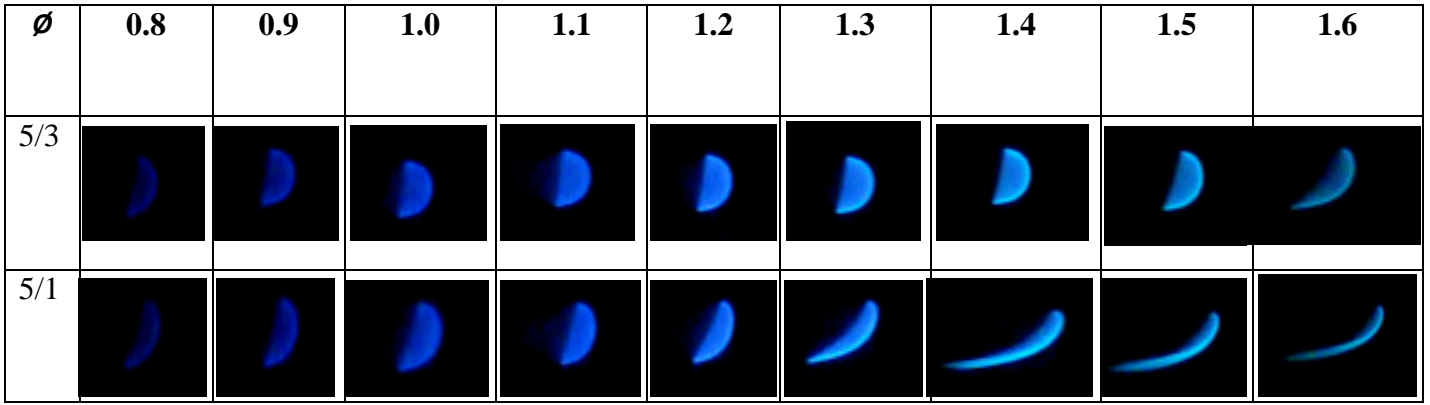


Figure 5.7 Flame shape across equivalence ratios of 5/3 and 5/1 mm orifice plates

Tables 5.2, 5.3 and 5.4 shows that the propagation of flames in a tube with orifice plates can be considered occur at constant velocity. The correlation coefficients R were good with values close to one.

Table 5.1 Velocities and correlation data for least squares linear fits for tube with 8 mm orifice plates

ϕ	0.8	0.9	1	1.1	1.2	1.3	1.4	1.5	1.6
Average flame speed, U_f (m/s)	0.97	1.01	1.15	0.97	0.74	0.66	0.54	0.49	0.39
Correlation Coefficient-R	0.992	1	0.999	0.997	0.993	0.991	0.986	0.993	0.998
Standard deviation of the fit (m/s)	0.004	0.005	0.03	0.11	0.04	0.03	0.03	0.02	0.06

Table 5.2 Velocities and correlation data for least squares linear fits for tube with 5 mm orifice plates

ϕ	0.8	0.9	1	1.1	1.2	1.3	1.4	1.5	1.6
Average flame speed, U_f (m/s)	0.52	0.78	0.91	0.96	0.93	0.87	0.78	0.59	0.43
Correlation Coefficient-R	0.999	1	0.999	0.999	0.999	0.999	0.999	0.999	0.999
Standard deviation of the fit (m/s)	0.01	0.01	0.02	0.01	0.01	0.01	0.01	0.02	0.01

Table 5.3 Velocities and correlation data for least squares linear fits for tube with 3 mm orifice plates

ϕ	0.8	0.9	1	1.1	1.2	1.3	1.4	1.5	1.6
Average flame speed, U_f (m/s)	0.48	0.64	0.79	0.88	0.87	0.82	0.65	0.44	0.39
Correlation Coefficient-R	0.999	0.999	1	0.999	1	1	0.999	0.999	0.99
Standard deviation of the fit (m/s)	0.04	0.01	0.002	0.01	0.002	0.01	0.01	0.02	0.01

Table 5.4 Velocities and correlation data for least squares linear fits for tube with 1 mm Orifice Plates

ϕ	0.8	0.9	1	1.1	1.2	1.3	1.4	1.5	1.6
Average flame Speed, U_f (m/s)	0.41	0.57	0.66	0.72	0.73	0.79	0.74	0.57	0.45
Correlation Coefficient-R	0.999	0.999	0.999	1	1	0.999	1	0.999	0.999
Standard deviation of the fit (m/s)	0.01	0.02	0.001	0.002	0.02	0.002	0.01	0.01	0.004

Flame speeds for all equivalence ratios and the four orifices are shown in Figure 5.8. The experiments performed with orifice plate of 5 mm had almost the same maximum flame speed as that obtained by Gerstien et al. [6], who found the peak flame speed to be approximately 0.99 m/s at $\phi = 1.1$ (as shown in Appendix L), while in the present work, it was about 0.96 m/s both at the same equivalence ratio. These results confirmed that the flame speed in a small diameter tube is less than in the large tube diameter [18, 111]. Where Gerstien et al. used a tube with outer diameter of 28 mm, in this work; the outer diameter was about 25 mm. Also, the main reason for this reduction is due to the effect of orifice plates. The flame speeds in tubes with orifice plates are however lower than the flame speeds in tube which are open both ends.

For orifice plates of 3 and 1 mm, the flame speeds decreased, and were ~ 0.88 and 0.72 m/s at $\phi = 1.1$ but the peak flame speed; with an average of 0.80 m/s, occurred at $\phi = 1.3$ for orifice plates of 1 mm. For the case of 1 mm orifice plates the flames became elongated under rich conditions (equivalence ratios of 1.4 to 1.6) as shown in Figure 5.1, resulting in an increased surface area and hence flame speed.

The flame speed results, using 8 mm orifice plates, are shown in the Figure 5.8. The flame speed was highest for these plates for equivalence ratios of 0.8 to 1.1. A peak flame speed of 1.15 m/s occurred at an equivalence ratio of 1.0. For equivalence ratios of 1.2 to 1.6, the flame speed was slower than for the smaller 5 and 3 mm orifice plates. This decrease in flame speed may be due to wall quenching, but also may be due to increases or changes in the pressure of the unburnt gases [5]. The configurations of orifice plates of 5/3 and 5/1 mm were nearly the same results as for orifice plates of 3 and 1 mm as shown in the Figure 5.9.

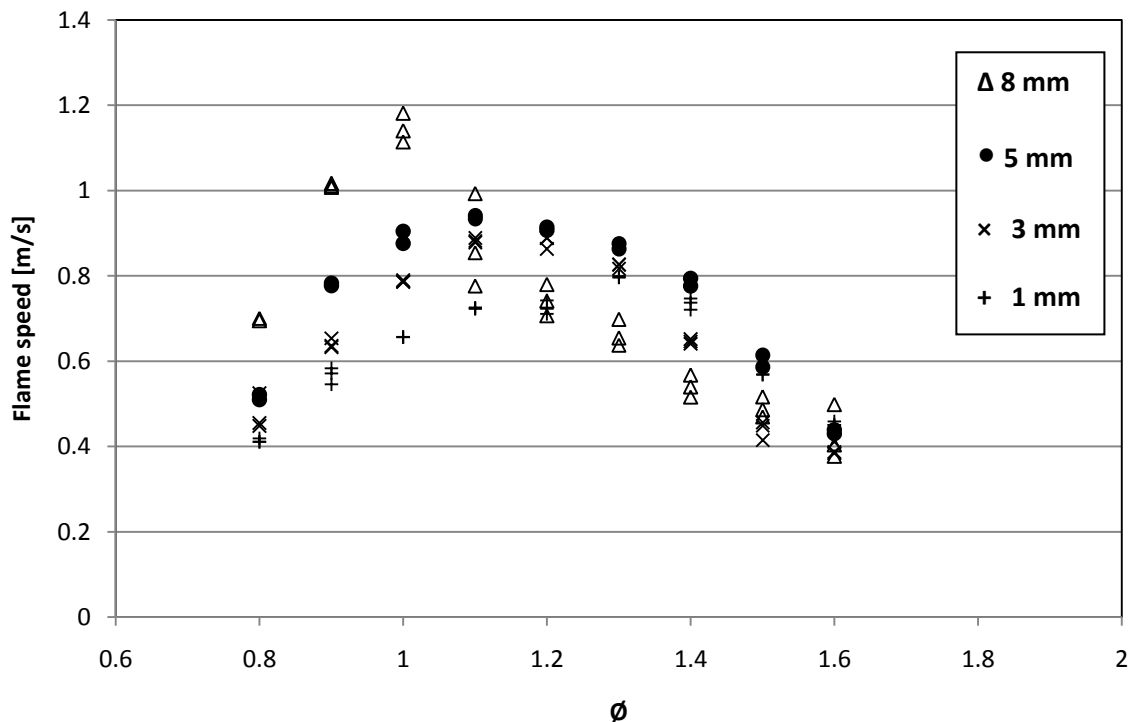


Figure 5.8 Flame speeds with the various orifice plates in flame tube

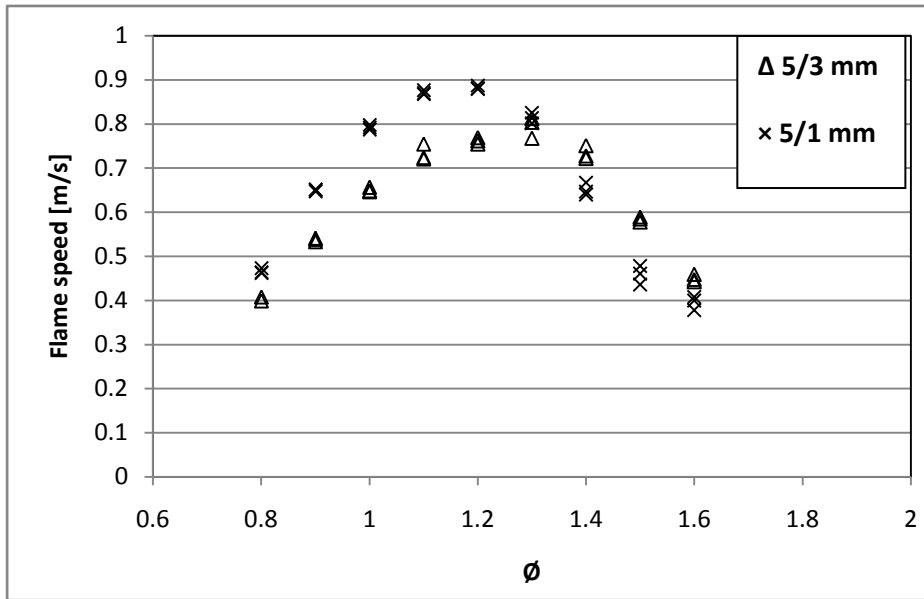


Figure 5.9 Flame speeds with the combination orifice plates in flame tube

These experiments can be compared with those of other workers. On the same rig Mallard [127] and Kat Kiu [141] achieved maximum flame speeds of up to 0.90 and 0.95 m/s respectively. Their results are similar to the maximum flame speeds recorded in this work for orifice plates of 5 mm, which was about 0.96 m/s.

5.2 Results of upwards and downwards propagation in a vertical tube, with orifice plates at both ends.

The experimental apparatus in its vertical configuration is shown in Figure 5.10. These experiments were conducted using orifice plates of 1 and 5 mm at both ends, the equivalence ratios varied from 0.8 to 1.6. Ambient temperature and pressure was used for all runs.

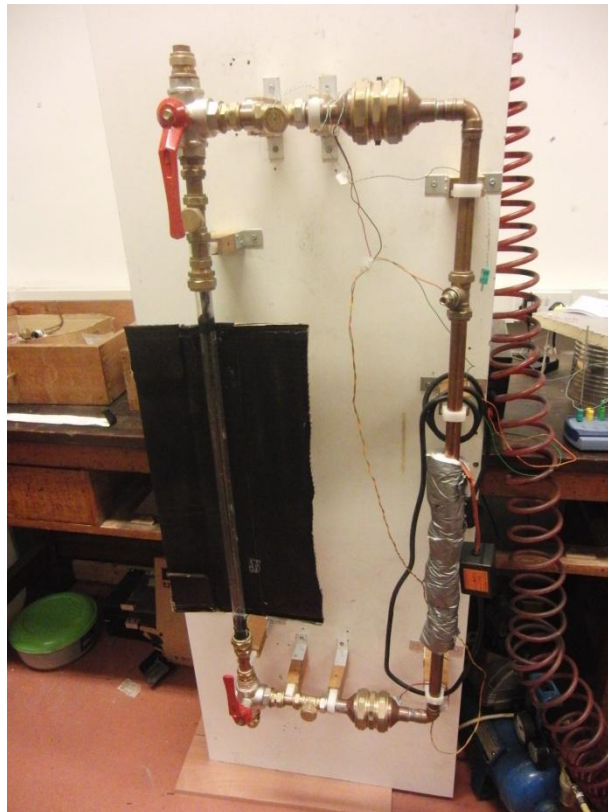


Figure 5.10 Vertical experimental apparatus

5.2.1 Upwards propagation in a vertical tube with 5 mm orifice plate at both ends

Typical images of the flame shape for upwardly propagating propane-air flames are shown in Figure 5.11. For $\phi = 0.8$ to 1, the flames were roughly hemispherical. For $\phi = 1.1$ to 1.4 the flames were approximately semi-ellipsoid but noticeably tilted. For equivalence ratios of 1.5 and 1.6, the flames were semi-ellipsoid in shape. The flames propagated steadily along the whole tube.

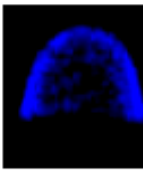
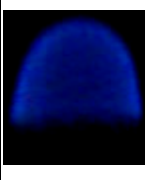
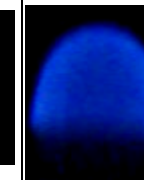
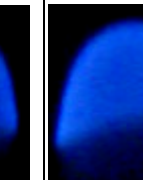
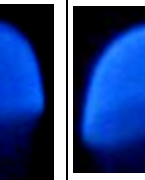
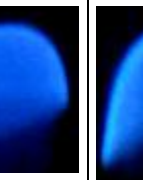
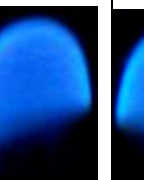

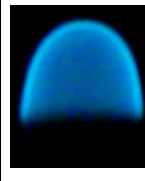
ϕ	0.8	0.9	1.0	1.1	1.2	1.3	1.4
							
	1.5	1.6					
							

Figure 5.11 Upwards propagation flame shape across equivalence ratios of 5 mm orifice plates

Distance against time plots with orifice plates of 5 mm are shown in Figure 5.12. The flames propagated at a constant velocity, resulting in straight lines. The propagation speed, correlation coefficient and standard deviation from the fit are given in the Table 5.5.

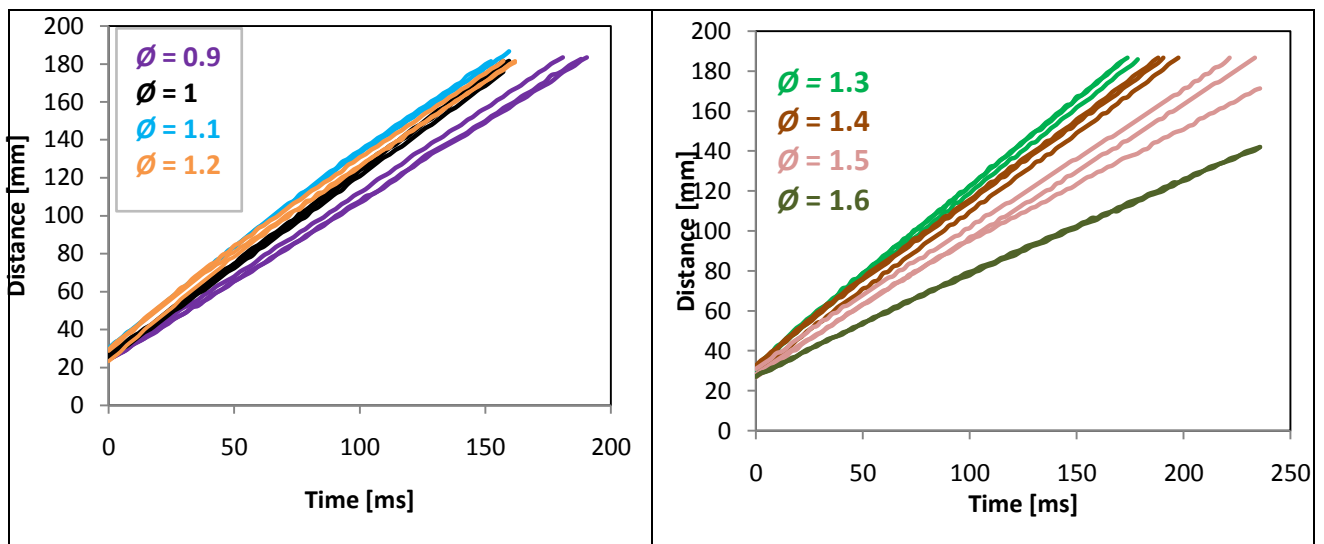


Figure 5.12 Flame distance against time of orifice plate 5 mm, at upward propagation

Table 5.5 Flame speed variation in test data 5 mm orifice plates of upward propagation

ϕ	0.8	0.9	1	1.1	1.2	1.3	1.4	1.5	1.6
Average flame speed, U_f	-	0.85	0.97	0.98	0.96	0.88	0.81	0.66	0.51
Correlation Coefficient- R	-	0.999	0.999	0.998	0.998	0.999	0.999	0.999	0.999
Standard deviation of the fit (m/s)	-	0.01	0.02	0.02	0.01	0.02	0.004	0.06	0.002

Figure 5.13, shows the flame speed with various equivalence ratios for upward propagation with 5 mm orifice plates. The peak propagation speed occurs at equivalence ratio of 1.1 and is 0.98 m/s.

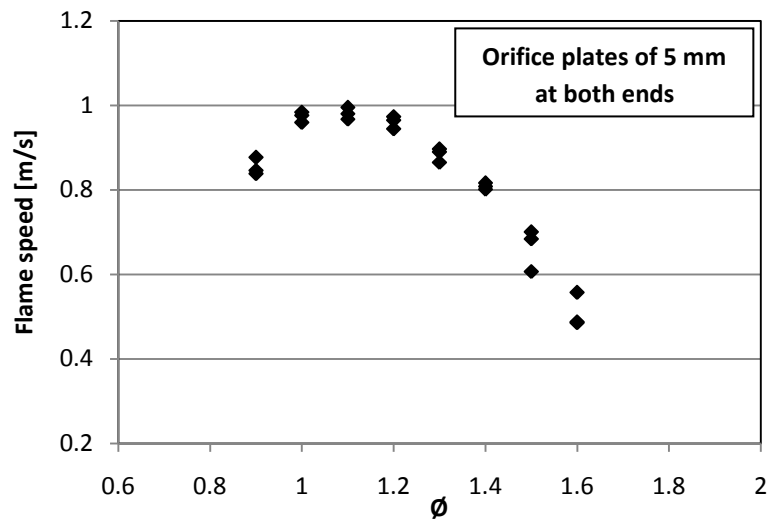


Figure 5.13 Flame speed with a range of equivalence ratios for upward propagation in a vertical tube with 5 mm orifice plate

Figure 5.14 compares horizontal and upward propagation with matching 5 mm orifices. The upwardly propagating flames were slightly faster than horizontal flames, for all equivalence ratios, due to the influence of gravity [63]. Mason and Wheeler [59] stated that the horizontally propagated flames were slower than the upwardly propagated, owing to the flame front shape which is an elliptical during propagating horizontally, while it is in a spherical shape when travelling upwards. For this reason the surface flame area is larger,

when travelling upward than when travelling horizontally. Thus the wall cooling effect of the tube becomes greater [59].

Downward propagation of flames for a 5 mm orifice plate was also investigated, but although the mixture ignited, it extinguishing before reaching the middle of the tube (at about 20 cm from the ignition point).

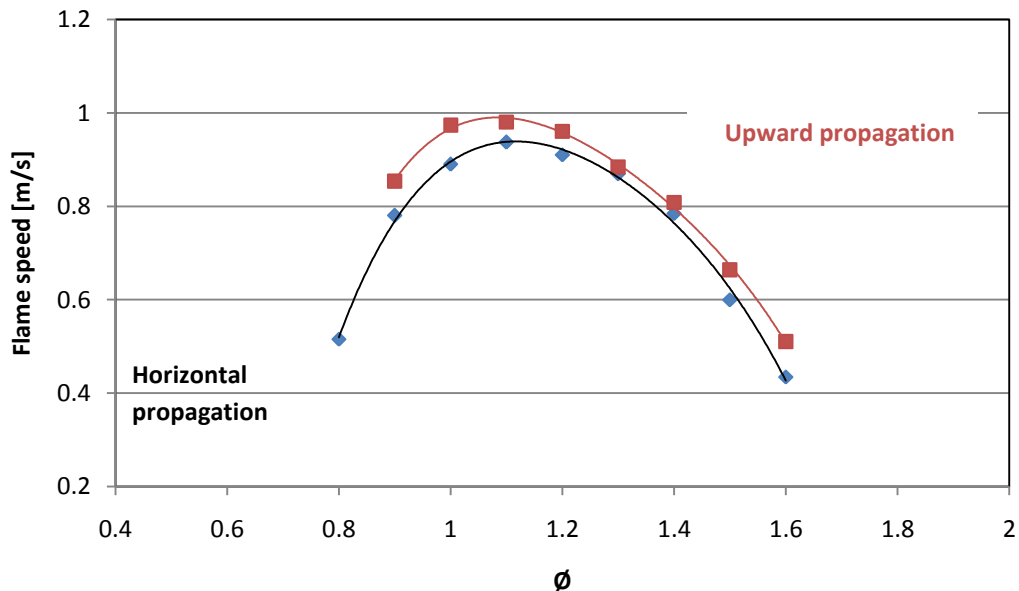


Figure 5.14 A comparison of horizontal and vertical propagation in tube

5.2.2 Upwards propagation in a vertical tube with 1 mm orifice plate at both ends

The flame shapes observed with orifice plates of 1 mm are shown in Figure 5.15. For $\phi = 0.8$ to 1.3, flames propagating in the upward direction were approximately hemispherical and moved steadily over the length of the tube as you seen in the Figure 5.15. For $\phi = 1.4$ to 1.6 the flame propagation remained stable, with an elongated, tipped shape.

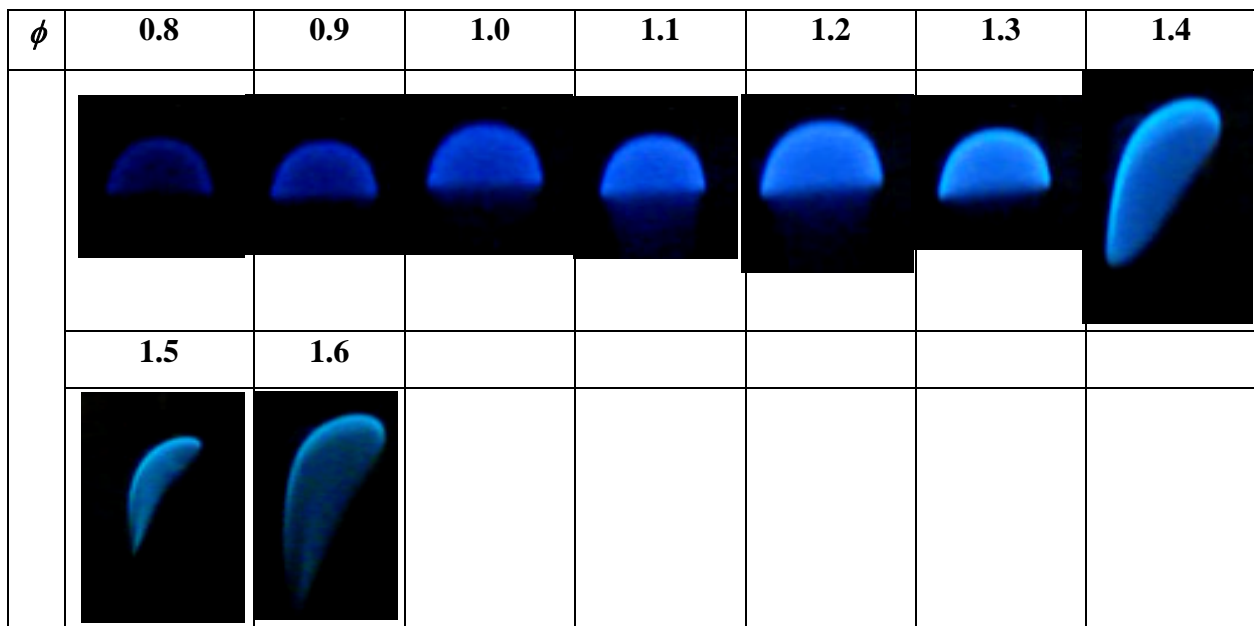


Figure 5.15 Images of flames propagating upward with orifice plate of 1 mm at various equivalence ratios

Flame distances are plotted in Figure 5.16. The flame propagated upwards for all equivalence ratios was steady along the length of the quartz tube.

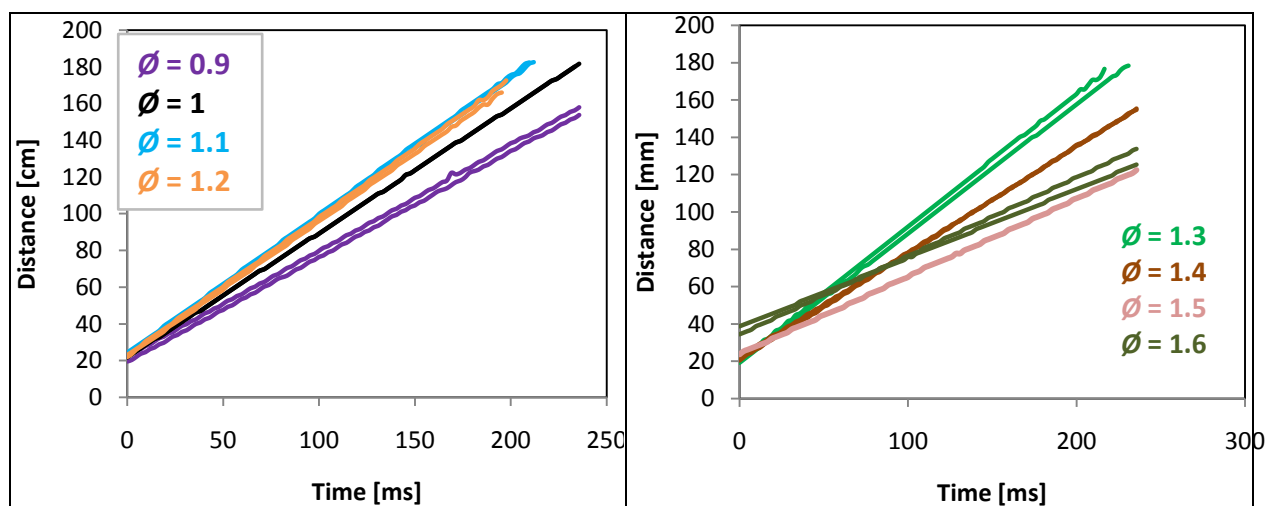


Figure 5.16 Flame distance against time of orifice plates 1 mm, at upwards propagation

The flame speeds are shown in Table 5.6 along with the correlation coefficient and standard deviation from the linear fit. Figure 5.17 shows the flame speed with a various equivalence ratios for upward propagation of 1 mm orifice plates, the peak flame speed was 0.75 m/s at $\phi = 1.1$.

Table 5.6 Flame speed variation in test data 1 mm orifice plates of upward

ϕ	0.8	0.9	1	1.1	1.2	1.3	1.4	1.5	1.6
Average flame speed, U_f (m/s)	-	0.57	0.68	0.75	0.74	0.70	0.56	0.47	0.36
Correlation Coefficient-R	-	0.999	1	1	0.999	0.999	0.999	0.999	0.999
Standard deviation of the fit (m/s)	-	0.003	0.0002	0.003	0.01	0.02	0.01	0.01	0.01

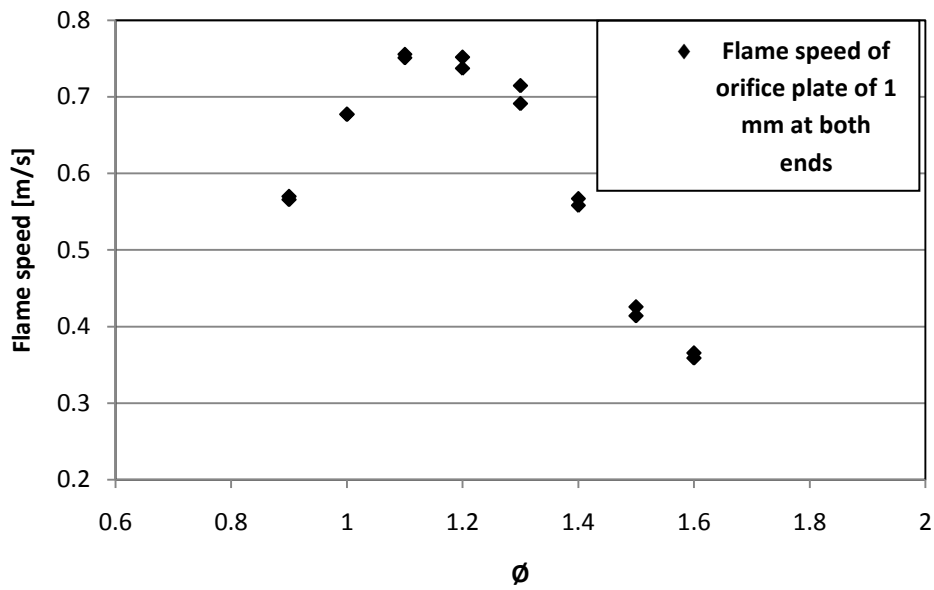


Figure 5.17 Flame speed with a range of equivalence ratios for upward propagation of 1 mm orifice plate

5.2.3 Downwards propagation in a vertical tube with 1 mm orifice plates

Images of flame shape for a propane-air mixture at a range of ϕ from 0.8 to 1.6, propagation downwards in the tube, with orifice plates of 1 mm at both ends, are shown in Figure 5.18. The flames of equivalence ratios from 0.8 to 1.2 remain smooth, with a hemispherical shape. However for $\phi = 1.1$ and 1.2 the flames propagated steadily with the hemispherical shape until approximately 50 cm from the point of ignition, where they became corrugated as can be seen in the Figures 5.19 and 5.20. The flame shape is almost flat with cellular structure. This phenomena may have occurred due to the influence of diffusive-thermal [142], or hydrodynamic instabilities [143]. For equivalence ratios from 1.3 to 1.5 the flames are tipped, with thick frontal shapes and became more elongated, at an equivalence ratio of 1.6, with a thin frontal shape. In downward propagation, the flame is markedly affected by gravity [63].


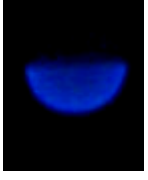
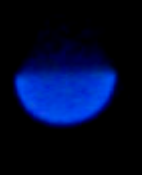

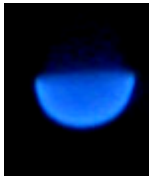
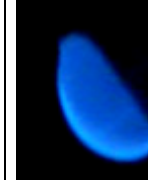
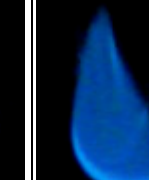


ϕ	0.8	0.9	1.0	1.1	1.2	1.3	1.4
							
	1.5	1.6					
							

Figure 5.18 Images of flames propagating downward with orifice plate of 1 mm at various equivalence ratios

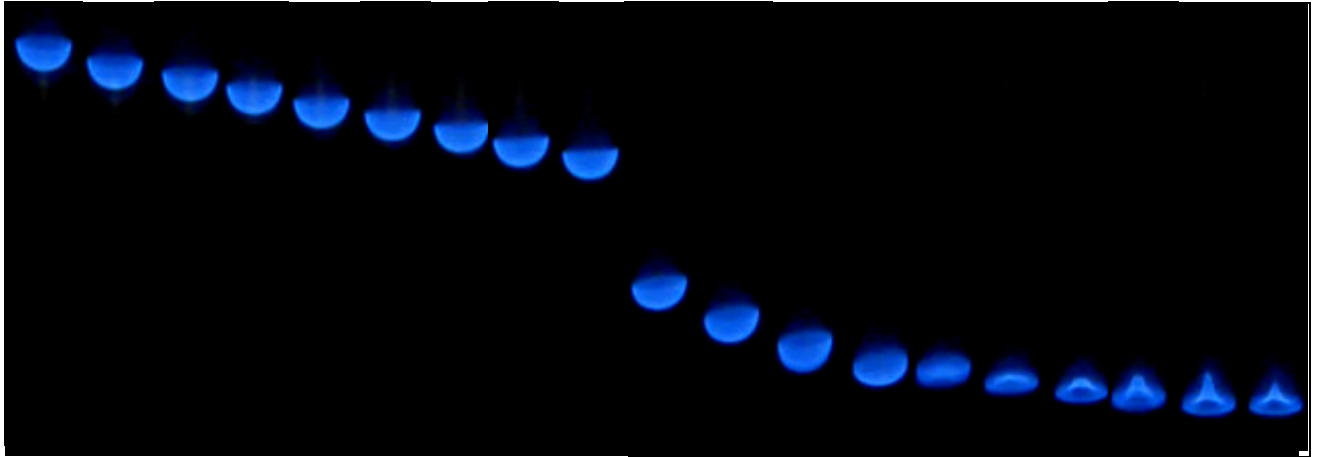


Figure 5.19 Images of flame propagating downward in the tube. Mixture equivalence ratio = 1.2, with orifice plate of 1 mm

In Figure 5.20 the distance is plotted against time for the downward propagating flame of propane-air mixture, at a range of equivalence ratios. As the plots are roughly linear, the flame travelled at a constant speed down the tube except at ϕ of 1.1 and 1.2 in the second part of the tube where fluctuations in the speed can be seen.

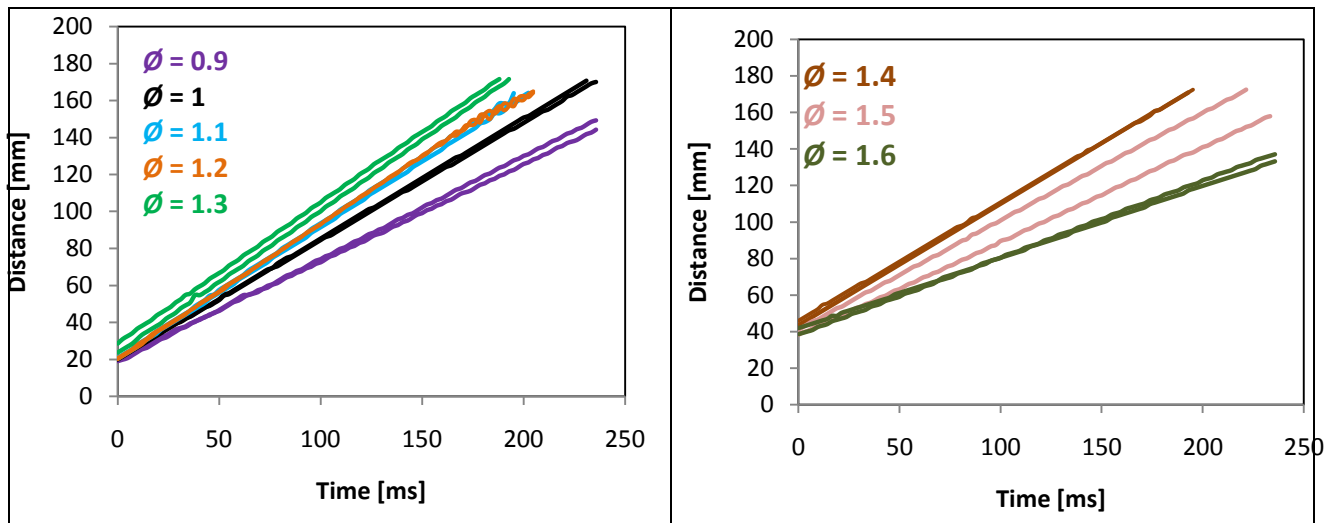


Figure 5.20 Flame distance against time of orifice plate 1 mm, at downwards propagation

The averaged values of flame speed observed with correlation coefficient and standard deviation of the fit are shown in the Table 5.7.

Table 5.7 Flame speed variation in test data 1 mm orifice plates of downward

ϕ	0.8	0.9	1	1.1	1.2	1.3	1.4	1.5	1.6
Average flame speed, U_f (m/s)	-	0.53	0.64	0.71	0.70	0.65	0.56	0.51	0.33
Correlation coefficient-R	-	0.999	1	0.999	0.999	1	1	0.999	0.999
Standard deviation of the fit (m/s)	-	0.02	0.01	0.02	0.002	0.003	0.05	0.03	0.01

The results obtained from the propagation speed of upward and downward flames, with a range of equivalence ratios from 0.9 to 1.6, are shown in the Figure 5.21. The maximum flame speed was 0.75 and 0.71 m/s at an equivalence ratio of 1.1 for both upward and downward propagation, respectively, as shown in Table 5.7. It can be seen that in the Figure 5.21 the upward propagation for orifice plates of 1 mm was faster than for downward propagating flames, as a result of gravitational effects on these flames [63]. A comparison of Figures 5.21 and 5.13 shows that the flame speed obtained from upward propagation with orifice plates of 5 mm is slightly higher than the flame speed of orifice plate 1 mm. Corrugations were observed in the images for equivalence ratios of 1.1 and 1.2 for orifice plates of 1 mm [63].

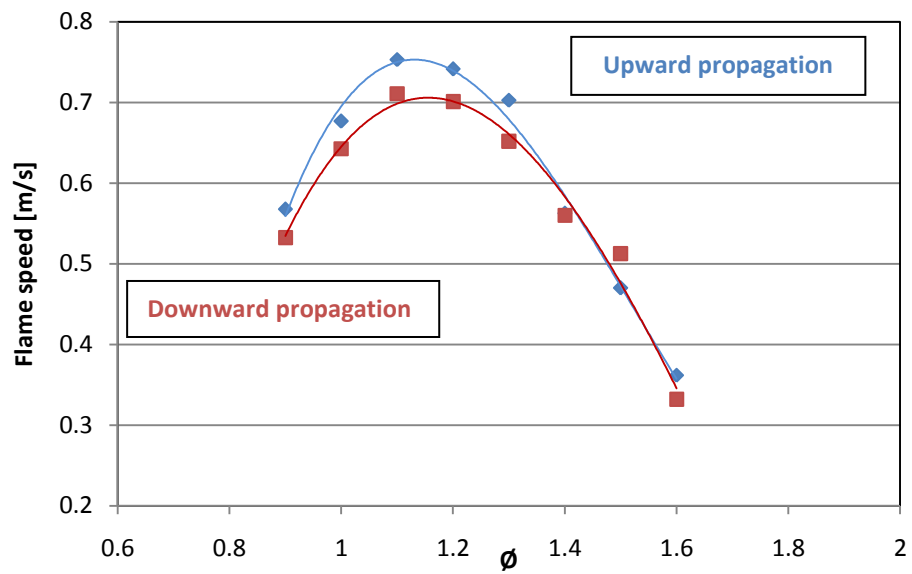


Figure 5.21 Flame speed with a range of equivalence ratio for upward and downward flames in 20 mm I.D tube with 1 mm orifice plate

5.3 Propane at elevated temperature

The effects of temperature on the flame speed and the laminar burning velocity of propane/air mixture were studied experimentally, using tube method at 333 K and 1 bar, with orifice plates of 5 mm. The aim of this test was to demonstrate that the tube method could be used for measuring laminar burning velocities at high temperature. The temperature inside was uneven and difficult to keep constant. For this reason a slight difference in flame speeds was noticeable between tests.

5.3.1 Results observation

The flames images of propane are propagated along the tube at high temperature for a range of equivalence ratio shown in Figure 5.22. The flames were steady, with a semi-ellipsoid shape, for all different equivalence ratios, and were symmetric for equivalence ratios of 0.8 to 1.6, while the flame of equivalence ratio of 1.7 was tilted.

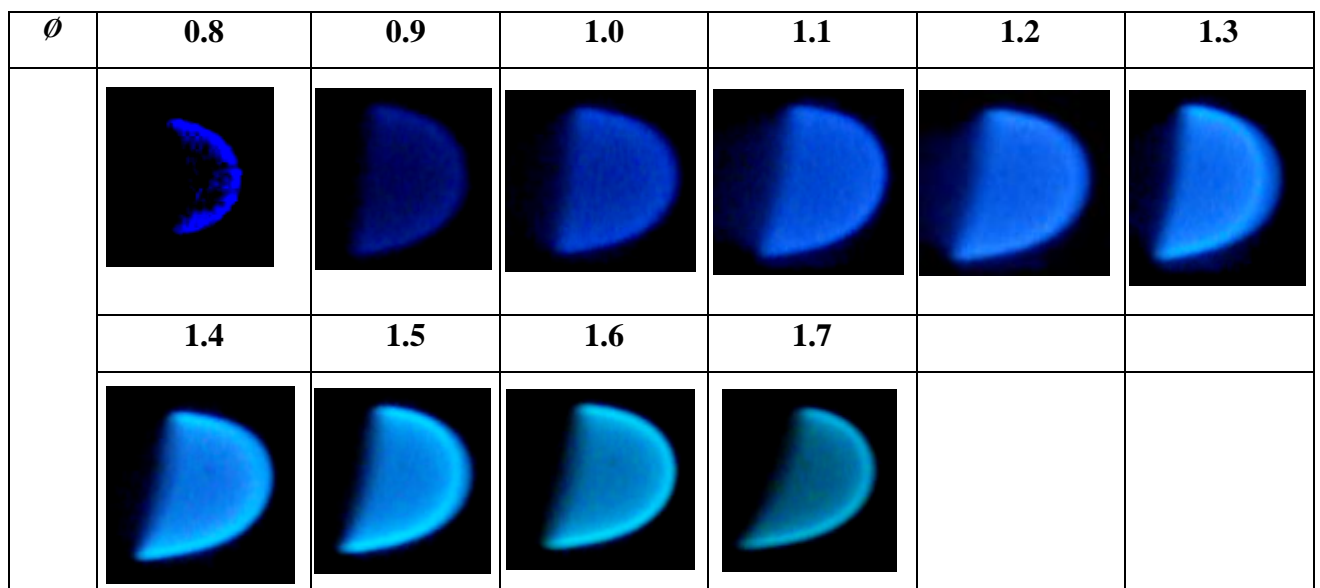


Figure 5.22 Flame shape of propane at 333 K across equivalence ratios of 5 mm orifice plate

Flames distances against time, for orifice plates of 5 mm, are plotted in the Figure 5.23. The flames propagated at constant speed resulting in linear plots.

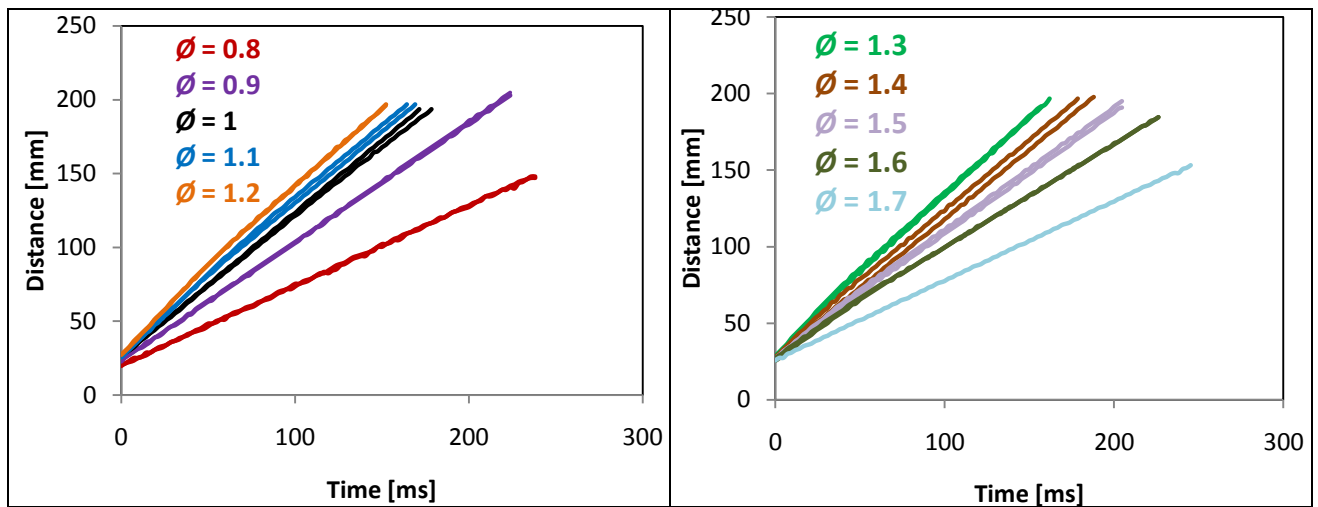


Figure 5.23 Flame distance against time of 5 mm orifice plate of propane at 333 K

Shown in Table 5.8 are the values of flame speed with the correlation coefficient and standard deviation from the fit. The speed of the flame can be seen to be higher than that at 300 K. For $\phi = 1.1$ flame speed was 1.03 m/s, compared to 0.94 m/s for orifice plates of 5 mm at ambient conditions.

The flame speed measurements plotted against equivalence ratio are presented in Figure 5.24. The flame speed peaks for an equivalence ratio of 1.2 and falls off for both lean and rich mixtures as shown in Table 5.8. The data demonstrate that the flame speed increases with initial temperature.

Table 5.8 Flame speed variation in test data 5 mm orifice plates at 333 K

ϕ	0.8	0.9	1	1.1	1.2	1.3	1.4	1.5	1.6	1.7
Average flame speed, U_f (m/s)	0.65	0.92	1.03	1.10	1.11	1.04	0.92	0.81	0.70	0.52
Correlation coefficient- R	0.999	1	1	0.999	0.998	0.999	0.999	0.999	0.999	0.999
Standard deviation of the fit (m/s)	0.0001	0.003	0.01	0.01	0.001	0.0002	0.02	0.01	0.003	

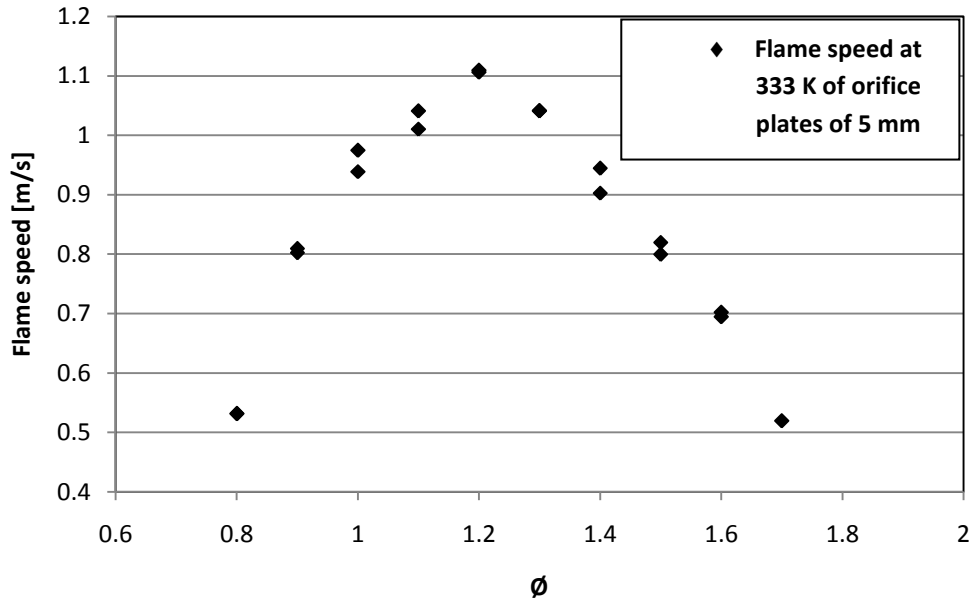


Figure 5.24 Flame speed with various equivalence ratios of 5 mm orifice plate at 333 K

5.4 Discussion

- **Comparison of flame speed between orifice plates and no orifice plate**

Coward and Hartwell [5] stated that the burning rates are expected to be higher for disturbed flames, due to their increased surface area. This occurred for all the disturbed flames in the tube with both ends open when compared to the orifice plate tests. There is also a discrepancy between the two repetitions of equivalence ratio of 1.2 at open both ends, shown in Figure 4.3. These differences confirm that the flame at this equivalence ratio and with tubes open at both ends, are non-linear. The flames propagated with an oscillatory motion, which was probably the result of pressure pulses, caused by the acceleration of gas from the flame [33]. Lewis and Elbe [33] cited that the oscillatory effect on flame propagation as a result of an acoustic vibration existed during transition to a detonation.

The results of flame speeds with orifice plates show low values, with small variations between the three repetitions of each orifice diameter, which proposes an increase in uniformity at rich conditions compared with the tube open both ends. They also recommend that the observed flame speed increases with increases of orifice diameter. This may be due to a lower decrease in pressure pulses, since the orifice plate diameter increase.

- **Flame speed variations between different orifice plates**

Increases in pressures may be causing the observed variations in flame speed. As the diameter of the orifice plates reduced, the flame speed dropped. For an orifice plate of 1 mm diameter the build up of pressure inside the tube may increase, resulting in a decrease in the flame speed [35]. A number of researchers confirmed that the laminar burning velocity decreased with increasing pressure, for different fuel-air mixtures [74, 144-145]. The flame length also decreases for an orifice plate of 1 mm [138].

To test this theory Mallard [127] performed a few tests with the flame tube closed at the end which the flame propagations towards, and the 5 mm orifice plate fitted near to ignition end. He conducted three tests for safety reasons, and to prevent damage to the rig, the results of the flame shape are shown in the Figure 5.25.

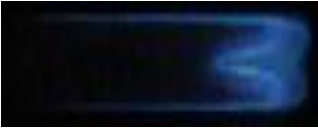
ϕ	0.9	1.2	1.6
Flame Shape			

Figure 5.25 Results of 5/0 mm orifice plates [130]

The flames have a similar appearance to those seen from the test with no orifice plates (open both ends), which produced similar oscillatory and disturbed flames. With close other end, the pressure disturbances develop and therefore the flame propagated at a slow speed.

For orifice plate of 8 mm, the flame speed increased, as shown in the Figure 5.8 and flame deformation occurred as well as shown in the Figure 5.2 for an equivalence ratio of 1.3, as the holes were widened too far and therefore the orifice plates could dampen pressure pulses in the tube.

- **Flame characteristics**

The flame could be observed for equivalence ratio of 0.8. At leaner equivalence ratios the flame image was weak such that the flame speeds were immeasurable. Tilted flames were a significant feature of propane combustion at high temperature. Linnett [18] and Hoare and Linnett [111] stated that the influence of convection upon slow flame caused the tendency for the flame to tilt forward in the upward half of the tube, and so the flame appears non symmetrical about the axis of the tube. Fast flame flames are roughly hemispherical enabling the surface area of the flames to be determined [18]. For tilted flames the speeds are smaller than non-tilted flame as shown in the Figure 5.1 for orifice plates of 1 mm. The tilted flames had a larger surface area than the upright flames [18, 111]. It is clear that for ambient temperature experiments, the flame speeds occurred more repeatedly and more stable than those at high temperature 333 K. The probable reason was that the reference temperature was the average of six thermocouples, and temperature gradients existed within the rig. Also, the inside rig temperature was unstable and it was difficult to keep it constant for a series of tests, as fresh cool air was used to flush the apparatus.

- **Effect of orifice plates**

The orifice plates absorbed the pressure waves and also allowed for the ejection of gases to prevent a build up of pressure. With an increased orifice hole in the plates, more gas can escape and stabilise the pressure, but this may compromise the plate's ability to absorb the pressure waves. An acoustics material is classified by giving it an absorption coefficient to compare materials and their ability to absorb sound/pressure waves, but this value can vary depending on the frequency [146]. This means that the absorption coefficient of the material, in this case the orifice plates, may be appropriate for one flame speed but not another. Gerstein et al. [57] used an 8 mm orifice at the ignition end and then added a second 1.7 mm diameter orifice plate at the end towards which the flame advanced. The larger hole at the ignition end was to release the high temperature expanded burned gas due to combustion. Gerstein et al. [6] produced uniform flames for all equivalence ratios, with a maximum flame speed of 0.99 m/s. In the case of Hoare and Linnett [111] they had lower flame speeds probably as a result of using smaller orifice plate holes.

- **Gravity effects**

The flame speed acquired in the vertical tube for flames propagating upwards were higher than those found when the tube was horizontal.

Maxworthy [60] and Coward and Hartwell [116] found that the upward propagation speeds were larger than the downward and horizontal movement of methane-air mixtures, in tube open both ends, for the leanest and richest mixtures. They did not research these results further and considered 1-2 cm/s deviations as satisfactory due to photographic difficulties and experimental variables in their study. A few decades later, Strehlow et al. [62] stated that the flame tip speeds of lean propane-air mixtures increased by roughly 0.07 m/s within a continuously increased gravity field of one-g. Though employing different techniques, Hamins and Libby [63] and Ronney and Wachman [147], found that for slower flames (leaner and richer mixtures) the effect of buoyancy played more important role than for stoichiometric mixtures.

5.5 Comparisons

Comparisons of flame speed of 5 mm orifice plates for propane-air mixtures at various equivalence ratios from 0.8 to 1.6 at 298 K and 1 bar are plotted in Figure 5.26. It can be seen that the maximum flame speed of propane at ambient temperature and pressure is about 0.94 m/s at an equivalence ratio of 1.1, which is close to the results obtained by Gerstein[6] and Qiang [148] of 0.99, and 0.88 m/s respectively. The peak flame speed attained at 333K is 1.11 m/s at an equivalence ratio of 1.2 also shown in Figure 5.26, which is a 14 % increase. That the increase of initial temperature leads to increased flame speed has been shown by [149] and Andrews and Bradley [150].

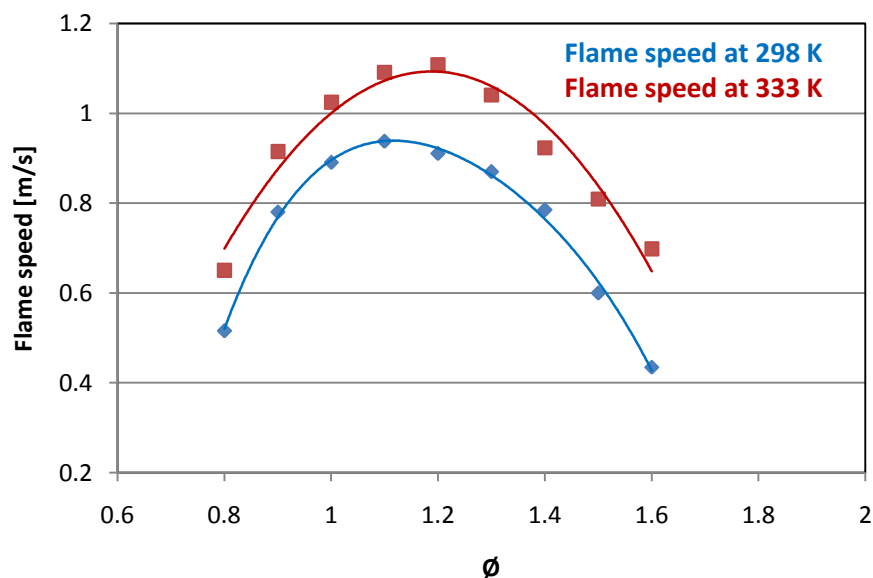


Figure 5.26 A comparison of flame speed propagating in a horizontal tube at both ambient and 333 K with 5 mm orifice plates placed at both ends

5.6 Liquid Fuel (Acetone)

The flame speed and the laminar burning velocity of acetone were also found. The initial temperature of 333 K was selected to ensure that the liquid fuel completely vaporised. Orifice plates of 5 mm were placed at both ends.

Lewis and Elbe and Glassman [16, 35] provided a tables for the flammability limits of gases and vapors with air in the tubes at atmospheric pressure and room temperature by percentage of volume. Acetone has a lower limit at $\phi = 0.52$ and upper limit at $\phi = 2.6$, the upper limit increases at high temperatures due to the vapour pressure.

5.6.1 Results observation

Flame images of acetone at 333 K for a range of equivalence ratios are shown in the Figure 5.27. The flames were steady, with semi- ellipsoid shapes, for all equivalence ratios, and were roughly symmetrical for $\phi = 0.9$ to 1.4, while for equivalence ratios of 1.5 and 1.6, they were slightly tilted.

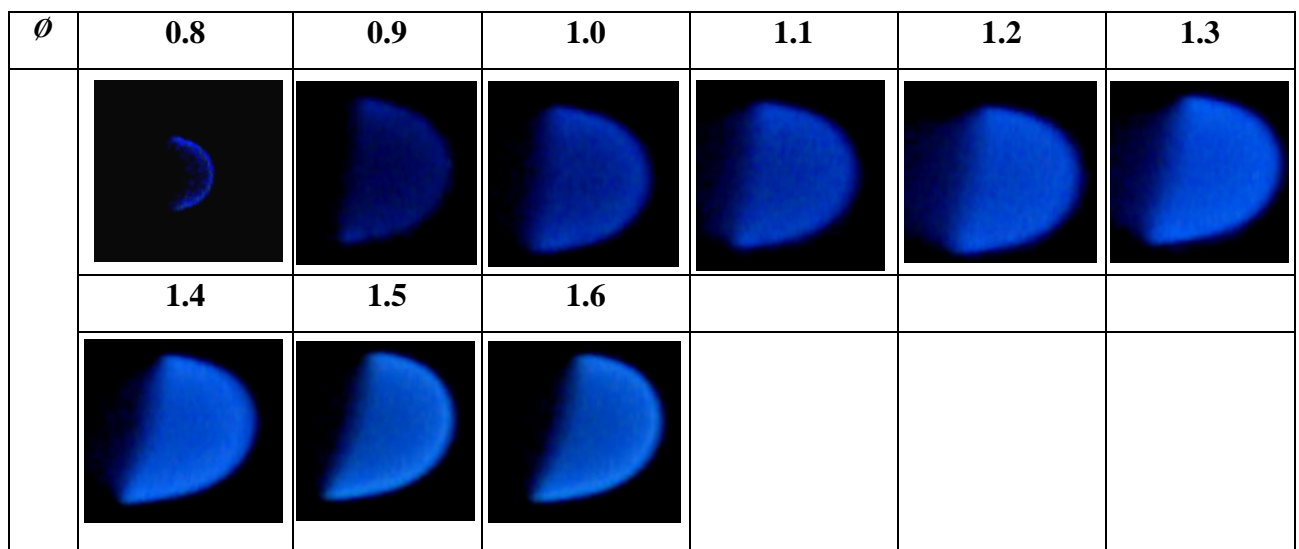


Figure 5.27 Flame shape of acetone at 333 K across equivalence ratios of 5 mm orifice plates

In Figure 5.28, the distance plotted against time, for the horizontal propagation of acetone-air mixture at 333 K and a range of equivalence ratios are given. As the plots are approximately linear, and the flames for all equivalence ratios travelled at a constant speed down the tube.

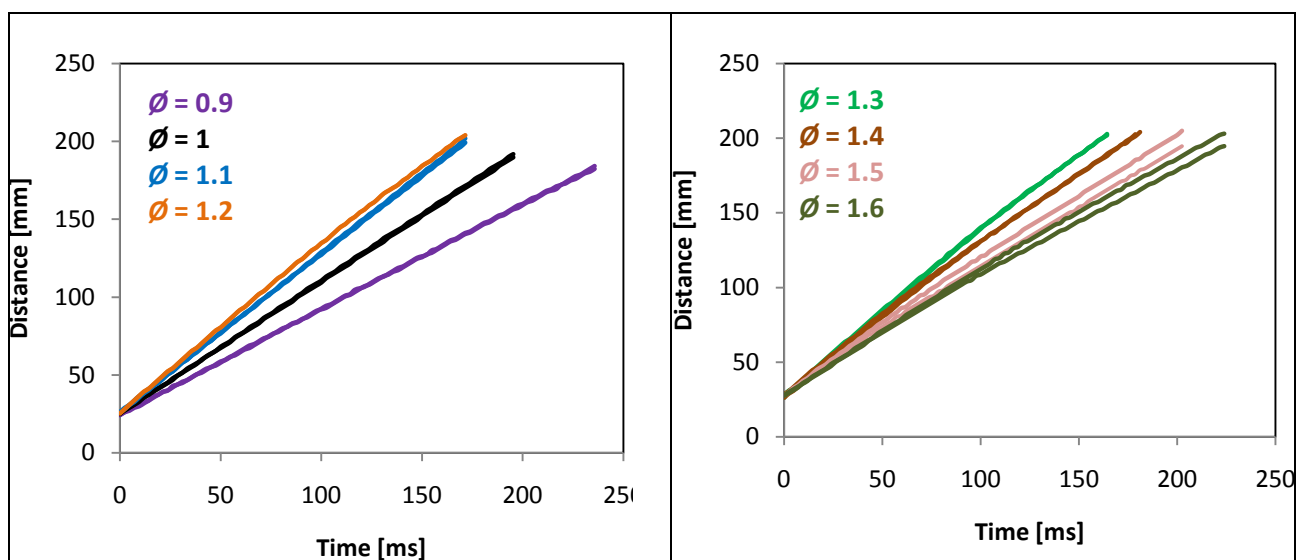


Figure 5.28 Flame distance against time of 5 mm orifice plate of acetone at 333 K

The average values of flame speed observed with correlation coefficient and standard deviations of the fit are shown in the Table 5.9.

Table 5.9 Flame speed variation of acetone in test data 5 mm orifice plates at 333 K

ϕ	0.8	0.9	1	1.1	1.2	1.3	1.4	1.5	1.6
Average flame speed, U_f (m/s)	-	0.66	0.85	1.02	1.04	1.07	0.98	0.85	0.76
Correlation Coefficient- R	-	0.999	1	1	0.999	0.998	0.998	0.998	0.998
Standard deviation of the fit (m/s)	0.01	0.01	0.01	0.0002	0.001	0.004	0.01	0.03	0.03

The flame speed for acetone-air mixture with orifice plates 5 mm at 333 K are presented in Figure 5.29. The flame speed peaks for an equivalence ratio of 1.3, with slightly different values of $\phi = 1.2$, as can be seen in the Table 5.9. However the flame speed falls off for both lean and rich mixture, as shown in Figure 5.28 and Table 6.1 confirms this.

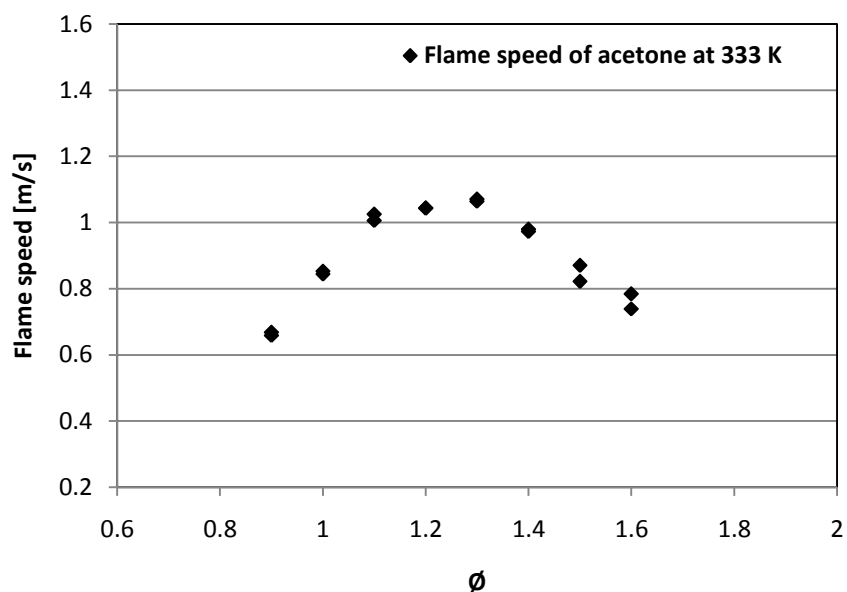


Figure 5.29 Flame speed of acetone with various equivalence ratios of 5 mm orifice plates at 333 K

5.6.2 Flame behaviour

From $\phi = 0.8$ the flame brightness was too weak to obtain the flame speed. Moreover the flame speed observed for $\phi = 1.5$ and 1.6 were not repeatable, as shown in Table 5.8 and Figure 5.28, the deviations were plotted from -2.83 to 3.4 % for equivalence ratio 1.6 and from -2.88 to 3.2 % for equivalence ratio of 1.5. These may be due to uncertainty in the temperature of the rig and photographic measurements.

The maximum flame speed was close to equivalence ratio of 1.3. These results have roughly a good agreement with Pichon et al. [107] using spherical bomb technique, at initial temperature and pressure and found a peak flame speed at $\phi = 1.25$. They attributed this to the “condensation” problem occurring inside the bomb. Gibbs and Calcote [105] used the same fuel at ambient conditions using a Bunsen burner and they reported a peak flame speed at $\phi = 0.93$. This discrepancy with Pichone et al. was attributed to the effect of stretch.

6 Measurement of laminar burning velocity

The determination of the laminar burning velocity is an important practical aspect of combustion. Most of the data of the laminar burning velocity in the literature have been obtained from measurements on constant volume spherical chambers and counterflow burners. The flame speed obtained directly from measurements of flame radius at different time using schlieren and shadow photograph.

In the present study, the laminar burning velocity of propane-air mixtures at equivalence ratios from 0.8 to 1.6 with orifice plates at both ends can be found using equation (1.1). Consequently, the unburned gas velocity and flame surface area must also be determined in addition to the speed of the flame down the tube. The gas velocity ahead of the flame (u_g) was measured using LDV system, as shown in the next section. The surface area was obtained by photography of the flame and then fitting with appropriate function, as shown in the section 6.2. As can be seen in Figure 6.5 near the centre, the unburned gas flows away from the combustion wave and near the wall it flows toward the wave. The wave surface therefore becomes curved and the formation of curved waves of this type is readily confirmed by casual visual observation of luminous combustion waves in tubes [116]. It is necessary to distinguish between the curvatures of the wave that is caused by the above described mechanism from curvature caused by the decrease of burning velocity close to the wall. This decrease of burning velocity is then limited to a small fraction of the wave area near to the wall, and the burning velocity is basically constant over the wave, since the radius of curvature is everywhere large compared to the wave width. The flame speed is strongly influenced by the experimental configuration, for a flame propagating in tube with open both ends, the speed is likely to be larger than for tube with orifice plates fitted at both ends, as shown in chapters 4 and 5. The main problem with measuring the flame surface area for tube with open both ends is that the flames are often non-symmetrical and takes on a characteristic 'tipped shape'. The measured flame speed for tube with orifice plates placed at both ends was smaller than the speed when the tube is open at both ends. Therefore, the gas velocity ahead of the flame is to be relatively small compared to the flame propagation velocity, as shown in the next section.

In this chapter, the values of the laminar burning velocities were found for orifice plates of 5mm at both ends and combination of 5 mm near to the ignition point and 3 mm far at the other end. The results were slightly smaller than the published values but of the right order.

6.1 Unburned gas velocity

In order to obtain the laminar burning velocity from the tube measurements, it is important to derive the LDV results of unburned gas velocity for orifice plates of 5 and 5/3 mm, as shown in Figure 6.1. The gas velocity in the tube during combustion is shown below

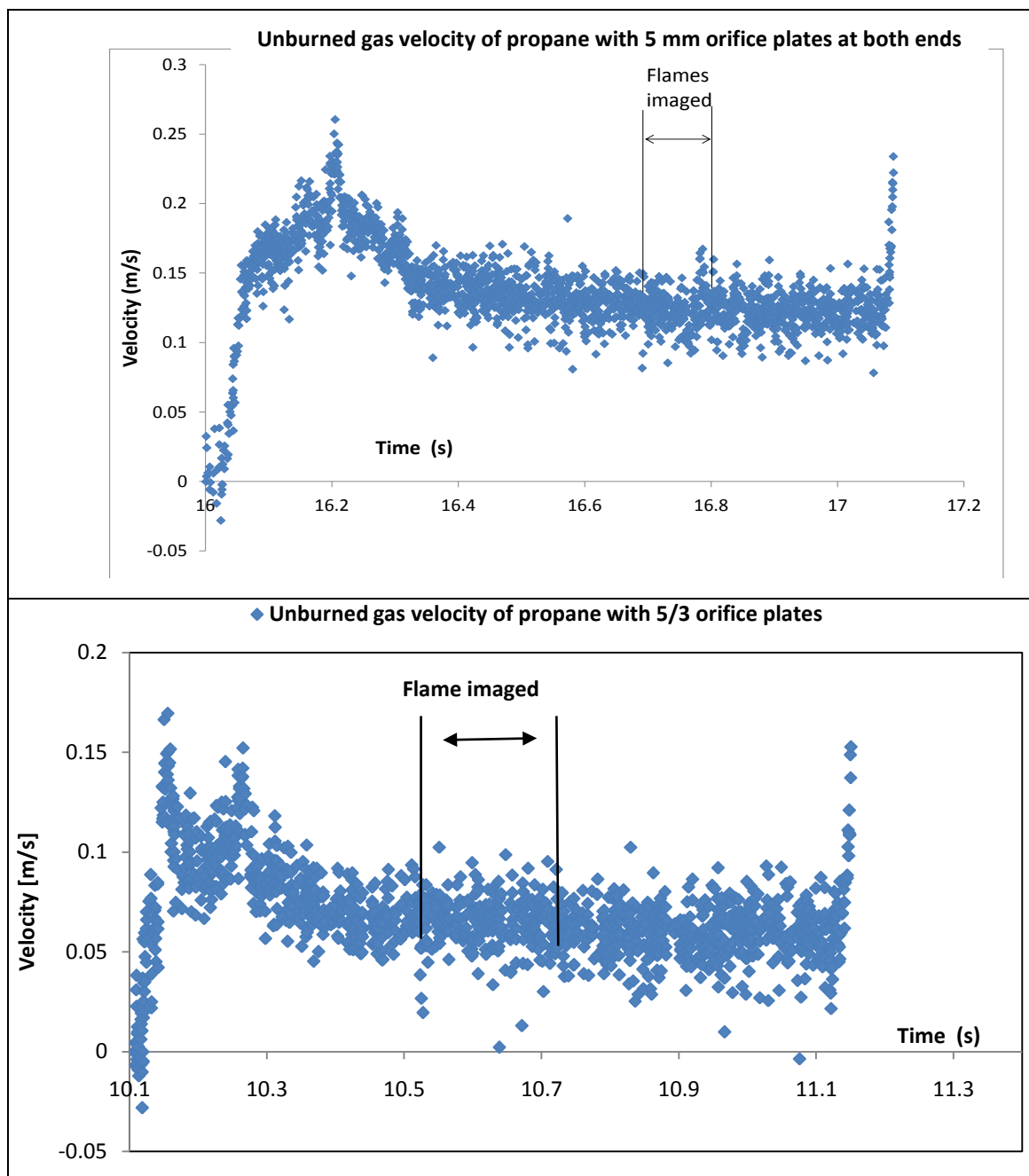


Figure 6.1 Results of unburned gas velocity of propane-air mixtures for equivalence ratio of 0.8

The gas velocity can be seen to be constant during filming. When the flame reached the control volume the signal was lost as the olive oil particles burned out. The high velocities observed for orifice plates of 5 and 5/3 mm around 16.2 and 10.15 s, respectively, are thought to be associated with the ignition process. This is followed by a fall in the speed, as the flame front contacts the walls, after which the gas velocity stabilises. This stable velocity, as seen in Figure 6.1, was taken to be the unburned gas velocity, as the time scale matches the flame propagation time scale. There were errors in this technique, mainly relating to the time sync of the camera and the LDV. These errors are about 0.01s, which could potentially be removed, probably by creating reference points, as shown in Figure 3.11. The results of the unburned gas velocity measurement of propane-air mixture with orifice plate of 5 at both ends and 5/3 mm are presented in Figure 6.2 and also in Table 6.1. The unburned gas velocity reached peak value at an equivalence ratio of 1.1 and then fell, for both lean and rich mixtures.

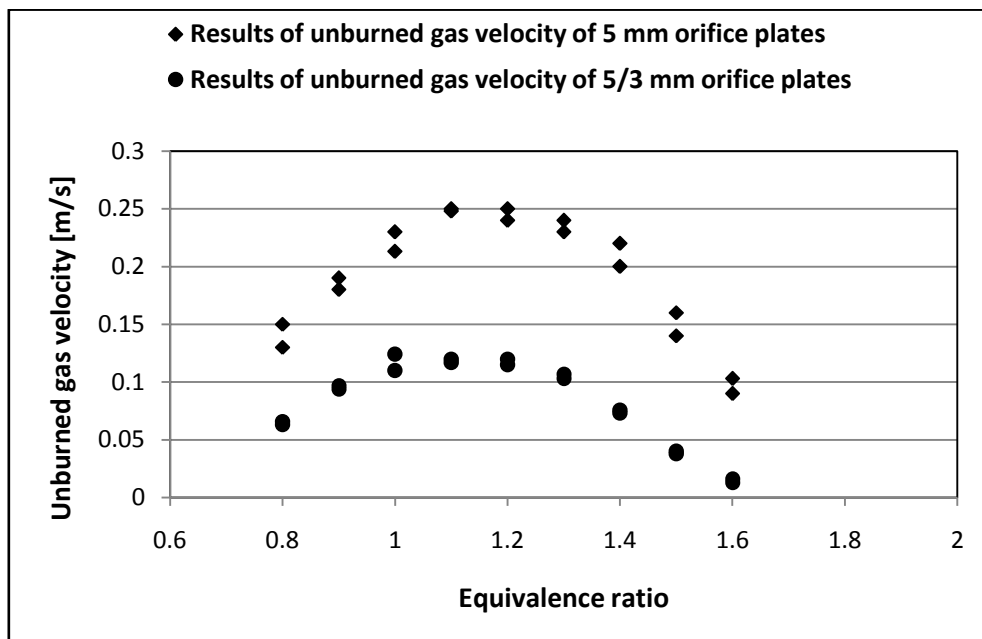


Figure 6.2 Unburned gas velocity of propane-air mixtures as a function of equivalence ratios with orifice plates of 5 and 5/3 mm, at ambient condition

The unburned gas velocity measured by LDV is plotted against the observed flame speed for a propane-air mixture with orifice plates of 5 mm, fitted at both ends and 5/3 mm orifice plates, as shown in Figure 6.3 and 6.4 respectively, following the approach by Gerstein et al. [6] a least squares straight line was fitted through the data over a range of observed flame speeds. The equation 6.1 and 6.2 are shown for derived for orifice plates of 5 mm, placed at both ends and 5/3 mm orifice plates.

$$U_g = 0.256 U_f + 0.024 \quad (6.1)$$

$$U_g = 0.176 U_f - 0.034 \quad (6.2)$$

The average standard deviations were determined to be small, about 2.4 %.

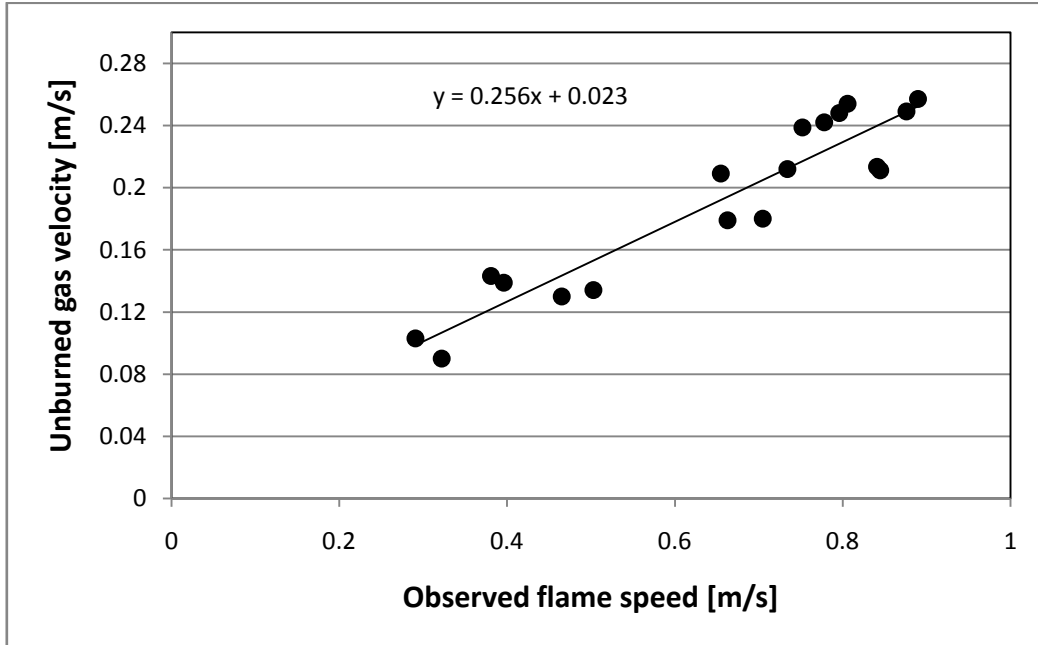


Figure 6.3 Unburned gas velocity as a function of observed flame speed of 5 mm orifice plates at both ends

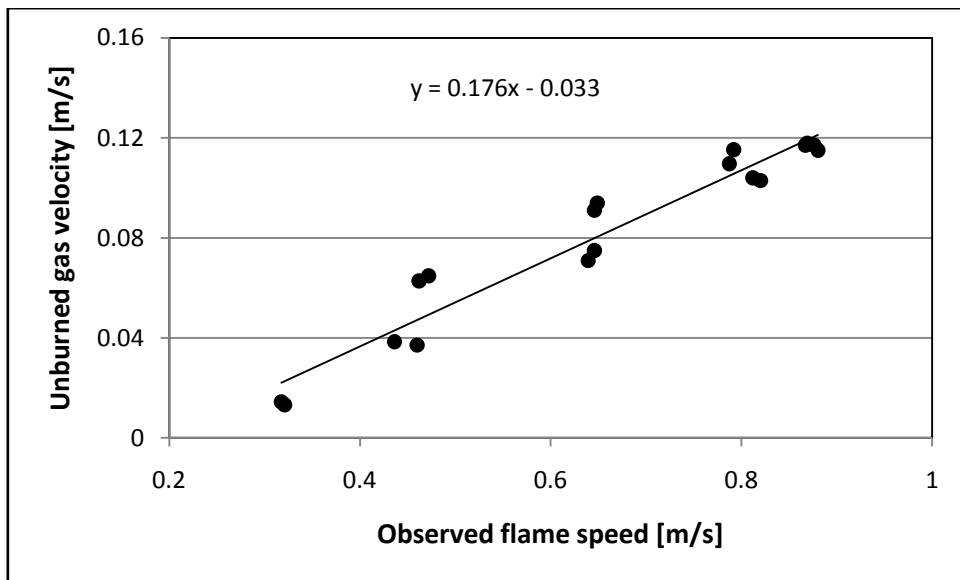


Figure 6.4 Unburned gas velocity as a function of observed flame speed of 5/3 mm orifice plates

Table 6.1 Table of Calculated Unburned Gas Velocities for the 5mm and 5/3 orifice plates

ϕ	Average flame speed (m/s)			Average of unburned gas velocity (m/s)	
	5 mm orifice plates	5/3 mm orifice plates	Deviation	5 mm orifice plate	5/3 mm orifice plates
0.8	0.52	0.47	0.04	0.13	0.06
0.9	0.78	0.65	0.09	0.18	0.09
1	0.91	0.79	0.08	0.21	0.11
1.1	0.96	0.87	0.06	0.25	0.12
1.2	0.93	0.88	0.04	0.25	0.12
1.3	0.87	0.81	0.04	0.24	0.10
1.4	0.78	0.65	0.09	0.21	0.07
1.5	0.59	0.45	0.09	0.14	0.04
1.6	0.42	0.32	0.07	0.11	0.02

6.2 Flame surface area

Figure 6.5 shows a representative set of flame images, captured from the top positions, for propane-air mixtures, for all the equivalence ratios and at initial conditions of temperature and pressure, with orifice plates of 5 mm fitted at both ends of the tube, 5 mm fitted at the ignition point and 3 mm at the other end, respectively. The top images are very symmetrical, with slight tilt, as shown in Figure 6.5, compared with the side images, which have more pronounced tilted. So in this study top images were used rather than the side image to obtain the surface area of flames. The flames were split into many little cones with their tops chopped off to find the surface area, as shown in Figure 6.6.

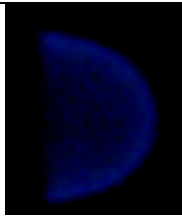
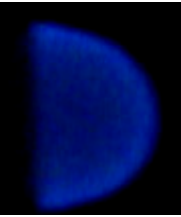


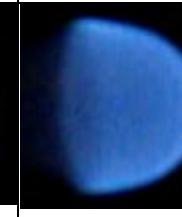
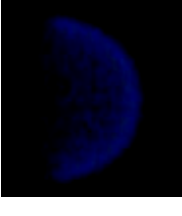
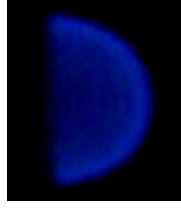
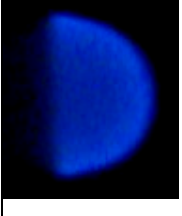
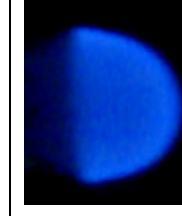
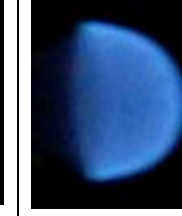
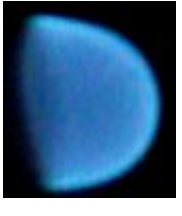
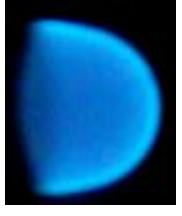
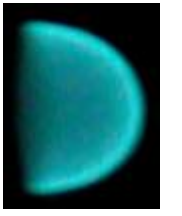
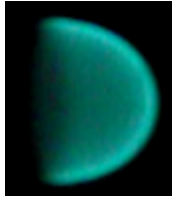
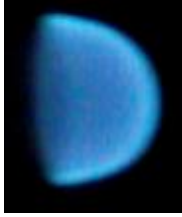
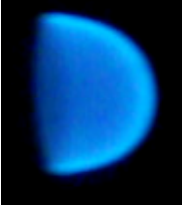
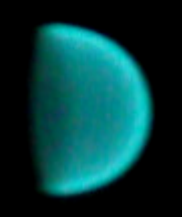
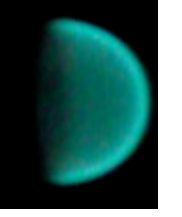
ϕ	0.8	0.9	1.0	1.1	1.2
Top image of 5 mm orifice plates					
Top images of 5/3 orifice plates					
ϕ	1.3	1.4	1.5	1.6	
Top image of 5 mm orifice plates					
Top images of 5/3 orifice plates					

Figure 6.5 Propane flame shape of top observation with 5 and 5/3 mm orifice plate

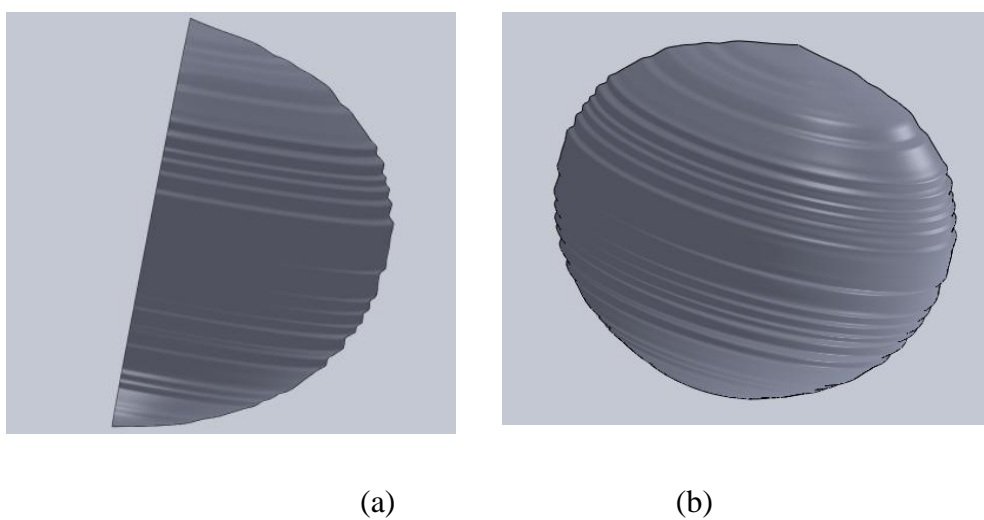


Figure 6.6 Flame shape (a) top image and (b) front view (an example of $\phi = 1.1$), produced by Solidworks software

The surface area is computed by the frustum equation:

$$A_f = \pi(R_1 + R_2) \sqrt{(R_1 - R_2)^2 + h^2} \quad (6.3)$$

Here, R_1 and R_2 is the top and bottom radius and h is the height between the top and the bottom circles, as shown in the Figure 6.7

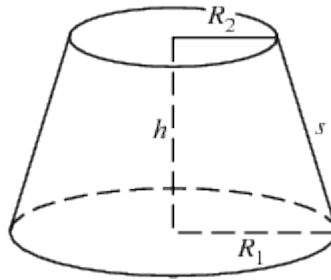


Figure 6.7 Frustum of right circular cone

Figure 6.8 shows a representative of the flame coordinate against a tube diameter to produce the six order polynomial equation that fits on pixels data in Microsoft Excel file (an example for $\phi = 1.1$, with 5 mm orifice plates fitted at both ends). To obtain the radius R_1 and R_2 are by fitting the mid-point on the x-axis and dividing the flame front into two parts, to obtain the surface area of the flame. An example had been presented in Appendix M.

SolidWorks was also used to create a 3-D shape of the flame. This is a solid modelling CAD (Computer- aided design), used to determine the shape or geometry of the model or assembly, such as a circle diameter, surface area and line length, etc. The flame coordinates were plotted using this software and spline was formed using points, then the flame surface was revolved by 180° around the axis joining the top and the bottom points to produce the surface as shown in Figure 6.6 and 6.9. The surface area computed by this software as shown in Figure 6.9, for $\phi = 1.1$. The result is higher than the results obtained from equation 6.3 by 15 %. This software might be not accurate, due to spline the flame coordinate manually. However, the results were checked against for a hemisphere shape ($A=2\pi r^2$), and gave nearly the same results with a variation of less than 3 %.

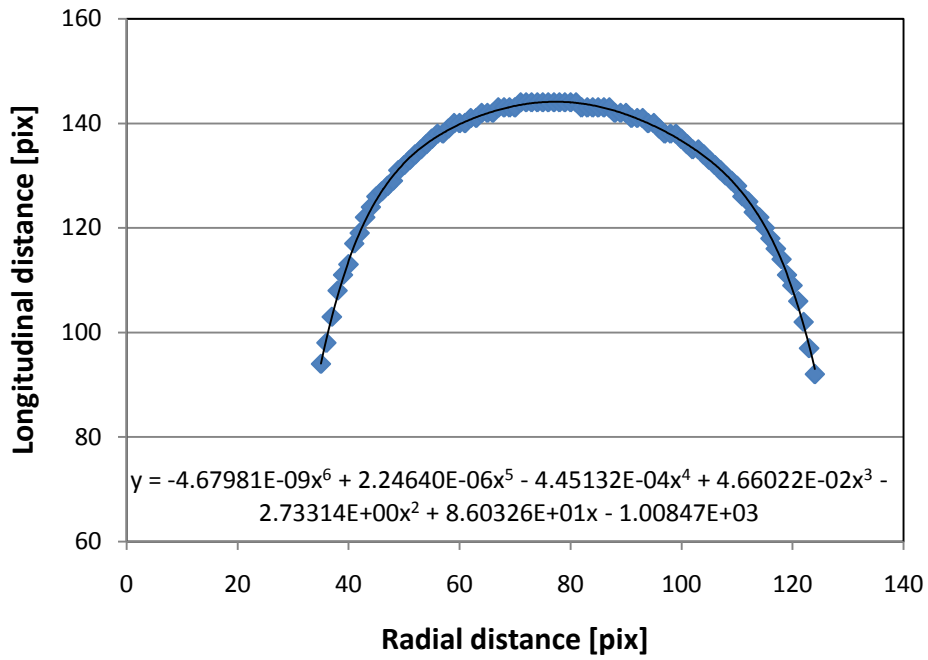


Figure 6.8 Example of computing flame surface area for equivalence ratio of 1.1, with 5 mm orifice plates

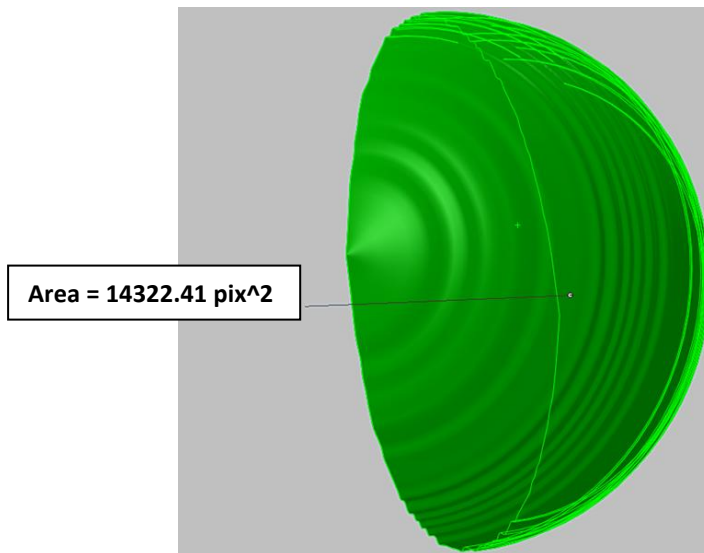


Figure 6.9 Flame surface area of $\phi = 1.1$, computed by Solidworks software

Table 6.2 shows the flame surface area for the top images of propane, under ambient conditions. The stoichiometric flame had the highest values of surface area. The leaner and richer flame had smaller surface areas. The standard deviations are very small, about 2.1 to 2.7 %, as shown in the Table 6.2. The flame surface area was found and compared against the diameter of the tube, to provide the ratio A_t/A_f . The results for all the varieties of equivalence ratios are shown in Table 6.2.

Table 6.2 Surface area measurements of propane at room temperature and atmospheric pressure

Equivalence ratios	Flame surface area (pix²) of 5mm orifice plate	A_t/A_f	Flame surface area (pix²) of 5/3 mm orifice plates	A_t/A_f
0.8	11432.23	0.507	10613.46	0.546
0.9	11709.33	0.495	10732.70	0.539
1.0	12538.98	0.462	11117.82	0.521
1.1	12142.87	0.478	11436.54	0.506
1.2	12538.82	0.463	12206.73	0.474
1.3	12149.33	0.477	11933.00	0.485
1.4	12312.04	0.471	11986.75	0.483
1.5	11341.41	0.511	11063.24	0.523
1.6	11234.72	0.516	10652.94	0.544
S. deviations		0.021		0.027

6.3 Laminar burning velocity

The laminar burning velocity was determined by placing the required variables into Equation 1.1. The resultant of the laminar burning velocity of propane-air mixtures at a temperature of 300 K and pressure of 1 bar with orifice plates of 5 mm at both ends and combination of 5/3 mm can be seen in Figure 6.10 and Table 6.3. The laminar burning velocity peaks at an equivalence ratio of 1.1, is 0.34 and 0.38 m/s for 5mm and 5/3 mm, respectively. In both cases u_l falls off for lean and rich mixtures. The laminar burning velocities values with 5 mm plate near to ignition point and 3 mm plate at the far end is higher than a configuration of 5 mm at both ends. The 3 mm plates at the end way from the ignition may be responsible for increased the pressure in the tube and potentially decreasing the laminar burning velocity [6].

Table 6.3 Laminar burning velocity calculations for both configurations

ϕ	Laminar burning velocity of propane with 5 mm (m/s)	Laminar burning velocity of propane with 5/3 mm (m/s)
0.8	0.197	0.224
0.9	0.297	0.302
1.0	0.323	0.354
1.1	0.340	0.380
1.2	0.320	0.360
1.3	0.301	0.344
1.4	0.268	0.280
1.5	0.229	0.214
1.6	0.159	0.163

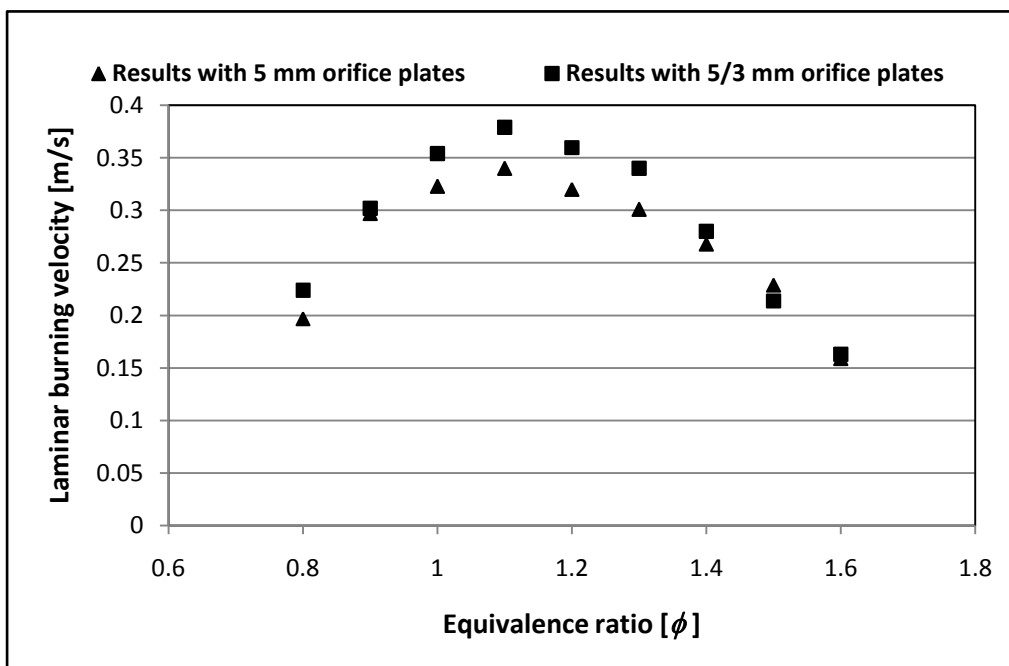


Figure 6.10 Laminar burning velocity of propane-air mixtures as a function of equivalence ratios with 5 mm orifice plates at both ends and at normal temperature and pressure

Figure 6.11 shows a comparison between these results and the literature values, for propane-air mixtures at atmospheric pressure and temperature. The present results for tube method for both configurations 5 and 5/3 mm plates are lower than those of other works using different

methods. Heat losses to the walls in this method may be the reason for this. The agreement is quite good, especially with those obtained by means of the tube method [6]. Only at the richest conditions for equivalence ratios of 1.5 and 1.6 are there considerable differences, with a variation of 30 and 26 % respectively, as can be seen in Figure 6.8. This result also has good agreement with Hassan et al. [42], Marley and Roberts [41] and Razus et al. [70] who used a spherical combustion bomb to obtain the burning velocity of propane-air mixture. In the first two cases, they used schlieren and high speed chemiluminescence imaging techniques to obtain flame radius as a function of time to determine unstretched laminar burning velocity. In the third case, the laminar burning velocity was derived from experimental pressure records during explosion in a spherical vessel from 0.03 to 0.2 MPa. Their results were a little low, as shown in Figure 6.8; this may be caused by curvature of the flame front, or by quenching and incomplete combustion in the electrode area near the centre of the exploding volume [44]. Vagelopoulos and Egolfopoulos [49] and Davis and Law [69] used the counterflow twin flame configuration to measure the laminar burning velocity of propane-air mixture with nearly stretch free. In the second case [69] they employed both linear and non linear extrapolation. They observed that the nonlinear extrapolation was slightly lower than the linear extrapolation for all equivalence ratios. A heat flux method was used by Bosschaart and Goey [72] to determine the laminar burning velocity of propane at normal condition and the maximum value was about 40 cm/s at $\phi = 1.1$, as shown in Figure 6.11 and flame stretch was absent.

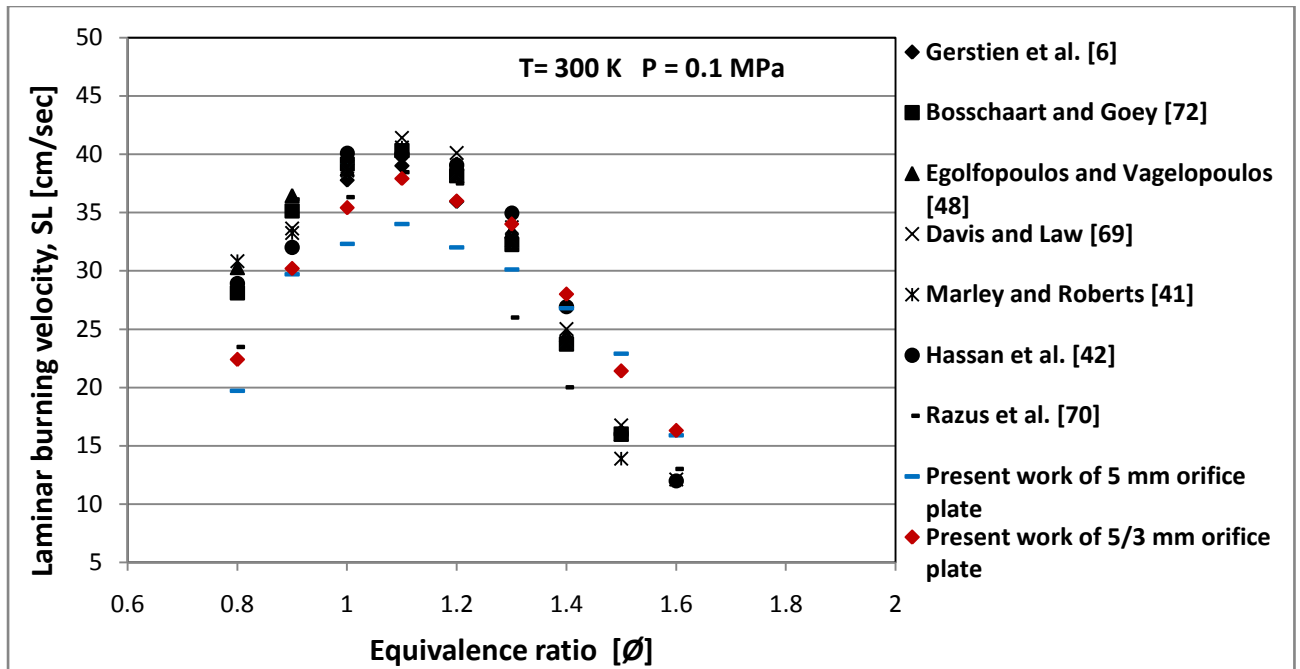


Figure 6.11 A comparison of measured laminar burning velocity of propane-air mixture at room temperature and atmospheric pressure

6.4 Laminar burning velocity of propane-air mixture at 333 K

The temperature was increased to 333 K, which was the average temperature in the entire rig at atmospheric pressure. Shown in Figure 6.12 are the side and the top images of propane-air flames at 333 K for a range of equivalence ratios.

As can be seen from the side images, at all equivalence ratios, the flames were semi-ellipsoid and tilted, while the top images are also semi-ellipsoid but symmetrical in shape. So in this study I will be considering the flame surface area of the top images. Equation 6.3 was used to calculate the surface area and the results are shown in Table 6.4. In this investigation at elevated temperature the flames were faster than the room temperature flames. The surface area of the flame increased with equivalence ratios up to $\phi = 1.2$ and then fell off under richer conditions, as shown in Table 6.4. Also, the ratios A_t/A_f had slightly increased as the quantities of fuel injected became either lean or rich from stoichiometric values. Moreover, the flames surface area at 333 K was lower than the values at room temperature by about 22%. This decrease caused an increase to the ratios of A_t/A_f , as shown in Table 6.4.

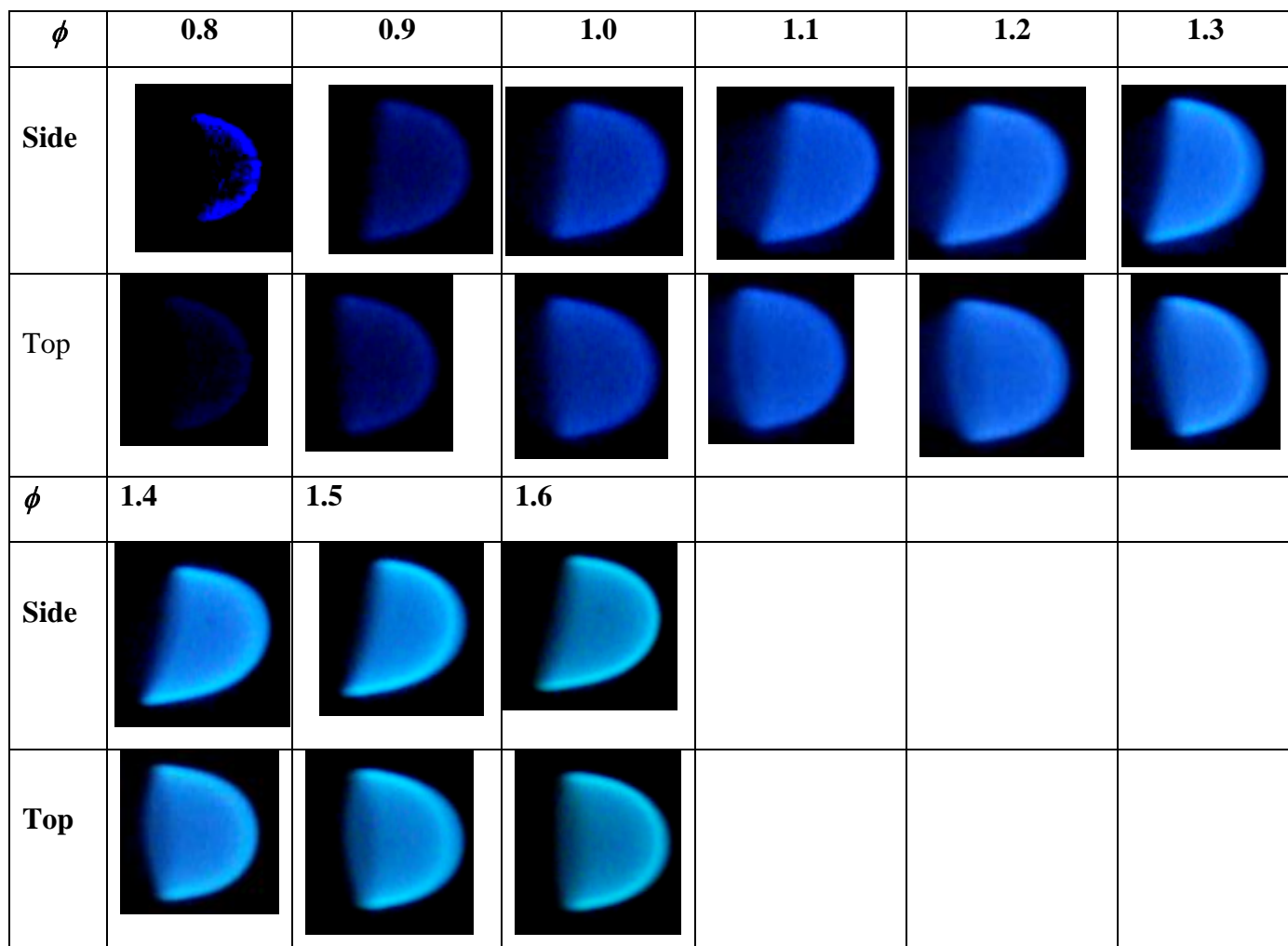


Figure 6.12 Propane flame shape of side and top observation with 5 mm orifice plates

Table 6.4 Surface area measurements of propane at 333K with 5 mm orifice plate

Equivalence ratios	Average flame speed (m/s)	Flame surface area, pix ²	A_t/A_f
0.8	0.65		
0.9	0.92	8789.20	0.661
1.0	1.03	9286.41	0.624
1.1	1.09	9637.00	0.601
1.2	1.11	10103.00	0.574
1.3	1.04	9522.13	0.608
1.4	0.92	9071.00	0.638
1.5	0.81	9393.00	0.617
1.6	0.69	9114.10	0.636

The laminar burning velocity for a propane-air mixture at 333 K was obtained using equation (1.1) and (6.1) for the unburned gas velocity of propane at 333 K. The values of unburned gas velocity, flame area and laminar burning velocity are given in Table 6.5 below.

Table 6.5 Laminar burning velocity of propane at 333 K and atmospheric pressure with 5 mm orifice plates

ϕ	Average flame speed (m/s)	Unburned gas velocity (m/s)	A_t/A_f	Laminar burning velocity (m/s)
0.8	0.65	0.19		
0.9	0.92	0.26	0.661	0.436
1.0	1.03	0.29	0.624	0.462
1.1	1.09	0.30	0.601	0.475
1.2	1.11	0.31	0.574	0.460
1.3	1.04	0.29	0.608	0.456
1.4	0.92	0.26	0.638	0.421
1.5	0.81	0.23	0.617	0.358
1.6	0.69	0.20	0.636	0.312

For comparison the power law relationship was used:

$$U_{l(333)} = U_{l(300)} \left(\frac{T_u}{T_o} \right)^\alpha \left(\frac{P}{P_o} \right)^\beta \quad (6.4)$$

The values of the constant α (temperature exponent) obtained by Akram et al. [101] are given in Table 6.6

Table 6.6 The temperature exponent of propane-air mixture with a range of equivalence ratios [101]

Equivalence ratios ϕ	0.8	0.9	1	1.1	1.2	1.3	1.4	1.5	1.6
Temperature exponent α	1.86	1.68	1.63	1.62	1.7	1.85	2.1	2.44	2.88

By substituting laminar burning velocity data for 300 K propane-air flames in Equation 6.4, the values of the laminar burning velocity of propane at 333 K were obtained, as given in Table 6.7 and presented in Figure 6.13.

Table 6.7 Laminar burning velocity of propane at 333 K and atmospheric pressure

Equivalence ratios	Laminar burning velocity at room temperature, $U_{L(300)}$ [m/s]	Laminar burning velocity, $U_{L(333)}$ [m/s]
0.8	0.197	
0.9	0.297	0.235
1	0.323	0.383
1.1	0.34	0.403
1.2	0.32	0.382
1.3	0.301	0.365
1.4	0.268	0.334
1.5	0.229	0.295
1.6	0.159	0.215

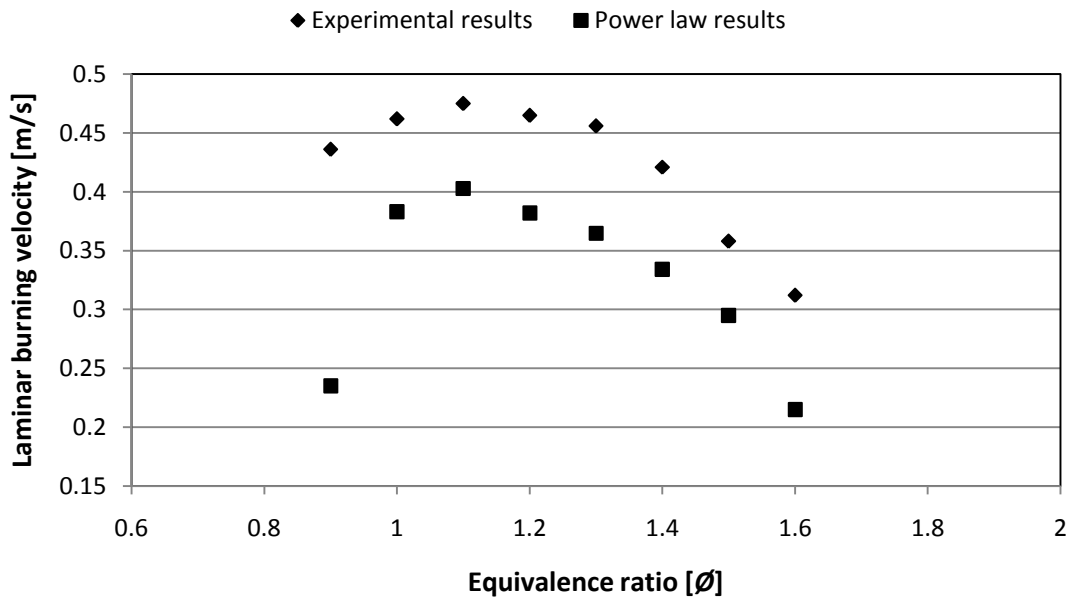


Figure 6.13 Laminar burning velocities of propane-air mixtures with 5 mm orifice plates fitted at both ends

Figure 6.13 shows a comparison of the laminar burning velocities of propane, measured in this study at 333 K, versus results obtained by Equation 6.2. As can be seen, the experimental results were higher than the results obtained by the power law relation, with deviations of 6 %, except at ($\phi = 0.9$) which were much higher at about 14 %. The maximum laminar burning velocity measured in this study was 0.47 m/s at $\phi = 1.1$, falling at both lean and rich sides. The laminar burning velocities for the entire range of equivalence ratios increased with increases in the temperature compared with the results obtained at room temperature. Razus et al. [70] measured the laminar burning velocity of propane at 333 K just at an equivalence ratio of 0.77 and 1.01, from pressure-time records over an extended time of spherical propagation, and the values were about 0.29 and 0.42 m/s respectively. These values have good agreements with the present results of equivalence ratios of 0.8 and 1 at about 0.33 and 0.46 m/s with a difference less than 9 % at stoichiometric. Metgalchi and Keck [22] also used the same method of [70] to determine the laminar burning velocity of propane at $\phi = 1$ and the same temperature of 333 K, the value was about 0.39 m/s with a difference of about 15 % .

6.5 Comparisons

Comparisons with laminar burning velocities at different temperatures were presented in Figure 6.14, for a range of equivalence ratios. From the graph, the present results at 300 K and atmospheric pressure were observed in good agreement with the literature data. There was limited previous data conducted at 333 K, at a variety of equivalence ratios to compare directly, except for Metgalchi and Keck [22] and Razus et al. [70] who achieved their results at 333 K at stoichiometric. Other results conducted to measure laminar burning velocities of propane at 363 and 423 K [70] were presented in Figure 6.14 by using a spherical bomb to show the correlations with the effect of temperature. Their results had maximum laminar burning velocities of roughly 52.2 and 66.7 cm/s respectively, which were about 9 and 28 % higher than the present study using the tube method, since temperatures were raised by 30 and 90 K. These results confirmed that as the initial temperature of unburned mixtures increased, the laminar burning velocity increased at a constant initial pressure.

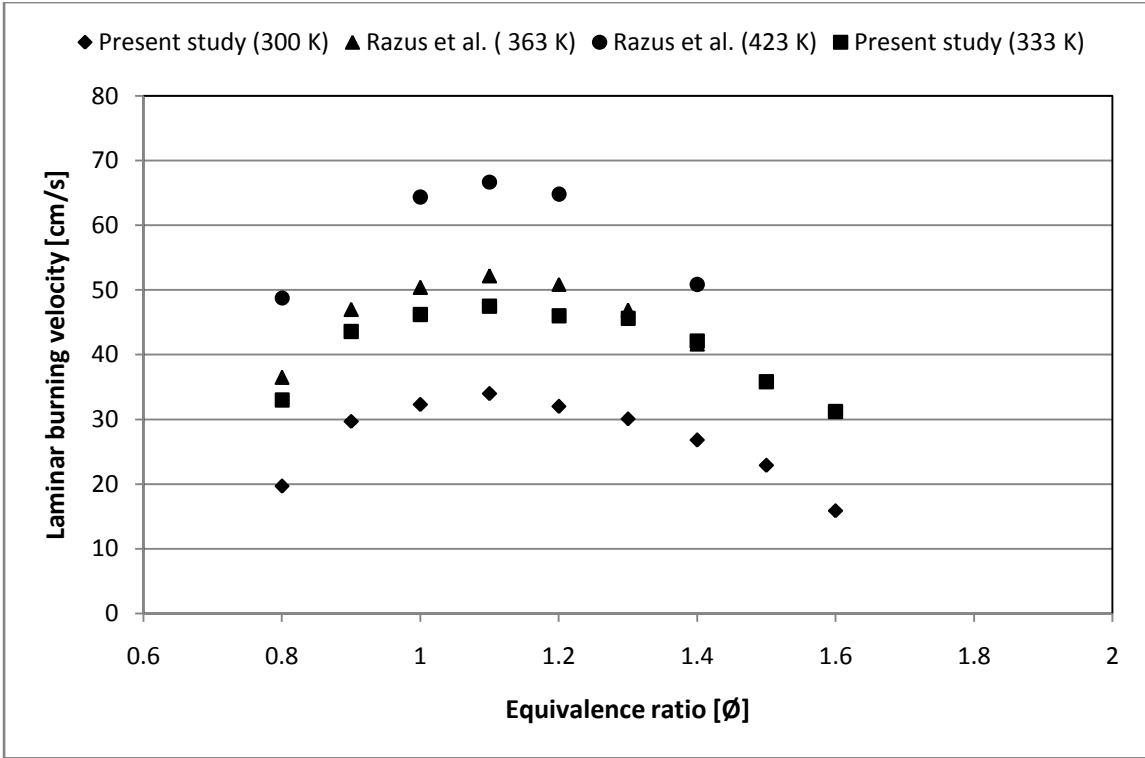


Figure 6.14 A comparison of laminar burning velocities of propane-air mixtures with 5 mm orifice plates at both ends

The tube method was found to be efficient and reliable during this study of the flame characteristics at elevated temperature. This data was comparable with other work despite the uncertainty of the temperature inside the tube and the approximate flame surface area measurements, which caused a slight variation in the laminar burning velocities. In the future an accurate method to measure the surface area of the flame should be developed and the rig modified so that it is more uniformly heated.

6.6 Discussion

6.6.1 Results of unburned gas velocity

The values of unburned gas velocity measured in this study with 5 mm plates fitted at both ends was higher than the results of 5 mm plates near to ignition point and 3 mm at the far end and those obtained by Gerstein et al. [6]. The probable reason for this is due to using small diameter plates at the far end, Gerstein et al. used 8 mm plates close to the ignition point and 2 mm plates at the other end. The large orifice plate caused an increase in the unburned gas velocity, as can be seen in the difference between the two configurations in this study. The unburned gas velocity depends not only upon the observed flame velocity, but also the boundary conditions of the tube. The maximum average variation of the unburned gas velocity was 2.4 %, these variations may be owing to the noise signals scattered away, as shown in Figure 6.1 which deformed the data. The higher values of unburned gas velocity observed with 5 mm plates at both ends lead to lower value of laminar burning velocity as shown in Table 6.3.

6.6.2 Effect of temperature

An increase in the initial temperature of the mixtures should cause a noticeable increase in burning velocity for low-temperature flames, see Figure 6.14. The laminar burning velocity at room temperature is 0.34 m/s with orifice plates of 5 mm at both ends, whilst with a temperature rise of 33 K, the laminar burning velocity increases to 0.47 m/s, by a factor of approximately 1.4. This increase was due to the chemical reaction in the preheat zone, which strongly effects the flames that have low burning velocities [76]. The effect of temperature on the laminar burning velocity has been shown to be strong for flames that have burning velocities in the range about 40 – 100 cm/s. This occurs due to the highly effective heat capacities of the dissociated product gases at these high temperatures which cause the flame temperature and, as a result, the burning velocities only vary slightly as the initial temperature of the mixture is altered. Andrews and Bradley [150] stated that an increase in temperature from 300 to 600 K, leads to increasing in the laminar burning velocity by a factor of 2.89.

Kuehl [151] using a Bunsen flame to measure the laminar burning velocity of propane-air mixture up to 811 K. At this temperature the laminar burning velocity had risen to 2.5 m/s.

He also studied the variations of burning velocity according to mixture strength, and his graphs show that the point of maximum burning velocity moves to less rich mixtures when the gas is preheated.

6.6.3 Effects of equivalence ratio and fuel structure

The effect of equivalence ratios on the laminar burning velocity is a result of how this parameter affects flame temperatures [12]. The laminar burning velocities should be a peak at a slightly rich mixture at $\phi = 1.1$ and falling at lean and rich conditions. Figure 6.14 indeed shows this behaviour in this study for propane-air mixture at ambient condition and at high temperature of 333 K. In the case of very lean or rich mixtures, it is difficult to propagate flames, due to too little fuel or oxidant to maintain a steady deflagration wave, as shown at equivalence ratio less than 0.8 in this study.

In the case of propane fuel (alkanes), the high flame speed is almost independent of the number of carbon atoms, unlike the alkenes and alkynes such as ethene (C_2H_4), the laminar burning velocity increased with a decrease in the number of carbon atoms. The laminar burning velocity of ethene is about 68 cm/s [6] compared with propane is 38 cm/s in this work. The effect of carbon atoms in different fuels on the laminar burning velocity, however, is not owing to the flame temperature; because most fuels have approximately the same adiabatic temperature, around 2200 K. The main probable reason is due to the change in thermal diffusivity [6], which is a function of the fuel molecular weight.

6.6.4 Reliability of tube method

The reliability of the tube technique for determining the laminar burning velocity depends strongly on the measurement of the flame surface area and the unburned gas velocity. Many researchers discarded this method, due to the difficulty in measurement of the flame area, as the surface is badly deformed close to the walls [44]. This method may not be a good absolute, but is useful for comparative measurements. One advantage of this method is that it can be used with small quantities of fuel and is easy to construct. Results by this method were compared with those by other methods and agreement was found to be excellent. In the case of a propane-air mixture at high temperature, the results appeared as good as most, although

the temperature could not be controlled in the rig, but as can be seen, the results were in good agreement.

Finally, some observations should be made about the various values of the laminar burning velocities of propane, found by different methods. As can be seen, the lower values were obtained by this method, owing to cooling walls. A spherical bomb has small values of laminar burning velocities, due to flame front curvature or heat losses near to electrode region [44]. The results obtained from counterflow technique appeared, however, to be rather high and seen most likely to be free from heat losses and non-uniformity effects [14].

7 Conclusions

The main purpose of this research was to establish a comprehensive study of flames in tubes. The investigations were experimental for gas (propane) and liquid (acetone) fuel which were propagated at room temperature and at a high temperature of 333 K, in the horizontal and vertical position. This study covered the flame shape, observed flame speed, ignition source, and the gravity effect, measurements of gas velocity ahead of the flame front, laminar burning velocities of propane at room and elevated temperature and the effect of temperature on the laminar burning velocity.

- There was a clear difference between the flame speed values propagating by spark ignition and by gas lighter ignition. The flame speed by spark ignitions were considerably higher than the speed by flame ignition owing to the effect of pressure waves built inside the tube with both ends open and with orifice plates
- The flame shapes with both ends open were stable at lean conditions and became subject to oscillations at equivalence ratios of 1.1 to 1.3. While at the rich conditions of equivalence ratios of 1.4 to 1.6 flames were steady. For equivalence ratios of 1.1 to 1.3 a high speed camera operating at 3000 fps was used (instead of the colour camera which only worked up to 1000 fps) to show the flame propagating inside the tube with greater clarity and precision. The flames started steadily at the beginning, later the concave shape became elongated with wrinkled in appearance. The flame shape with orifice plates was more stable with a semi-ellipsoid shape at all equivalence ratios and orifice plate sizes in both horizontal and vertical positions. This flame shape is formed due to cooling of the walls and viscous forces. Tilted flames were observed, especially at the horizontal position, with the slower flame speed. The flame shapes in the vertical position were roughly hemispherical and semi-ellipsoid under rich condition, and the upward propagation was larger than the downward travelling, resulting in an increased the flame speed. At a temperature of 333 K with orifice plates of 5 mm at both ends, the flames were steady with a semi-ellipsoid shape almost for almost all varieties of equivalence ratios. For liquid fuel acetone at 333 K and at atmospheric pressure, the flame shape was semi-ellipsoid and uniform with a tipped shape at rich conditions
- Placing orifice plates at the ends of the tube resulted in flame speeds that were more uniform and linear in speed with distance along the tube. With the smallest orifice plates of 1 mm the pressure was increased, resulting in a change to the shape and

thickness of the flame and reduced the flame speed. With orifice plates of 5 mm placed at both ends the peak flame speed was nearly the same as the values published in 1951 [6], and the configurations of the flame shape were roughly the same at all the different equivalence ratios. However, for the biggest orifice plates 8 mm, fitted at both ends, a distorted flame was observed in the second half of the tube for rich conditions. The recombination of orifice plates 5/3 and 5/1, by fitting the biggest plate near to ignition point and the smallest in the other ends offered a good shape of flame and the speed was nearly the same for orifice plates of 3 and 1 mm at both ends. The biggest close to ignition point was responsible for excluding vibrations, whilst the smallest at the other end was used to change the flame shape.

- The flame speed observed at 333 K and at atmospheric pressure with 5 mm orifice plates at both ends for a propane-air mixture was constant, resulting in linear plots. The maximum flame speed was 1.11 m/s and higher than the speed at room temperature with the same orifice plates, by less than 15 %. These results are in good agreement with the previous results, which confirmed that, an increase in initial temperature caused an increase in the flame speed. For an acetone-air mixture at 333 K and at atmospheric pressure the peak flame speed was at an equivalence ratio of 1.3 and, generally, in good agreement with the published data, which used a spherical bomb technique in 2009 [107]
- The unburned gas velocity is measured by the Laser Doppler Velocimetry system (LDV) for propane - air mixture with 5 mm orifice plate at both ends and 5 mm plate next to ignition point and 3 mm plate at far end. The gas velocity ahead of the flame front was about 74 % less than the observed flame speed for orifice plate of 5 mm placed at both ends and about 86 % for recombination orifice plates of 5/3 mm.
- The surface area of the symmetrical flame requires only one image to obtain an accurate measurement, while the tilted and hemispherical flame required side and top images to get an accurate measurement of the flame surface area
- The laminar burning velocities were measured, with good agreement with the literature, for propane-air mixtures at room and high temperature and at atmospheric pressure. These results at room conditions, compared with the previous results in a similar tube method technique and with a small deviation with those who used spherical bomb and counterflow techniques, probably due to the heat loss by the wall. On the other hand, the laminar burning velocity of a propane-air mixture at 333 K and at normal pressure increased with increases in the initial temperature. These results

have good agreement with the previous work with a few exceptions which can be attributed to the inaccurate temperature inside the tube. However, the repeatability provided roughly the same results and this confirms that the apparatus used in this study is more accurate. In general, by means of the tube method these results of laminar burning velocities are in close agreements with the experimental data obtained by the different techniques in the literature.

7.1 Future work

In the future, further experiments will likely investigate the laminar burning velocity at high pressure and perform the experiment with different fuels. The final aim is to employ this method in the design of micro combustor for powering a small-scale machine.

The accuracy of laminar burning velocity data obtained experimentally at high temperature for tube method suffered from a number of factors. Firstly, the temperature inside the tube is not accurate. Secondly there is the problem of measuring the surface area of the flame. Therefore, some improvements and additional work are required in order to obtain the laminar burning velocity more accurately:

- ◆ Some modification to the rig, like reducing the quartz tube from 70 cm to 15 cm in length and increasing the distance of the copper tube to get more space for the heater to take place, to obtain a more accurate temperature inside
- ◆ The alternative method is to measure the surface area of the flame, by using suitable software, to capture three dimensional shape of the flame
- ◆ Perform a number of experiments for propane-air mixtures at high temperature with combination orifice plates of 5/3 and 5/1 mm. By placing 5 mm plate near to ignition point and 3 & 1 mm at the far end where the flame travels there.
- ◆ Perform a number of experimental configurations using different tube diameters. This is an important aim to study the effect of tube diameter on the flame speed.
- ◆ The measurement of the unburned gas velocity of liquid fuels to obtain the accurate values of the laminar burning velocity
- ◆ Study the effect of viscous drag on the flame speed close to the wall and may be using PIV to measure it
- ◆ Study the stretch effects in the tube with open at both ends and measure the stretch rate to obtain the stretched laminar burning velocity

References

- 1 **Al-mahalawy, F. and Habik, S.** *Fundamentals and Technology of Combustion*. (Elsevier Science Ltd., UK, 2000).
- 2 **Griffiths, J.F. and Barnard, J.A.** *Flame and Combustion*. (Alden Press., Oxford, 1995).
- 3 **Mossa, F. and Woolley, R.** Flame propagation in the tubes. *European Conference Meeting* (Proceedings of the European Meeting Cardiff - UK, 2011).
- 4 **Mallard, E. and Chateliar, H.L.** *Ann. Mines*, 1883, **8**.
- 5 **Coward, H.F. and Hartwell, F.J.** Studies in the mechanisms for flame movements. Part 2. The fundamental speed of flame in mixtures of methane and air. *Journal of chemical Society*, 1933, 2676-2684.
- 6 **Gerstein, M., Levine, O. and Wong, E.L.** The determination of fundamental burning velocities of hydrocarbons by a Revised Tube Method. *Journal of The American Chemical Society*, 1951, **73**(1), 418-422.
- 7 **Guenoche, H.** *Non-steady flame propagation*. (The Macmillan Company, New York, 1964).
- 8 **Coward, H.F. and Payman, W.** Problems in flame propagation. *Chemical Review*, 1937, **21**, 359-366.
- 9 **Urtiew, P.A. and Oppenheim, A.K.** Experimental observations of the transition to detonation in an explosive gas. *Proceedings of the Royal Society (London)*, 1966, **295**, 13-28.
- 10 **Wu, M., Burke, M.P., Son, S.F. and Yetter, R.A.** Flame acceleration and the transition to detonation of stoichiometric ethylene/oxygen in microscale tubes. pp. 2429-2437 (Proceedings of the Combustion Institute, 2007).
- 11 **Akkerman, V., Law, C.K., Bychkov, V. and Eriksson, L.E.** Analysis of flame acceleration induced by wall friction in open tubes. *Physics of Fluids*, 2010, **22**, 053606.
- 12 **Turns, S.R.** *An Introduction to Combustion - Concepts and Applications*. (McGraw-Hill International Editions, Mechanical Engineering Series, Singapore, 1996).
- 13 **Kuo, K.K.** *Principles of Combustion*. (John Wiley, United State of America, 2005).
- 14 **Law, C.K.** *Combustion Physics*. (Cambridge University press., Cambridge, 2006).
- 15 **Ragland, K.W. and Bryden, K.M.** *Combustion Engineering*. (Taylor and Francis Group, LLC, 2nd edition - 2011).

- 16 **Glassman, I. and Yetter, R.A.** *Combustion*. (Elsevier Inc., USA, 2008).
- 17 **Bunkute, B.** Burning velocities of coal-derived syngas mixtures. *School of Engineering* (Cranfield University, Shrivenham, UK, 2008).
- 18 **Linnett, J.W.** Methods of measuring laminar burning velocities. *Fourth symposium on combustion*, pp. 21-35 (Combustion and Detonation Waves, 1953).
- 19 **Andrewa, G.E. and Bradley, D.** Determination of burning velocities: A critical review. *Combustion and Flame*, 1972, **18**, 133 -153.
- 20 **Gulder, O.L., Smallwood, G.J., Wong, R., Snelling, D.R. and Smith, R.** Flame front surface characteristics in turbulent premixed propane/air combustion. *Combustion and Flame*, 2000, **120**, 407 - 416.
- 21 **Bradley, D., Lawes, M. and Mansour, M.S.** Explosion bomb measurements of ethanol-air laminar gaseous flame characteristics at pressures up to 1.4 MPa. *Combustion and Flame*, 2009, **156**, 1462-1470.
- 22 **Metghalchi, M. and Keck, J.C.** Laminar burning velocity of propane-air mixtures at high temperature and pressure. *Combustion and Flame*, 1980, **38**(2), 143-154.
- 23 **Saeed, K. and Stone, C.R.** Measurements of the laminar burning velocity for mixtures of methanol and air from a constant-volume vessel using a multizone model. *Combustion and Flame*, 2004, **139**(1-2), 152-166.
- 24 **Dahoe, A.E.** Laminar burning velocities of hydrogen-air mixtures from closed vessel gas explosions. *Journal of Loss Prevention in the Process Industries*, 2005, **18**(3), 152-166.
- 25 **Liao, S.Y., Jiang, D.M., Gao, J. and Huang, Z.H.** Measurements of Markstein Numbers and Laminar Burning Velocities for Natural Gas-Air Mixtures. *Energy & Fuels*, 2004, **18**, 316-326.
- 26 **Liao, S.Y., Jiang, D.M. and Cheng, Q.** Determination of laminar burning velocities for natural gas. *Fuel*, 2004, **83**(9), 1247-1250.
- 27 **Stone, R., Clarke, A. and Beckwith, P.** Correlations for the laminar-burning velocity of methane/diluent/air mixtures obtained in free-fall experiments. *Combustion and Flame*, 1998, **114**(3-4), 546-555.
- 28 **Crayford, A.P., Bowen, P.J., Rosa, D. and Tam, V.H.** Laminar burning characteristics of methane/water-vapour/air flames. *ECMCardiff - UK*, 2011).

- 29 Broustail, G., Halter, F., Moreac, G. and Rousselle, C.** Experimental determination of laminar burning velocity of butanol/iso-octane and ethanol/iso-octane blends as a function of initial pressure. *ECMCardiff* - UK, 2011).
- 30 Takizawa, K., Takahashi, A., Tokuhashi, K., Kondo, S. and Sekiya, A.** Burning velocity measurements of fluoropanes by the spherical-vessel method. *Journal of Fluorine Chemistry*, 2008, **129**, 713 - 719.
- 31 Bradley, D., Lawes, M., Liu, K., Verhelst, S. and Woolley, R.** Laminar burning velocities of lean hydrogen-air mixtures at pressures up to 1.0 MPa. *Combustion and Flame*, 2007, **149**, 162-172.
- 32 Hu, E., Fu, J., Pan, L., Jiang, X., Huang, Z. and Zhang, Y.** Experimental and numerical study on the effect of composition on laminar burning velocities of H₂/CO/N₂/CO₂/air mixtures
International Journal of Hydrogen Energy, 2012
37, 18509-18519.
- 33 Lewis, B. and Elbe, G.V.** Determination of the speed of flames and the temperature distribution in a spherical bomb from time-pressure explosion records. *Journal of chemical physics*, 1934, **2**, 283 - 290.
- 34 Fiock, E.F. and Marvin, C.F.** Flame speeds and energy considerations for explosions in a spherical bomb. (Technical Report 682, National Advisory Committee for Aeronautics, 1939).
- 35 Lewis, B. and Elbe, G.V.** *Combustion, Flames and Explosion of Gases*. (Academic Press, INC, Pittsburgh, Pennsylvania, 1987).
- 36 Groff, E.G.** The cellular nature of confined spherical propane-air flames. *Combustion and Flame*, 1982, **48**, 51-62.
- 37 Dowdy, D.R., Smith, D.B., Taylor, S.C. and Williams, A.** The use of expanding spherical flames to determine burning velocities and stretch effects in hydrogen/air mixtures. *23rd Symposium (International) on Combustion*, pp. 325-332 (The Combustion Institute, 1990).
- 38 Clavin, P.** Dynamic behavior of premixed flame fronts in laminar and turbulent flows. *Progress in Energy and Combustion Science*, 1985, **11**, 1-59.

- 39 Verhelst, S., Woolley, R., Lawes, M. and Sierens, R.** Laminar and unstable burning velocities and Markstein lengths of hydrogen-air mixtures at engine-like conditions. *30th International Symposium on Combustion*, pp. 209-216 (The Combustion Institute, 2005).
- 40 Al-Shahrany, A.S., Bradley, D., Lawes, M. and Woolley, R.** Measurement of unstable burning velocities of iso-octane-air mixtures at high pressure and the derivation of laminar burning velocities. *30th International Symposium on Combustion*, pp. 225-232 (The Combustion institute, 2005).
- 41 Marley, S.K. and Roberts, W.L.** Measurements of laminar burning velocity and Markstein number using high-speed chemiluminescence imaging. *Combustion and Flame*, 2005, **141**, 473 - 477.
- 42 Hassan, M.I., Aung, K.T., Kwon, O.C. and Faeth, G.M.** Properties of laminar premixed hydrocarbon/air flames at various pressures. *Journal of Propulsion and Power*, 1998, **14**, 479-488.
- 43 Jomaas, G., Zheng, X.L., Zhu, D.L. and Law, C.L.** Experimental determination of counterflow ignition temperatures and laminar flame speed of C2-C3 hydrocarbons at atmospheric and elevated pressures. pp. 193-200 (Proceeding of The Combustion Institute, 2005).
- 44 Gaydon, A.G. and Wolfhard, H.G.** *Flames: their structure radiation and temperature*. (Chapman and Hall etc., , London, 1979).
- 45 Powling, J.** A new burner method for the determination of law burning velocities and limits inflammability. *Fuel*, 1949, **28**, 105 - 118.
- 46 Maaren, A.V. and Goey, L.P.H.** Laser doppler thermometry in at flames. *Combustion Science and Technology*, 1994, **99**, 105 - 118.
- 47 Yu, G., Law, C.K. and Wu, C.K.** Laminar flame speed of hydrocarbon + air mixtures with hydrogen addition *Combustion and Flame*, 1986, **63**(3), 339-347.
- 48 Vagelopoulos, C.M., Egolfopoulos, F.N. and Law, C.K.** Further considerations on the determination of laminar burning velocities with the counterflow twin-flame technique. *25th Symposium (International) on Combustion*, pp. 1341 - 1347 (The Combustion Institute, 1994).
- 49 Vagelopoulos, C.M. and Egolfopoulos, F.N.** Direct experimental determination of laminar flame speeds. *27th Symposium (International) on Combustion*, pp. 513 - 519 (The Combustion Institute, 1998).

- 50 Chao, B.H., Egolfopoulos, F.N. and Law, C.K.** Structure and propagation of premixed flame in nozzle-generated counterflow. *Combustion and Flame*, 1997, **109**(4), 620-638.
- 51 Saso, Y., Zhu, D.L., Wang, H., Law, C.K. and Saito, N.** Laminar burning velocities of trifluoromethane-methane mixtures: Experiment and numerical simulation. *Combustion and Flame*, 1998, **114**(3-4), 457-468.
- 52 Wang, C.H., Ueng, G.J. and Tsay, M.S.** An experimental determination of the laminar burning velocities and extinction stretch rates of benzene/air flames. *Combustion and Flame*, 1998, **113**(1-2), 242-248.
- 53 Wu, C.k. and Law, C.K.** On the determination of laminar flame speeds from stretched flames. *20th symposium (International) on Combustion*, pp. 1941 -1949 (The Combustion Institute, 1984).
- 54 Egolfopoulos, F.N., Cho, P. and Law, C.K.** Laminar flame speeds of methane-air mixtures under reduced and elevated pressures. *Combustion and Flame*, 1989, **76**, 375-391.
- 55 Zhao, Z., Kazakov, A. and Dryer, F.L.** Measurements of dimethyl ether/air mixture burning velocities by using particle image velocimetry. *Combustion and Flame*, 2004, **139**(1-2), 52-60.
- 56 Wheeler, V.R.** The propagation of flame in mixture of methane and air; the uniform movement. *Journal of the Chemical Society*, 1914, **105**, 2606-2613.
- 57 Gerstein, M., Levine, O. and Wong, E.L.** Fundamental burning velocities of hydrocarbons. *Industrial and Engineering Chemistry*, 1951, 2770-2772.
- 58 Markstein, G.H.** Experimental and theoretical studies of flame-front stability. *Journal of the Aeronautical Science*, 1951, **18**, 199-209.
- 59 Mason, W. and Wheeler, R.V.** The propagation of flame in mixtures of methane and air - part II. *Trans. Chem. Society*, 1920, **117**, 1226-1234.
- 60 Maxworthy, T.** Flame propagation in tubes. *Physics of Fluids*, 1962, **5**, 407-417.
- 61 Jarosinski, J., Strehlow, R.A. and Azarbarzin, A.** The mechanisms of lean limit extinguishment of an upward and downward propagating flame in a standard flammability tube. *19th Symposium (International) on Combustion*, pp. 1549-1557 (The Combustion Institute, 1982).
- 62 Strehlow, R.A., Non, K.A. and Wherley, B.R.** The effect of gravity on premixed flame propagation and extinction in a vertical standard flammability tube. *21th Symposium (Internationa) on Combustion*, pp. 1899-1908 (The Combustion Institute, 1986).

- 63 Hamins, A., Heitor, M. and Libby, P.A.** Gravitational effects on the structure and propagation of premixed flames. *37th Congress of the International Astronautical federation*, pp. 503-514 (Acta Astronautica, Innsbruck, Austria, 1988).
- 64 Stevens, F.W.** The rate of flame propagation in gaseous explosive reactions. *Journal of American chemical society*, 1926, **48**, 1896-1906.
- 65 Rallis, C.J. and Garforth, A.M.** The determination of laminar burning velocity. *Progress in Energy and Combustion Science*, 1980, **6**, 303-329.
- 66 Bradley, D. and Hundy, G.** Burning velocities of methane-air mixtures using hot-wire anemometers in closed-vessel explosions. *Thirteenth Symposium (International)*, pp. 575-583 (The Combustion Institute, Pittsburgh, 1970).
- 67 Andrews, G.E. and Bradley, D.** Determination of burning velocities: A critical review. *Combustion and Flame*, 1972, **18**, 133 -153.
- 68 Henderson, H.T. and Hill, G.R.** A kinetic study of methyl chloride combustion. *The Journal of Physics and Chemistry*, 1956, **60**, 874-878.
- 69 Davis, S.G. and Law, C.K.** Determination of and fuel structure effects on laminar flame speeds of C1 to C8 hydrocarbons. *Combustion Science and Technology*, 1998, **140**, 427-449.
- 70 Razus, D., Brinzea, V., Mitu, M., Movileanu, C. and Oancea, D.** Burning velocity of propane-air mixtures from pressure-time records during explosions in a closed spherical vessel. *Energy & Fuels*, 2012, **26**, 901-909.
- 71 Borman, G.L. and Ragland, K.W.** *Combustion Engineering*. (McGraw Hill, 1998).
- 72 Bosschaart, K.J., de Goey, L.P.H. and in collaboration with, J.M.B.C.f.F.M.** The laminar burning velocity of flames propagating in mixtures of hydrocarbons and air measured with the heat flux method. *Combustion and Flame*, 2004, **136**(3), 261-269.
- 73 Toshio, H.** Effects of temperature and pressure on burning velocity. *Combustion and Flame*, 1986, **65**, 35-43.
- 74 Farrell, J.t., Johnston, R.j. and Androulakis, I.P.** Molecular structure effects on laminar burning velocities at elevated temperature and pressure. *SAE International*, pp. 1-22(Tampa, Florida USA, 2004).
- 75 Razus, D., Oancea, D., Brinzea, V., Mitu, M. and Movileanu, C.** Experimental and computed burning velocities of propane-air mixtures. *Energy conversion and management*, 2010, **51**, 2979-2984.

- 76 Strehlow, R.A.** *Combustion fundamentals*. (McGraw-Hill International Company, Singapore, 1985).
- 77 Hassan, M.I., Aung, K.T. and Faeth, G.M.** Measured and predicted properties of laminar premixed methane/air flames at various pressures. *Combustion and Flame*, 1998, **115**(4), 539-550.
- 78 Gu, X.J., Haq, M.Z., Lawes, M. and Woolley, R.** Laminar burning velocity and Markstein lengths of methane-air mixtures. *Combustion and Flame*, 2000, **121**(1-2), 41-58.
- 79 Kitagawa, T.** Effects of pressure on burning velocity and instabilities of propane-air premixed flames. *The Japan Society of Mechanical Engineers*, 2005, **48**, 2-8.
- 80 Tang, C., Zheng, J., Huang, Z. and Wang, J.** Study on nitrogen diluted propane-air premixed flames at elevated pressures and temperatures. *Energy conversion and management*, 2010, **51**, 288-295.
- 81 Bradley, D., Lawes, M. and Mansour, M.S.** Explosion bomb measurements of ethanol-air laminar gaseous flame characteristics at pressures up to 1.4 MPa. *Combustion and Flame*, 2009, **156**(7), 1462-1470.
- 82 Burbano, H.J., Pareja, J. and Amell, A.A.** Laminar burning velocities and flame stability analysis of syngas mixtures at sub-atmospheric pressures. *International Journal of Hydrogen Energy*, 2011, **36**, 3243-3252.
- 83 Tse, S.D., Zhu, D.L. and Law, C.K.** Morphology and burning rates of expanding spherical flames in H₂/O₂/Inert mixtures up to 60 atmospheres. *Proceedings of the Combustion Institute*, 2000, **28**, 1793-1800.
- 84 McHale, E.T., Geary, R.W., Elbe, G.V. and Huggett, C.** Flammability limits of H₂-O₂-hydrocarbon mixtures. *Combustion and Flame*, 1971, **16**, 167-175.
- 85 Holland, S., Jones, D.T. and Gray, P.** Combustion supported by nitrous oxide: Flame speeds and flammability limits in the hydrogen+ethane+nitrous oxide system. *Combustion and Flame*, 1971, **17**, 31-35.
- 86 Schoor, F. and Verplaetsen, F.** The upper flammability limit of methane/hydrogen/air mixtures at elevated pressures and temperatures. *International Journal of Hydrogen Energy*, 2007, **32**, 2548-2552.
- 87 Lovachev, L.A., Babkin, V.S., Bunev, V.A., Vyun, A.V., Krivulin, V.N. and Baratov, A.N.** Flammability limits: An invited review. *Combustion and Flame*, 1973, **20**, 259-289.

- 88 Halstead, M.p., Pye, D.B. and Quinn, C.P.** Laminar burning velocities and weak flammability limits under engine-like conditions. *Combustion and Flame*, 1974, **22**, 89-97.
- 89 Shebeko, N., Tsarichenko, S.G., Korolchenko, A., Trunev, A.V., Navzenya, V., Papkov, S.N. and Zaitzev, A.A.** Burning velocities and flammability limits of gaseous mixtures at elevated temperatures and pressures. *Combustion and Flame*, 1995, **102**, 427-437.
- 90 Cashdollar, K.L., Zlochower, I.A., Green, G.M., Thomas, R.A. and Hertzberg, M.** Flammability of methane, propane and hydrogen gases. *Journal of Loss Prevention in the Process Industries*, 2000, **13**, 327-340.
- 91 Law, C.K. and Faeth, G.M.** Opportunities and challenges of combustion in microgravity. *Progress in Energy and Combustion Science*, 1994, **20**, 65-113.
- 92 Law, C.K.** Dynamics of stretched flames. In *Twenty-second Symposium (International) on Combustion*, pp. 1381-1402 (The Combustion Institute, 1989).
- 93 Karlovitz, B., Denniston, D.W., Knapschacfer, D.H. and Wells, F.E.** Studies on turbulent flames. *4th Symposium (International) on Combustion*, pp. 613-620 (The Combustion Institute, 1953).
- 94 Tseng, L.K., Ismail, M.A. and Faeth, G.M.** Laminar burning velocities and Markstein number of hydrocarbon/air flames. *Combustion and Flame*, 1993, **95**, 410-426.
- 95 Halter, F., Tahtouh, T. and Mounaim-Rousselle, C.** Nonlinear effects of stretch on the flame front propagation. *Combustion and Flame*, 2010, **157**, 1825-1832.
- 96 Tang, C., Zheng, J., Huang, Z. and Wang, J.** Study on nitrogen diluted propane-air premixed flames at elevated pressures and temperatures. *Energy conversion and management*, 2010, **51**, 288-295.
- 97 Andersen, J.W. and Fein, R.S.** Measurements of normal burning velocities and flame temperatures of Bunsen flames. *The Journal of Chemical Physics*, 1949, **17**, 1268-1273.
- 98 Warnatz, J.** The structure of laminar alkane, alkene, and acetylene flames. *18th Symposium (International) on Combustion*, pp. 369-384 (The Combustion Institute, 1981).
- 99 Maas, U. and Warnatz, J.** Ignition processes in hydrogen-oxygen mixtures. *Combustion and Flame*, 1988, **74**, 53-69.
- 100 Razus, D., Brinzea, V., Mitu, M. and Oancea, D.** temperature and pressure influence on explosion pressures of closed vessel propane-air deflagrations. *Journal of Hazardous Materials*, 2010, **174**, 548-555.

- 101 Akram, M., Kishore, V. and Kumar, S.** Laminar burning velocity of propane/CO₂/N₂-air mixtures at elevated temperatures. *Energy & Fuels*, 2012, **26**, 5509-5518.
- 102 Lozano, A., Yip, B. and Hanson, R.K.** Acetone: a tracer for concentration measurements in gaseous flows by planar laser-induced fluorescence. *Experiments in Fluids*, 1992, **13**, 369-376.
- 103 Yip, B., Miller, M.F., Lozano, A. and Hanson, R.K.** A combined OH/acetone planar laser-induced fluorescence imaging technique for visualizing combustions flows. *Experiments in Fluids*, 1994, **17**, 330-336.
- 104 Li, Y., Wei, L., Tian, Z., Yang, B., Wang, J., Zhang, T. and Qi, F.** A comprehensive experimental study of low-pressure premixed C₃-oxygenated hydrocarbon flames with tunable synchrotron photoionization. *Combustion and Flame*, 2008, **152**, 336-359.
- 105 Gibbs, G.J. and Calcote, H.F.** Effect of molecular structure on burning velocity. *Journal of chemical and Engineering Data*, 1959, **4**, 226-237.
- 106 Molkov, V.V. and Nekrasov, V.P.** Normal propagation velocity of acetone-air flames versus pressure and temperature. *Combustion Explosion, Shock Waves*, 1981, **17**, 280-283.
- 107 Pichon, S., Black, G., Chaumeix, N., Simmie, J.M., Curran, H.J. and Donohue, R.** The combustion chemistry of a fuel tracer: measured flame speeds and ignition delays and a detailed chemical kinetic model for the oxidation of acetone. *Combustion and Flame*, 2009, **156**, 494-504.
- 108 Burluka, A.A., Harker, M., Osman, H., Sheppard, C.G.w. and Konnov, A.A.** Laminar burning velocities of three C₃H₆O isomers at atmospheric pressure. *Fuel*, 2010, **89**, 2864-2872.
- 109 Chong, C.T. and Hochgred, S.** Measurements of laminar flame speeds of acetone/methane/air mixtures. *Combustion and Flame*, 2011, **158**, 490-500.
- 110 Nilsson, E.J., Goey, L.P. and Konnov, A.A.** Laminar burning velocities of acetone in air at room and elevated temperatures. *Fuel*, 2013, **105**, 496-502.
- 111 Hoare, M.F. and Linnett, J.W.** Burning velocity determination, part 10 Flame propagation along horizontal tubes. *Trans. Faraday Soc.*, 1953, **49**, 1038-1049.
- 112 Yeh, Y. and Cummins, H.Z.** Localized fluid flow measurements with an He-Ne laser spectrometer. *Applied Physics Letters*, 1964, **4**, 176-178.
- 113 Foreman, J.W., George, E.W. and Lewis, R.D.** Measurement of localized flow velocities in gases with a Laser Doppler Flowmeter. *Applied Physics Letters*, 1965, **7**, 77-78.

- 114 Wang, C.P.** Laser Doppler Velocimetry. *Journal of Quantitative spectroscopy and Radiative Transfer*, 1988, **40**, 309-319.
- 115 Pennington, P.** Flames in Tubes. *Mechanical Engineering* (Sheffield University, Sheffield, 2009).
- 116 Coward, H.F. and Hartwell, F.J.** Studies in the mechanism of flame movement. Part I. The uniform movement of flame in mixtures of methane and air, in relation to tube diameter. *Journal of American chemical society*, 1932, 1996-2004.
- 117 Akkerman, V., Bychkov, V., Petchenko, A. and Eriksson, L.E.** Acceleration flames in cylindrical tubes with nonslip at the wall. *Combustion and Flame*, 2006, **145**, 206-219.
- 118 Bjerketvedt, D., Bakke, J.R. and Wingerden, K.V.** Gas explosion handbook. *Journal of Hazardous Materials*, 1997, **52**, 1-150.
- 119 Jensen, K.D.** Flow measurements. *The Journal of The Brazilian Socitey of Mechanical Sciences and Engineering*, 2004, **26**, 400-419.
- 120** (TSI), T.S.I., Laser Doppler Velocimetry/Phase Doppler Particle Analyzer(PDPA)- Operation Manual, July,2011.
- 121** www.laum-vld-univ-lemans.fr/principes.htm.
- 122** T.S.I., Partical Instruments Six-Jet Atomizey Instruction Manual. In TSI, ed2003).
- 123 Joklik, R.G., Daily, J.W. and Pitz, W.j.** Measurements of CH radical concentrations in an aacetylene/oxygen flame and comparisons to modeling calculations. *21th Symposium (International) on Combustion*, pp. 895-904 (The Combustion Institute, 1986).
- 124 Devriendt, K. and Peeters, J.** Direct identification of the $C_2H(X(2) \sigma^+) + O(p-3) \rightarrow CH(A(2)\Delta) + CO$ reaction as the source of the $CH(A(2)\Delta \rightarrow X(2)\pi)$ chemiluminescence in $C_2H_2/O/H$ atomic flames. *Journal of physical chemistry*, 1997, **101**, 2546-2551.
- 125 Gaydon, A.G.** *Spectroscopy and combustion theory*. (Chapman & Hall LTD, 1942).
- 126 Haber, L.C.** An investigation into the origin, measurement and application of chemiluminescent light emissions from premixed flames. *Mechanical Engineering* (Virginia Polytechnic Institute and State University, Virginia, 2000).
- 127 Mallard, S.** Flames in Tubes. *Mechanical Engineering* (Sheffield University, Sheffield, 2011).
- 128 Mason, W. and Wheeler, V.R.** The "Uniform Movement" during the propagation of flame. *Journal of the Chemical Society, Transactions*, 1917, **111**, 1044-1057.

- 129 Lavante, E.V. and Strehlow, R.A.** The mechanism of lean limit flame extinction. *Combustion and Flame*, 1983, **49**, 123-140.
- 130 Shoshin, Y. and Jarosinski, J.** On extinction mechanism of lean limit methane-air flame in a standard flammability tube. pp. 1043-1050 (Proceedings of the Combustion Institute, 2009).
- 131 Shoshin, Y.L. and Goey, L.P.H.** Experimental study of lean flammability limits of methane/hydrogen/air mixtures in tube of different diameters. *Experimental Thermal and Fluid Science*, 2010, **34**, 373-380.
- 132 Ellis, O. and Wheeler, R.V.** Explosion in closed cylinders. part III. The manner of movement of flame. *Journal of the Chemical Society*, 1928, 3215-3218.
- 133 Cui, C., Moshe, M. and Jackson, T.L.** Pulsating mode of flame propagation in two-dimensional channels. *The American Institute of Aeronautics and Astronautics (AIAA)*, 2005, **43**, 1284-1292.
- 134 Petchenko, A., Bychkov, V., Akkerman, V. and Eriksson, L.E.** Flame-sound interaction in tubes with nonslip walls. *Combustion and Flame*, 2007, **149**, 418-434.
- 135 Akkerman, V., Bychkov, V., Petchenko, A. and Eriksson, L.** Flame oscillations in tubes with nonslip at the walls. *Combustion and Flame*, 2006, **145**, 675-687.
- 136 Lee, T. and Lee, S.** Direct comparison of turbulent velocity and flame surface properties premixed flames. *Combustion and Flame*, 2003, **132**, 492-502.
- 137 Fleifil, M., Annaswamy, A.M., Ghoneim, Z.A. and Ghoniem, A.F.** Response of a laminar premixed flame to flow oscillations: A kinematic model and thermoacoustic instability results. *Combustion and Flame*, 1996, **106**, 487-510.
- 138 Gerstein, M.** The structure of laminar flames. *4th Symposium on Combustion*, pp. 35-43 (Combustion and Detonation Waves, 1953).
- 139 Markstein, G.H.** Instability phenomena in combustion waves. *International Symposium on Combustion*, pp. 44-59 (1953).
- 140 McIntos, A.C.** Pressure-driven disturbances in fluid dynamic interactions with flames. *Modeling in Combustion Science, Lecture Notes in Physics*, 1995, **449**, 176-192.
- 141 HO, Y.K.** Flames in Tubes. *Thesis (BSc) Mechanical Engineering* (University of Sheffield, Sheffield, 2011).
- 142 Markstien, G.H.** *Non-steady flame propagation*. (Macmillan, New York, 1964).

- 143 Williams, F.A.** *Combustion theory, 2nd edition.* (Benjamin-Cummings, Menlo Park, Calif, 1985).
- 144 Law, C.K., Peter, N. and Rogg, B.** *Reduced kinetic mechanisms for application in combustion system.* (Berlin; London: Springer-Verlag, 1993).
- 145 Ulinski, M., Moore, P., Elia, M. and Metghalchi, M.** Laminar burning velocities of methane-air-diluent mixtures. *Journal of Engineering for Gas Turbines and Power-Transactions of the Asme*, 1998, **32**.
- 146 Bruel, P.V.** *Sound insulation and room acoustics.* (London, Chapman& Hall, 1951).
- 147 Ronney, P.D. and Wachman, H.Y.** Effect of gravity on laminar premixed gas combustion I: Flammability limits and burning velocities. *Combustion and Flame*, 1985, **62**, 107-119.
- 148 Qiang, H.** Flames in Tubes. *Thesis (MSc), Mechanical Engineering* (University of Sheffield, Sheffield, 2012).
- 149 Dugger, G.L., Weast, R.C. and Heimel, S.** Flame velocity and preflame reaction in heated propane-air mixtures. *Industrial and Engineering Chemistry*, 1955, **47**, 114-116.
- 150 Andrews, G.E. and Bradley, D.** The burning velocity of methane-air mixtures. *Combustion and Flame*, 1972, **19**, 275-288.
- 151 Kuehl, D.K.** Laminar burning velocities of propane-air mixtures. *Symposium (International) on Combustion*, pp. 510-521,1961).

Appendix A

Calculate the internal volume of the apparatus

a- volume of the tube

Length of copper tube = 1970 mm

Length of quartz tube = 650 mm

Radius of tube = 10.2 mm

Volume = 822.68 cm³

b- volume of the fans

Length of fan = 70 mm

Radius of fan = 26 mm

Volume = 297.17

c- Volume of conical from 54mm to 22 mm reducer

Length = 20 mm

Base Radius = 26 mm

Length of tube (22 diameter) = 17 * 4 = 68 mm

Volume = 82.436 cm³

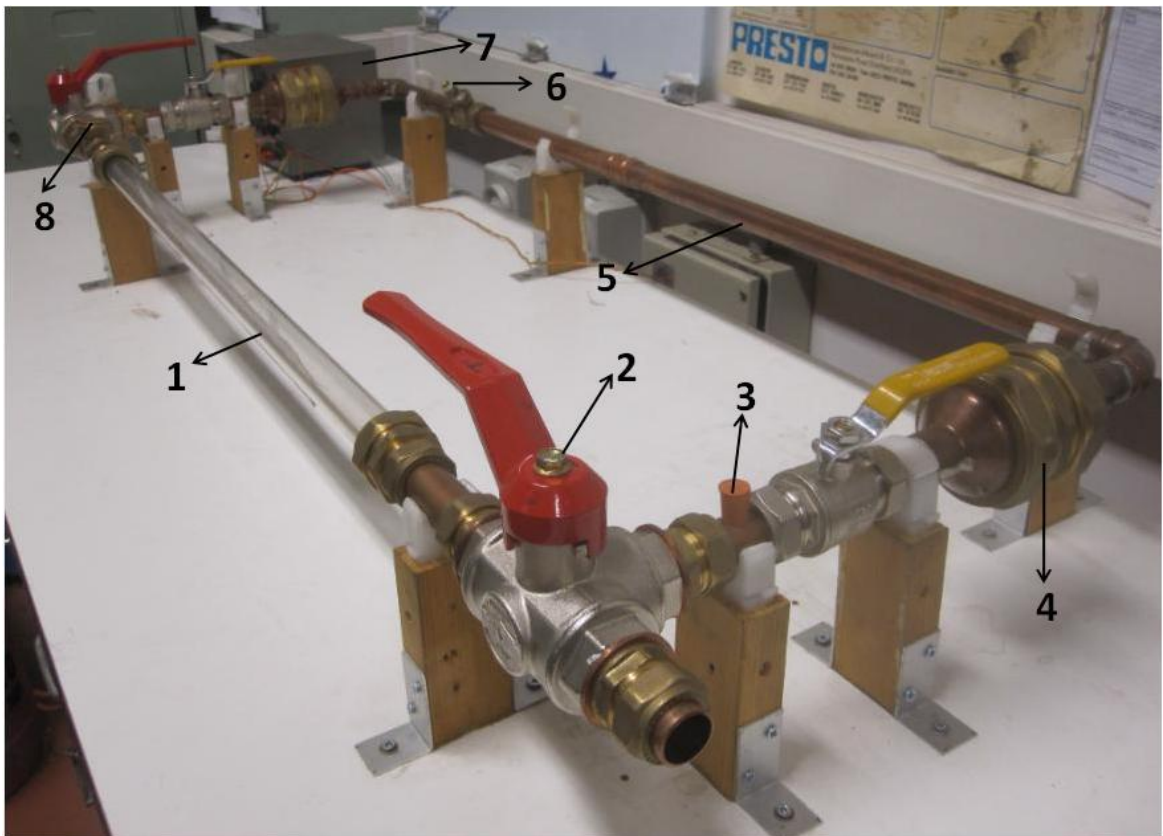
Total volume = 1202.286 cm³

Appendix B

B1 - Experimental procedures

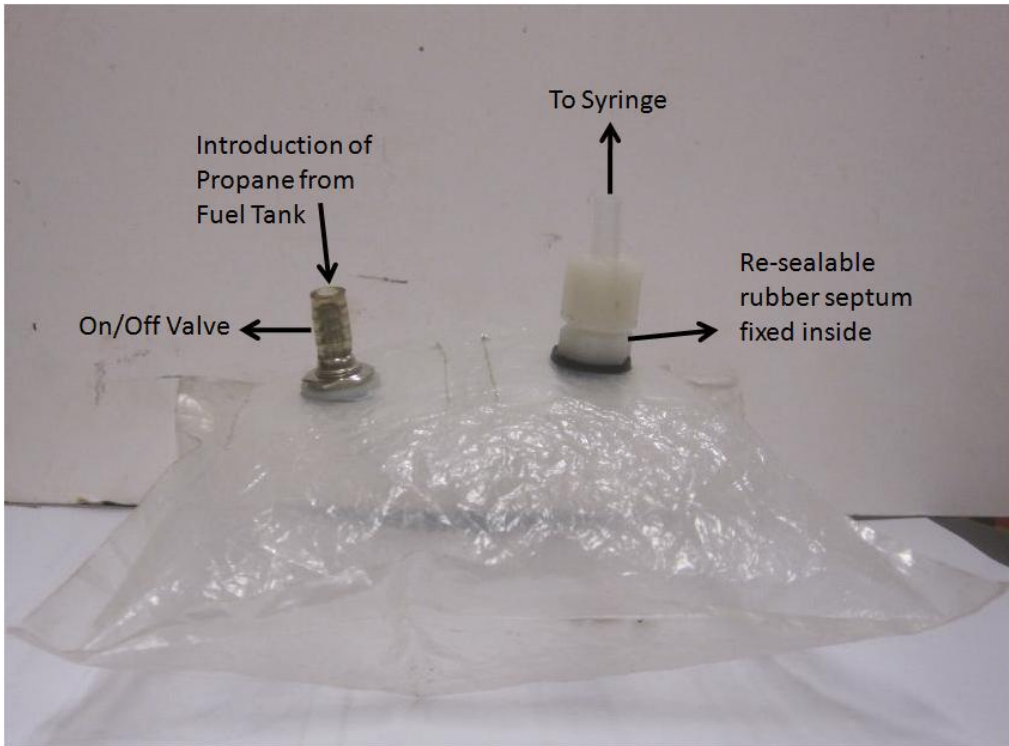
To prepare for the test, firstly is ensuring no air in the transfer bag shown below and propane cylinder tube, also ensure that the two three-way valves is in the right position through the loop. Switch on the fans for mixing and the fuel is injected into the system used needle and syringe. Leave the system 3 – 4 minutes to mix the fuel and air, and then switch off the fans and allow the mixture to be settled down for approximately 1 minute. Set up a high speed camera and turn lights off and the three-way valves towards the atmosphere. Open the cover of ignition point to insert the gas lighter and ignite the gases. Finally end the recording on the camera and compressed the air through cleaning hole and activate it to purge unburned gases.

Liquid fuel (Acetone) is injected using syringe sized according to the amount of fuel injec



- 1- Flame tube 2- Three way valve 3- Cleaning hole 4- Mixing Fan 5- Copper tube 6- Fuel injection hole 7- DC power supply 8- Ignition point

Flame tube apparatus



Gas transfer bag



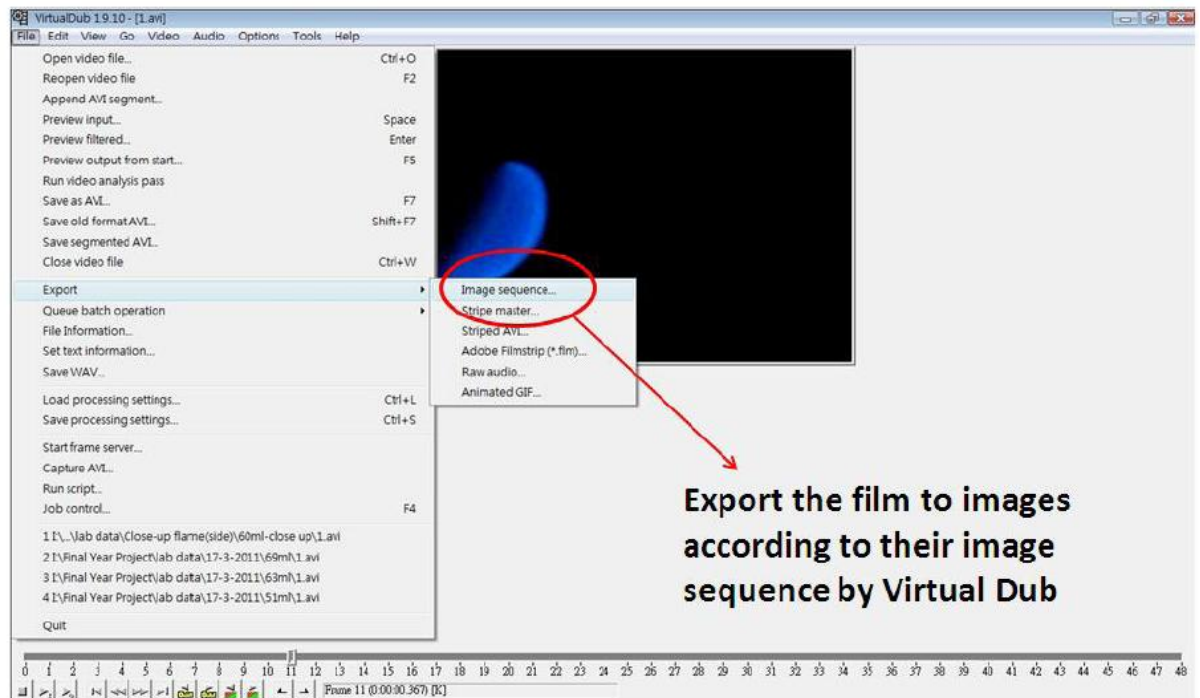
Experimental apparatus with high temperature of 333 K

B2 – Flame speed calculating:

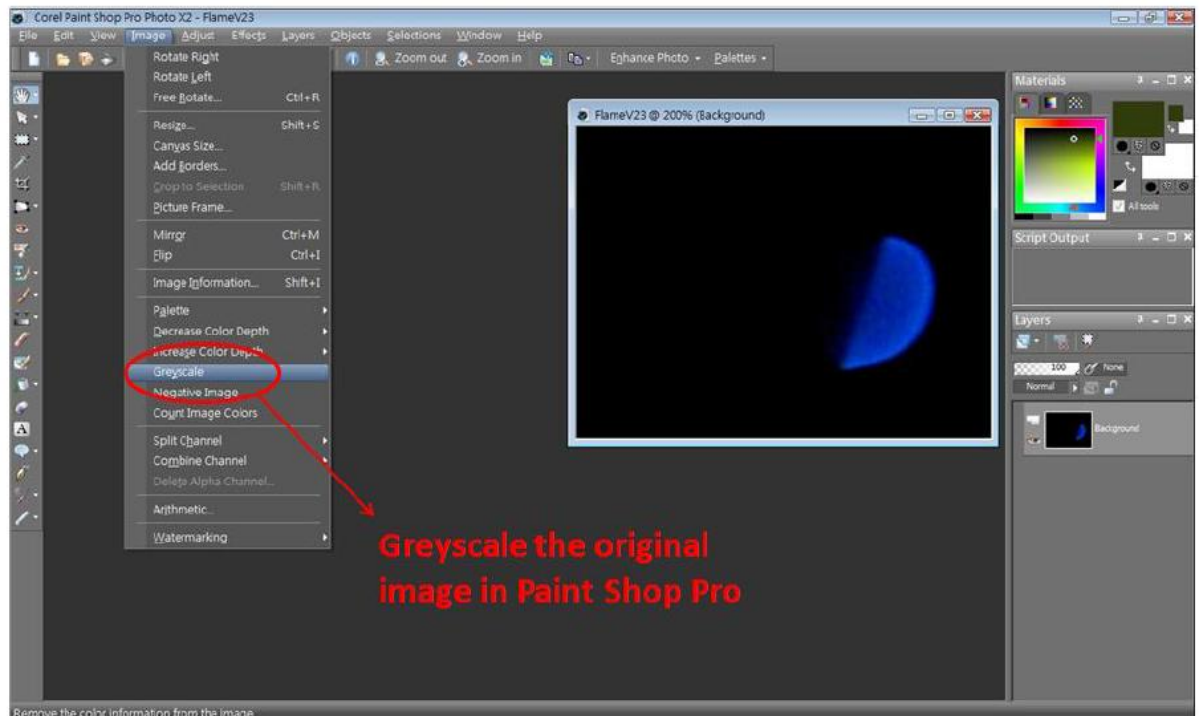
1. Films captured using a digital camera.
2. Moved video was captured to computer.
3. Open video in Virtual dub software.
4. The 'avi video files' were converted into 'bmp' images and unnecessary parts of the film cut. This was done using Virtual dub.
5. The captured flames images are then processed in Corel paint Shop Pro. A concept of image segmentation is employed. This is a technique of partitioning the flames images into multiple segments.
6. Open middle frame of the sequence in a Corel paint Shop photo and then start recording.
7. Converted the image into grayscale and brightness & contrast is applied. Then saved it as a script file into a folder.
8. Performed batch process on all frames was saved before into EPS image.
9. The data were collected can be opened in Excel and then the flame speed can be calculated.
10. The flame speed was calculated using the function 'LINEST' together with following five readings.

B3 – Flame speed processing

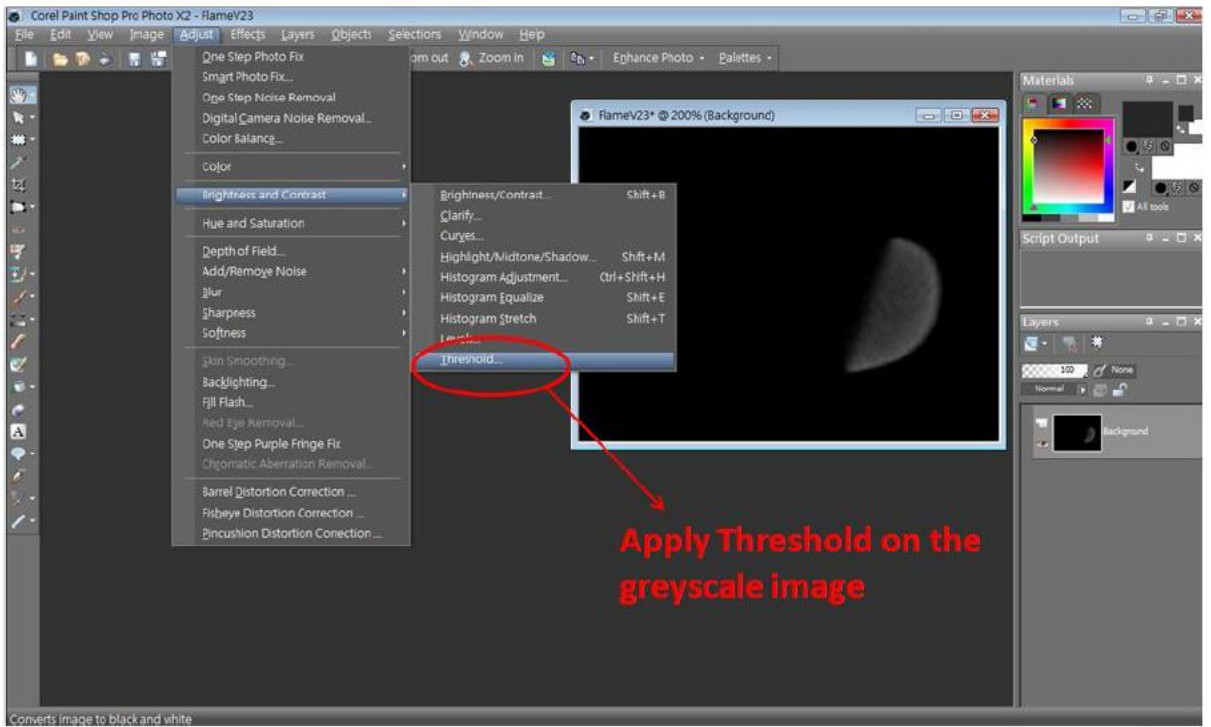
Step 1:



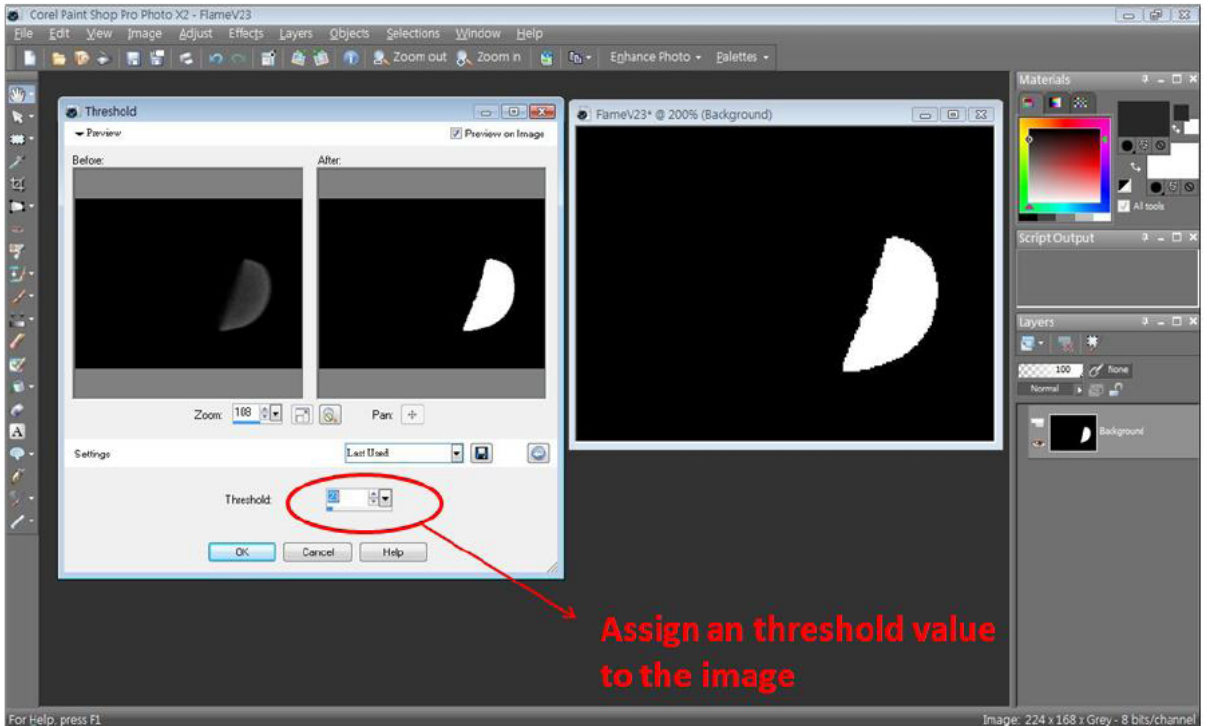
Step 2:



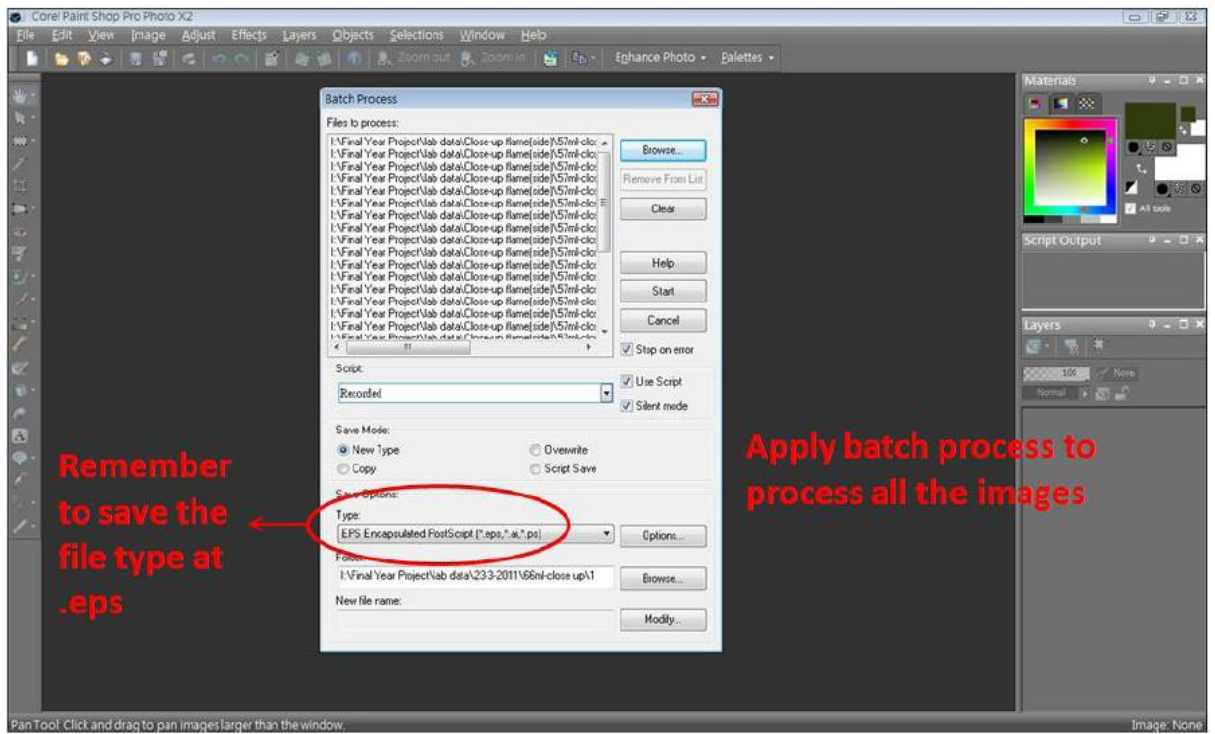
Step 3:



Step 4:



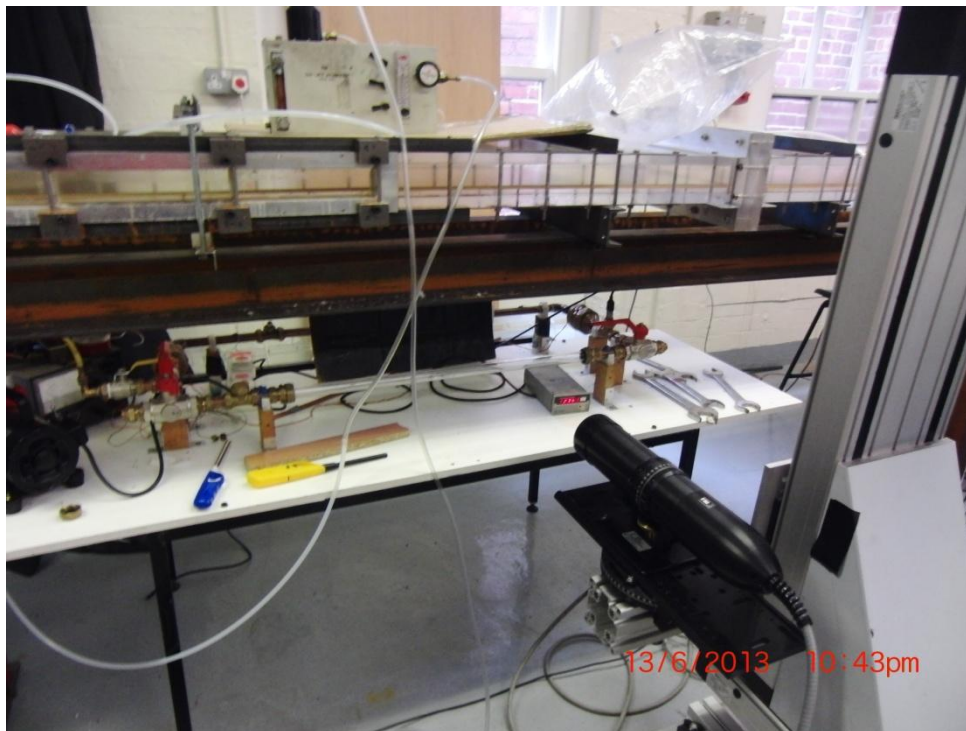
Step 5:

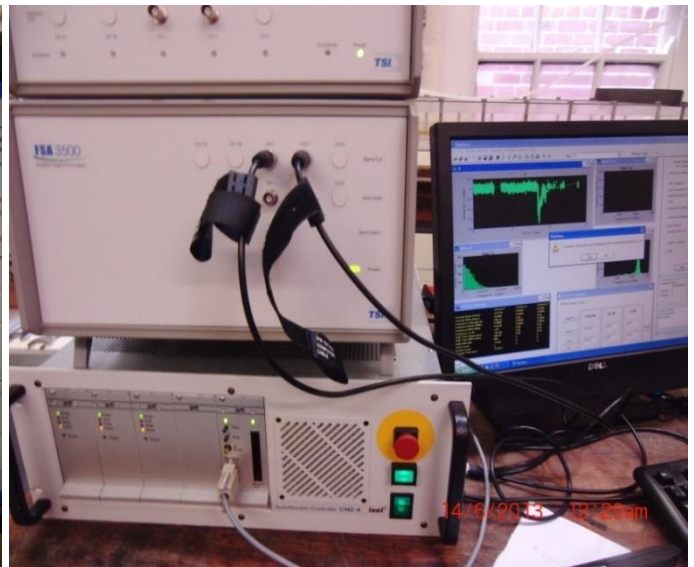
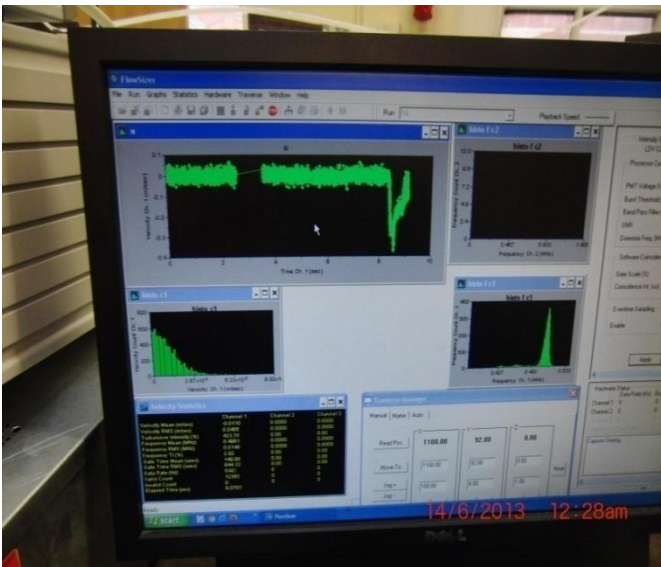


Appendix C

LDV procedure and data collection

Prepare the rig and the mixture as explained in Appendix –A for propane-air mixtures. Put the laser system close to the rig and used the traverse to move the laser and setting the apparatus to the suitable point on the tube when data need to be start collected. The traverse can move automatically based on the matrix of the position selected as shown in the Figure below. The software package should be installed and a new main folder created to monitor for each equivalence ratio. Before inject the mixture insert the seeding inside the tube for 10 to 15 second and then turn the laser on and ignite the mixture. Next save the data recorded by press the (scan capture) button to obtain the unburned gas velocity directly for each equivalence ratios. Finally moved all the data obtained to the Excel software and then scattered the data of time against speed and find the average of speed between the two source points on the tube.





Appendix D

Temperature recordings

		Propane	Acetone
Thermocouples	Room Tem.	(High) °C	(High) °C
1- Heater	21.16	64.13	63.79
2- Fuel input	22.11	61.31	60.93
3- Before L/H valve	21.19	66.02	65.78
4- L/H Tube	20.14	61.31	61.33
5- R/H Tube	21.16	51.88	52.33
6- After R/H Tube	22.30	54.76	54.66
Average of Temperature		59.90	59.803

The temperature unit in this work by Kelvin [K] = [°C] + 273

These temperatures were recorded in the first test begin.

Appendix E

Quantity of Propane at 333 K with a range of equivalence ratio

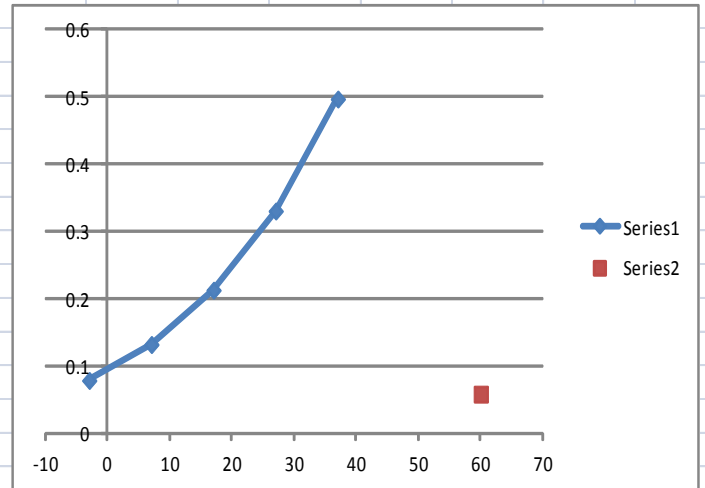
	0	-250							
Pressure =	1.03 bar		Text in red should depends on the fuel						
Vol. Of tube =	0.00120365 m ³		Text in blue should depends on the vessel, an should not be changed						
Gas Const. (R) =	8.31E-02 m ³ .bar/kmol.K								
Temperature =	333 K	60 C							
lamda	1								340
Equivalence ratio	1.2				52.2224 ml				
density of fuel at room temp.28C	1.815 Kg/m3								
					1.75823				
No. of moles in vessel =	4.48E-05 kmol	PV=nRT							
	0.04 mol								
No. of atoms in fuel									
C	3								
H	8								
O	0								
N	0								
For 1 mole of fuel									
Required moles of O2	5								
Required moles of N2	18.8								
Total moles air and fuel	24.8								
mole fraction fuel (stoich.)	0.040322581 bar								
	0.042016807								
mole fraction of fuel =	0.048								
moles of fuel at injection =	0.002149436 mole								
	2149.435555								
mass of fuel =	44.097								
Vol of Fuel injected	0.052222402 m3								

Equivalence ratio [ϕ]	0.8	0.9	1	1.1	1.2	1.3	1.4	1.5	1.6
Quantity of propane [ml]	35	40	44	48	52	56	60	64.5	68.5

Appendix F

Quantity of Acetone at 333 K with a range of equivalence ratio

	1203.63		
	1.20363		
	Acetone		
Pressure =	1 bar		Text in red should depends on the fuel
Vol. Of tube =	0.00120363 m ³		Text in blue should depends on the bomb, an should not be changed
Gas Const. (R) =	8.31E-02 m ³ .bar/kmol.K		
Temperature =	333 K		
lamda	0.833333333		
Equivalence ratio	1.2		
density of liquid fuel room temp.	0.789 Kg/ml		
No. of moles in bomb =	4.35E-05 kmol	PV=nRT	
	0.04 mol		
No. of atoms in fuel			
C	3		
H	6		
O	1		
N	0		
For 1 mole of fuel			
Required moles of O2	4		
Required moles of N2	15.04		
Total moles air and fuel	20.04		
mole fraction fuel (stoich.)	0.0499002 bar		
	0.052521008		Red square
mole fraction of fuel =	0.059288538	60	0.05929
moles of fuel at injection =	0.002577564		
Mass of fuel.	58.08 g		
Vol. Of fuel to inject	0.189740086 ml		
	189.7400857 micro l		



Equivalence ratio [ϕ]	0.8	0.9	1	1.1	1.2	1.3	1.4	1.5	1.6
Quantity of Acetone [microL]	130	145	160	175	190	205	220	234	248

Appendix G

Example of flame speeds calculation for open both ends and with an equivalence ratio of 1.1.

		Scale		18 cm		203 pix
Time (ms)	Frame	Distanc Pixels	Speed Pix/fram	Distance mm	Speed m/s	
0	0	49		43.44828		
2.380952	1	55		48.76847		
4.761905	2	63	7.3	55.86207	2.718621	
7.142857	3	70	7.5	62.06897	2.793103	
9.52381	4	78	7.5	69.16256	2.793103	
11.90476	5	85	7.5	75.36946	2.793103	
14.28571	6	93	7.7	82.46305	2.867586	
16.66667	7	100	7.6	88.66995	2.830345	
19.04762	8	109	7.7	96.65025	2.867586	
21.42857	9	115	7.5	101.9704	2.793103	
23.80952	10	124	7.7	109.9507	2.867586	
26.19048	11	130	7.8	115.2709	2.904828	
28.57143	12	140	8	124.1379	2.97931	
30.95238	13	146	8	129.4581	2.97931	
33.33333	14	156	7.8	138.3251	2.904828	
35.71429	15	162	7.9	143.6453	2.942069	
38.09524	16	171	8	151.6256	2.97931	
40.47619	17	178	8.1	157.8325	3.016552	
42.85714	18	188	8.2	166.6995	3.053793	
45.2381	19	194		172.0197		
47.61905	20	204		180.8867		
				Av.	2.887302	

Appendix H

Example of flame speed calculation for upward propagating at open both ends, with an equivalence ratio of 1.2.

			Scale	20 cm	210 pix		
Time (ms)	Frame	Distanc Pixels	Speed Pix/fram	Distance mm	Speed m/s		
0	0	56		53.33333			
2.380952	1	59		56.19048			
4.761905	2	73	7.5	69.52381	3		
7.142857	3	74	6.5	70.47619	2.6		
9.52381	4	86	7.5	81.90476	3		
11.90476	5	85	7.5	80.95238	3		
14.28571	6	105	8.5	100	3.4		
16.66667	7	102	8.5	97.14286	3.4		
19.04762	8	120	9.6	114.2857	3.84		
21.42857	9	120	11	114.2857	4.4		
23.80952	10	144	10.7	137.1429	4.28		
26.19048	11	145	10.7	138.0952	4.28		
28.57143	12	161	9	153.3333	3.6		
30.95238	13	165	9.2	157.1429	3.68		
33.33333	14	179	7.3	170.4762	2.92		
35.71429	15	182	6	173.3333	2.4		
38.09524	16	189	4.8	180	1.92		
40.47619	17	190	5.8	180.9524	2.32		
42.85714	18	199	6.2	189.5238	2.48		
45.2381	19	206	5.7	196.1905	2.28		
47.61905	20	212		201.9048			
50	21	212		201.9048			
				Av.	3.155556		

Appendix I

Example of Flame Speeds Calculation for orifice plate of 5 mm, at equivalence ratio of

1.1

		Scale	18.8	cm	214	pix
Time	Frame	Distance	Speed	Distance	Speed	
(ms)		Pixels	pixels/fram	mm	m/s	
0	0	32		28.11215		
2.380952	1	34		29.86916		
4.761905	2	37	2.8	32.50467	1.033121	
7.142857	3	40	2.8	35.14019	1.033121	
9.52381	4	43	2.7	37.7757	0.996224	
11.90476	5	45	2.7	39.53271	0.996224	
14.28571	6	48	2.6	42.16822	0.959327	
16.66667	7	51	2.7	44.80374	0.996224	
19.04762	8	53	2.5	46.56075	0.92243	
21.42857	9	56	2.5	49.19626	0.92243	
23.80952	10	58	2.5	50.95327	0.92243	
26.19048	11	61	2.5	53.58879	0.92243	
28.57143	12	63	2.5	55.34579	0.92243	
30.95238	13	66	2.5	57.98131	0.92243	
33.33333	14	68	2.5	59.73832	0.92243	
35.71429	15	71	2.5	62.37383	0.92243	
38.09524	16	73	2.5	64.13084	0.92243	
40.47619	17	76	2.5	66.76636	0.92243	
42.85714	18	78	2.5	68.52336	0.92243	
45.2381	19	81	2.5	71.15888	0.92243	
47.61905	20	83	2.7	72.91589	0.996224	
50	21	86	2.4	75.5514	0.885533	
52.38095	22	89	2.6	78.18692	0.959327	
54.7619	23	90	2.3	79.06542	0.848636	
57.14286	24	94	2.5	82.57944	0.92243	
59.52381	25	95	2.5	83.45794	0.92243	
61.90476	26	99	2.5	86.97196	0.92243	
64.28571	27	100	2.5	87.85047	0.92243	
66.66667	28	104	2.3	91.36449	0.848636	
69.04762	29	105	2.4	92.24299	0.885533	

Average speed, m/s **0.96**

Appendix J

Example of Flame Speeds Calculation of propane with orifice plate of 5 mm, at equivalence ratio of 1.1 and at high temperature 333K

		Scale	19.5	cm	214
Time (ms)	Frame	Distance Pixels	Speed pixels/frame	Distance mm	Speed m/s
0	0	28		25.51402	
2.380952	1	31		28.24766	
4.761905	2	34	3	30.98131	1.148131
7.142857	3	37	3	33.71495	1.148131
9.52381	4	40	3	36.4486	1.148131
11.90476	5	43	2.8	39.18224	1.071589
14.28571	6	46	2.9	41.91589	1.10986
16.66667	7	48	2.8	43.73832	1.071589
19.04762	8	52	3	47.38318	1.148131
21.42857	9	54	3	49.20561	1.148131
23.80952	10	58	2.8	52.85047	1.071589
26.19048	11	60	2.9	54.6729	1.10986
28.57143	12	63	2.8	57.40654	1.071589
30.95238	13	66	3	60.14019	1.148131
33.33333	14	69	3	62.87383	1.148131
35.71429	15	72	3	65.60748	1.148131
38.09524	16	75	2.8	68.34112	1.071589
40.47619	17	78	2.9	71.07477	1.10986
42.85714	18	80	2.8	72.8972	1.071589
45.2381	19	84	2.8	76.54206	1.071589
47.61905	20	86	2.7	78.36449	1.033318
50	21	89	2.5	81.09813	0.956776
52.38095	22	91	2.7	82.92056	1.033318
54.7619	23	94	2.8	85.65421	1.071589
57.14286	24	97	2.8	88.38785	1.071589
59.52381	25	100	2.7	91.1215	1.033318
61.90476	26	102	2.5	92.94393	0.956776
64.28571	27	105	2.5	95.67757	0.956776
66.66667	28	107	2.5	97.5	0.956776
69.04762	29	110	2.5	100.2336	0.956776

Average speed, m/s 1.01

Appendix K

Example of Flame Speeds Calculation of acetone with orifice plate of 5 mm, at equivalence ratio of 1.2 and at high temperature 333K

		1.2-a				
		Scale	20.3 cm		217 pix	
Time (ms)	Frame	Distance Pixels	Speed pixels/frame	Distance mm	Speed m/s	
0	0	27		25.25806		
2.380952	1	30		28.06452		
4.761905	2	33	3	30.87097	1.17871	
7.142857	3	36	3	33.67742	1.17871	
9.52381	4	39	2.8	36.48387	1.100129	
11.90476	5	42	2.7	39.29032	1.060839	
14.28571	6	44	2.7	41.16129	1.060839	
16.66667	7	47	2.8	43.96774	1.100129	
19.04762	8	50	3	46.77419	1.17871	
21.42857	9	53	2.8	49.58065	1.100129	
23.80952	10	56	2.7	52.3871	1.060839	
26.19048	11	58	2.7	54.25806	1.060839	
28.57143	12	61	2.8	57.06452	1.100129	
30.95238	13	64	3	59.87097	1.17871	
33.33333	14	67	2.8	62.67742	1.100129	
35.71429	15	70	2.7	65.48387	1.060839	
38.09524	16	72	2.7	67.35484	1.060839	
40.47619	17	75	2.8	70.16129	1.100129	
42.85714	18	78	3	72.96774	1.17871	
45.2381	19	81	2.8	75.77419	1.100129	
47.61905	20	84	2.7	78.58065	1.060839	
50	21	86	2.7	80.45161	1.060839	
52.38095	22	89	2.8	83.25806	1.100129	
54.7619	23	92	3	86.06452	1.17871	
57.14286	24	95	2.8	88.87097	1.100129	
59.52381	25	98	2.7	91.67742	1.060839	
61.90476	26	100	2.7	93.54839	1.060839	
64.28571	27	103	2.8	96.35484	1.100129	
66.66667	28	106	2.8	99.16129	1.100129	
69.04762	29	109	2.7	101.9677	1.060839	
71.42857	30	111	2.7	103.8387	1.060839	
73.80952	31	114	2.8	106.6452	1.100129	
76.19048	32	117	2.8	109.4516	1.100129	

Average speed, m/s **1.044**

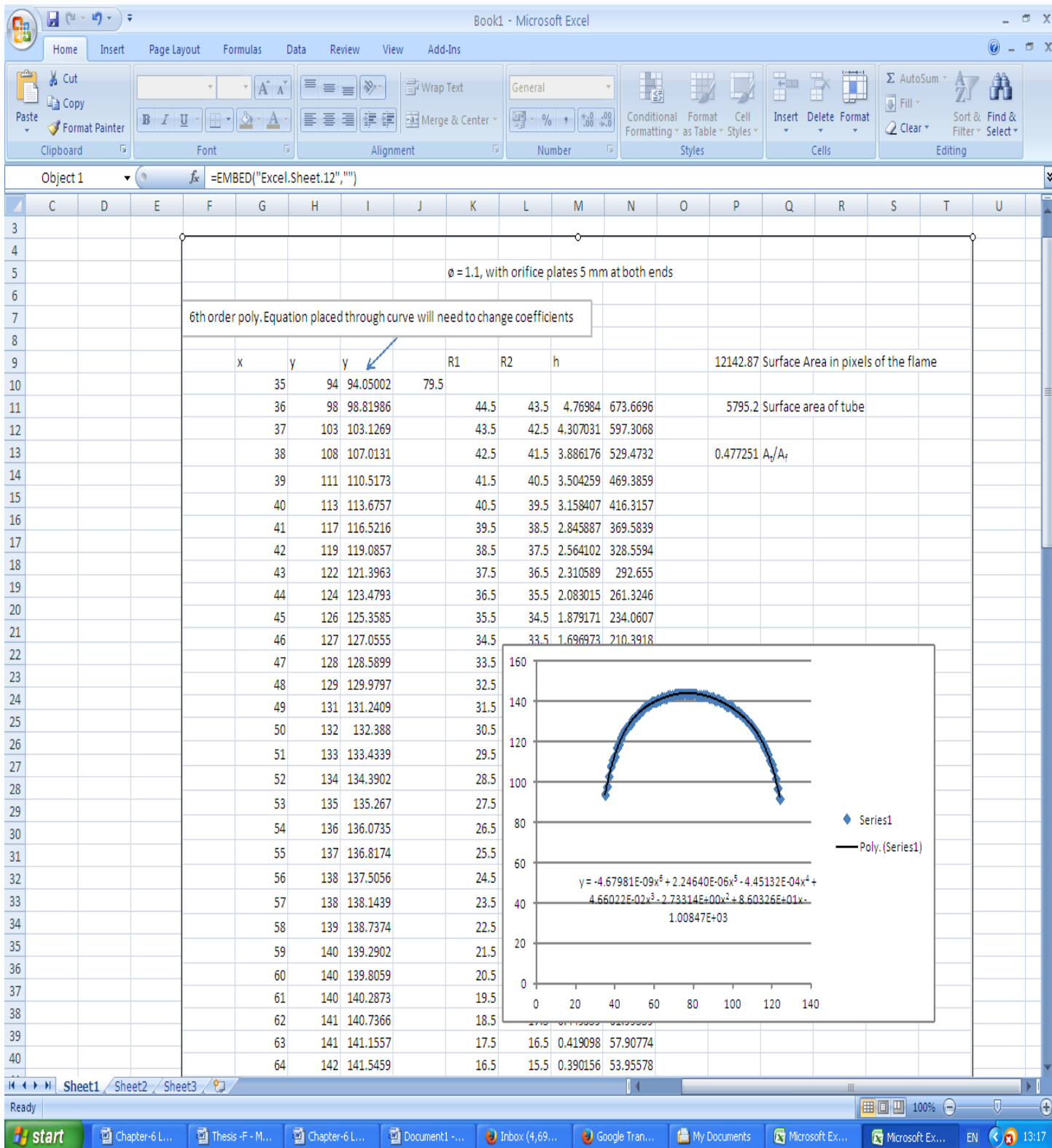
Appendix L

The variation of the maximum flame speed of different fuel obtained by Gerstein [6]

Fuel	Max. of laminar burning velocity, cm/sec	Vol. % of fuel at maximum laminar burning velocity
Methane	33.8	9.96
Ethane	40.1	9.28
Propane	39.0	4.54
Butane	37.9	3.52
Hexane	38.5	2.51

Appendix M

Example of surface area calculation



Appendix N– Published

Yang J, Mossa F.M.S, Huang H.W, Wang O, Woolley R and Zhang Y “*Oscillating flames in open tubes*”, 35th Symposium (International) on Combustion, San Francisco (USA), August 2014, Proceedings of the Combustion Institute, *In Press corrected proof*, Available online 16 September 2014.